



1



2
MAX PLANCK INSTITUTE
FOR DYNAMICS OF COMPLEX
TECHNICAL SYSTEMS
MAGDEBURG



BIOPROCESS ENGINEERING

Hochschule Anhalt

Anhalt University of Applied Sciences

Department of Applied Biosciences
and Process Engineering

Clonal heterogeneity of the MDCK cell population: Effect on cell-to-cell variability in influenza A virus replication

MASTER THESIS

presented to the department of Applied Biosciences and Process Engineering
at Anhalt University of Applied Sciences
in partial fulfilment of the requirements for the degree of

Master of Science (M.Sc.)

submitted on January 26th, 2017 by

Annekathrin Leupelt

matriculation number: 4054298

First examiner: Prof. Dr. Hans-Jürgen Mägert¹

Second examiner: Prof. Dr.-Ing. Udo Reichl²

Supervisor: Dipl.-Ing. Sascha Young Kupke²

Statement of authorship

I, Annekathrin Leupelt, born on September 8th, 1989 in Lutherstadt Wittenberg, hereby declare that the present thesis is my own work and effort. All facilities and sources I used have been acknowledged. This work or a similar version neither has been submitted to any other course or exam authority nor has been published before.

Magdeburg, January 26th, 2017

Acknowledgements

I want to thank those people who directly or indirectly promoted me to accomplish this master thesis. Without their contributions listed below it would not be possible to cope it.

First of all, Prof. Hans-Jürgen Mägert not only assumed the position as first examiner but provided highly significant and never tiring lectures during five years of my studies in beautiful Köthen.

Thank You!

Second, Prof. Udo Reichl gave me the opportunity to work in his Bioprocess Engineering research group at Max Planck Institute and readily assumed the position as second examiner.

Thank You!

Third, Sascha Y. Kupke provided the very exciting subject of this thesis and supervised me throughout the entire time. He pushed me into the main direction, always asked the right questions and thus made me concentrate on the essentials and cut overgrowing trees.

Thank You!

Further, the whole Molecular Biology team provided a really nice working atmosphere. Everyone contributed to inspiring and helpful discussions that opened my mind and enabled me looking further ahead. Also the members of the Upstream Processing team provided valuable scientific exchange.

Thank You!

Beyond, Nancy Wynserski, Claudia Best and Ilona Behrendt provided excellent technical assistance. They readily taught me methods and skills, answered my questions and made me feel welcome.

Thank You!

Last but not least, my family supported and motivated me throughout my studies ensuring my well-being. The same is true for my betrothed Fabian Gielsdorf. He took the load off me in stressful times and spent countless great times.

Thank You!

Abstract

Madin-Darby canine kidney (MDCK) cells are a continuous epithelial cell line and comprise a heterogeneous non-clonal cell population with clonal subpopulations displaying differences in various characteristics. Furthermore, a large cell-to-cell variability in influenza A virus (IAV) replication was revealed among individual MDCK cells by single-cell analysis (Heldt and Kupke et al., 2015, *Nat Commun* **6**, 8938). The present thesis is the first study that aims to reveal if the clonal heterogeneity of the MDCK cell population contributes to the large cell-to-cell variability in IAV replication.

31 clonal MDCK cell lines were derived from a parental MDCK cell population by limiting dilution cloning. The individual clones reflected heterogeneous characteristics in terms of morphology, cell size and cell density. Strikingly, two distinct groups of clones became apparent: 1) clones of small cells growing to high cell densities and 2) clones of big cells growing to low cell densities. All clones were infected with IAV and investigated for the virus titer they produce at the population level. However, no significant differences in volumetric virus titers were observed between the clones. Yet, further analysis showed that 1) clones of small cells were associated to lower and 2) clones of big cells were associated to higher cell-specific virus yields. It was therefore assumed that the combination of cell size, cell density and cell-specific virus yield, in turn, resulted in similar volumetric virus titers produced by similar cell volumes.

Finally, the IAV replication was investigated at the single-cell level comparing two clones, one representing small cells and one representing big cells, with the parental MDCK cells. Single-cell analysis demonstrated that the cell-to-cell variability in extracellular virus yields and intracellular vRNA content was similarly high in all three populations. Therefore, it seems that the heterogeneity in the MDCK cell population does not contribute to the large cell-to-cell variability in IAV replication. Hence, other factors, such as biological noise, are likely to play a role.

Table of contents

1	Introduction	1
2	Aim of the thesis	2
3	Theoretical background.....	3
3.1	Influenza virus	3
3.1.1	Classification.....	3
3.1.2	Structure, genetics and replication	4
3.1.3	Influenza vaccines and vaccine production.....	8
3.2	Madin-Darby canine kidney (MDCK) cells	10
3.2.1	Properties and applications.....	10
3.2.2	Heterogeneity within the cell population	10
3.3	Single-cell analysis	12
3.3.1	Approaches: Chances and limitations	14
3.3.2	Applications	15
3.3.3	Application for virus replication studies	16
4	Material and methods	18
4.1	Material.....	18
4.1.1	Technical equipment and plastic ware	18
4.1.2	Chemicals and reagents	19
4.1.3	Buffers and media	20
4.1.4	Primers	22
4.1.5	Cell line and virus strain.....	22
4.2	Methods	23
4.2.1	MDCK cell culture	23
4.2.1.1	Maintenance and expansion	23
4.2.1.2	Measurement of cell count, viability and cell diameter	23
4.2.1.3	Calculation of the cell volume	24

4.2.1.4	Harvesting of conditioned medium.....	24
4.2.1.5	Cloning and expansion of subclones.....	25
4.2.1.6	Cryopreservation and thawing	26
4.2.1.7	Maintanance of clonal MDCK cell populations	27
4.2.2	Influenza A virus (IAV) infection of MDCK cells	28
4.2.2.1	Population level	28
4.2.2.2	Single-cell level	30
4.2.3	Virus quantification assays.....	31
4.2.3.1	Hemagglutination (HA) assay.....	31
4.2.3.2	50 % Tissue culture infection dose (TCID ₅₀) assay.....	32
4.2.3.3	Plaque assay	33
4.2.3.4	Plaque assay for single cells	34
4.2.4	Absolute intracellular vRNA quantification in single cells by RT-qPCR	35
4.2.5	Statistical analysis	40
5	Results	41
5.1	Cloning and characterization of clonal MDCK cell populations	41
5.1.1	Cloning procedure	41
5.1.2	Morphological characteristics	46
5.1.3	Growth characteristics.....	48
5.2	IAV infection of clonal and parental MDCK cell populations.....	51
5.2.1	Screening at the population level	51
5.2.1.1	Analysis of the virus yield	51
5.2.1.2	Analysis of the virus yield under alternative infection conditions.....	56
5.2.2	Single-cell analysis.....	60
5.2.2.1	Selection of clonal MDCK cell populations	60
5.2.2.2	Analysis of the virus yield	61
5.2.2.3	Analysis of the intracellular vRNA content.....	65

6	Discussion	69
6.1	Clonal MDCK cell populations	69
6.2	IAV infection of clonal and parental MDCK cell populations.....	75
6.2.1	Screening at the population level	76
6.2.2	Single-cell analysis.....	79
7	Conclusions and outlook	86
8	Bibliography.....	88
	List of abbreviations.....	I
	List of symbols	III
	List of figures	V
	List of tables	VIII
A	Appendix	X
A 1	Standard operating procedures (SOPs).....	X
A 1.1	SOP V/05, version 2.2 (20.01.2011): Hemagglutination assay (HA assay)	X
A 1.2	SOP V/08, version 2.1 (02.06.2008, 09.01.2013): TCID ₅₀ Assay	XV
A 2	Supplemental material	XXI

1 Introduction

Influenza viruses cause highly contagious respiratory disease with potentially fatal outcome posing a persisting and unpredictable global threat: Seasonal influenza epidemics yearly cause millions of cases of severe illness and up to half a million of deaths worldwide. Additionally, infrequently occurring influenza pandemics have dramatic health, social and economic impact around the world. Vaccination is the most effective intervention preventing infections. Since the virus strains adapt and alter every year, the vaccine production additionally faces the challenge of updating the composition accordingly (WHO, 2014, 2016a; Wright et al., 2013).

Traditionally, influenza vaccines are produced in embryonated chicken eggs. But especially in pandemic scenarios when large amounts of vaccine doses are needed, the production capacity is critical. In contrast, the cell culture based vaccine production is expandable in short terms and comes along with additional benefits. Though, cell culture based production processes need further optimization and increased virus yields in order to become the predominant technology (Hegde, 2015).

The research on influenza A (IAV) production in cell cultures is one focus of the Bioprocess Engineering group at Max Planck Institute for Dynamics of Complex Technical Systems in Magdeburg. Different approaches, such as the variation of the cell line, the variation of culture and infection conditions, the testing of different bioprocess strategies and mathematical modeling are used to aim high virus yields. Moreover, the Molecular Biology team aims, for instance, to increase the understanding of viruspropagation by identifying bottlenecks of intracellular virus replication and of virus-host cell interactions. For this purpose, Madin-Darby canine kidney (MDCK) cells are a well established cell line which comprises a heterogeneous non-clonal cell population. In particular, performing single-cell analysis, a large cell-to-cell variability in influenza virus titers was revealed among the infected MDCK cell population (Heldt and Kupke et al., 2015). Finding out the origin of this variability potentially provides a strategy to increase the cell-specific virus yield.

2 Aim of the thesis

The aim of the present thesis is to assess the contribution of the clonal heterogeneity of the MDCK cell population to the cell-to-cell variability in IAV replication.

To achieve this, three milestones were set (Figure 2-1). First, the MDCK cell population is to be cloned which is intended to reduce the heterogeneity and to obtain virtually homogeneous clonal MDCK cell populations. This is done by a limiting dilution technique followed by the expansion of the clones. The clones are cryopreserved for subsequent experiments.

Second, the clonal MDCK cell populations are to be screened for the average virus titer they produce at the population level in order to identify high and low yielding clones. Potentially, clones producing higher virus titers than the non-clonal MDCK cell population could be used for production processes increasing the yield. The screening is done by IAV infection of the clonal populations and subsequent quantification of the virus titers by different virus titration assays.

Third, using selected clones, the cell-to-cell variability in IAV replication is to be compared to that of the non-clonal MDCK cell population. This is done by IAV infection of the population and the subsequent separation of the infected cells. Quantifying the extracellular virus yield and the intracellular vRNA content at the single-cell level reveals the distribution of these parameters among the cells. Finally, the results of the single-cell experiments should expand the understanding of cell-to-cell variability in IAV replication.

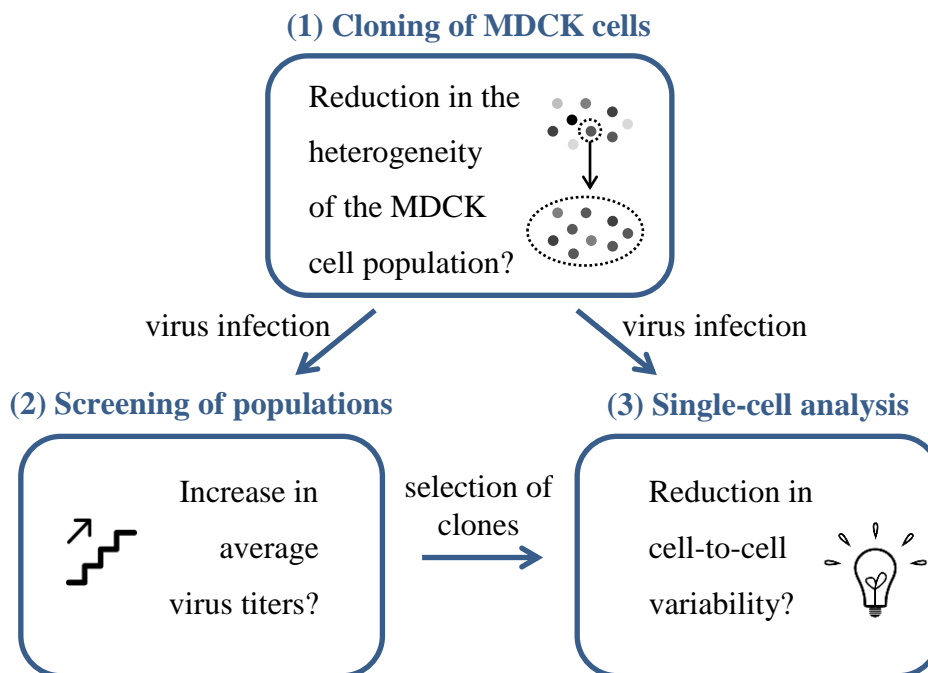


Figure 2-1: Milestones of the present thesis and questions to be addressed.

3 Theoretical background

The theoretical fundamentals and the current state of the major subjects relevant for the present thesis are introduced in the following.

3.1 Influenza virus

Influenza viruses are pathogens causing highly contagious and often serious acute respiratory illness (the flu). Symptoms, usually lasting for 3-7 days, include cough, sore throat and a runny nose as well as fever, chills and muscle aches and thereby differs from the common cold. Severe cases can end up with a generalized infection and even lead to death (Modrow et al., 2013; Zinserling and Dedov, 2016). Overall, influenza virus infections and the secondary complications are possibly the most important infectious cause of human morbidity and mortality (Hegde, 2015). Aside from humans, a variety of animals including birds, swine, horses and dogs are susceptible to influenza viruses and a large natural reservoir is found in aquatic birds. The inter-species transmission of specific influenza virus variants and constant evolution of the virus keep it a major, global health threat (Wright et al., 2013).

Seasonal influenza viruses circulate yearly spreading from person-to-person through sneezing, coughing or touching contaminated surfaces (WHO, 2014). It is estimated that about three to five million cases of severe illness and quarter to half a million deaths are caused by these annual epidemics worldwide (WHO, 2016a). Additionally, global pandemic outbreaks of completely new influenza virus variants coming up in 1918/1919, 1957, 1968 and 2009 resulted in millions of deaths (WHO, 2014).

3.1.1 Classification

Influenza viruses are enveloped RNA viruses with a segmented, linear, single-stranded genome of negative polarity and so belong to the family *Orthomyxoviridae*. They represent three out of five different genera – influenza A, influenza B and influenza C viruses (McCauley et al., 2012; Shaw and Palese, 2013). Especially influenza A viruses are further classified into serotypes according to their hemagglutinin (currently H1-H18) and neuraminidase (currently N1-N11) subtypes (WHO, 2016b). Moreover, strains can be distinguished by the nomenclature of influenza virus isolates. This includes the virus type, the host species (if non-human), the geographical location of the isolate, the isolate number, the year of isolation and the H and N variants (WHO, 2016b). For example, the virus strain A/Puerto Rico/8/34 (H1N1) was the eighth isolate of an influenza A virus taken from a human in Puerto Rico in 1934 and has an H1 and N1 subtype.

3.1.2 Structure, genetics and replication

Influenza viruses have a complex structure with each component being critical for virus replication. The viral geno- and phenotype is altered frequently due to the specific genetics of influenza viruses which consequently challenges fighting the pathogen (Bouvier and Palese, 2008). The following sections are restricted to influenza A viruses (IAV) which are of most interest since this is the most pathogenic genus (Julkunen et al., 2001).

Structure

Influenza viruses are spherical or filamentous particles with an approximate diameter of 100 nm or a length of about 300 nm. They basically consist of the envelope, the viral genome and viral proteins (Bouvier and Palese, 2008). A schematic depiction of the virus structure is shown in Figure 3-1.

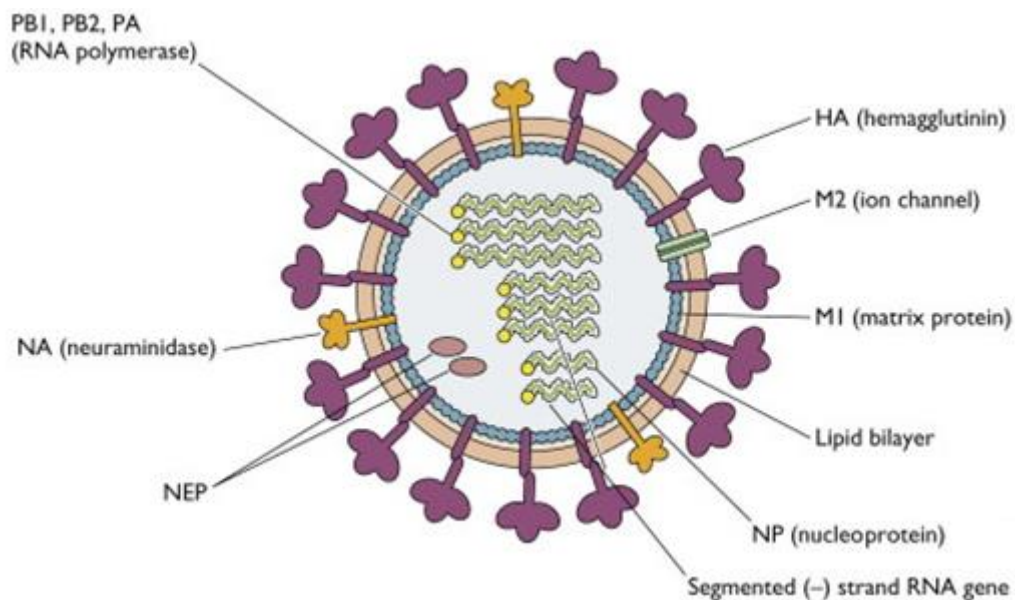


Figure 3-1: Schematic depiction of the influenza A virus particle structure; the complex of RNA polymerases, NP and a viral RNA segment is called viral ribonucleoprotein complex (vRNP); NEP: nuclear export protein; PB1 and PB2: polymerase basic 1 and 2; PA: polymerase acidic; adapted from Flint et al. (2009).

The envelope is formed by a lipid bilayer which is derived from the host cell and exposes three viral proteins. These are the antigenic peripheral glycoproteins hemagglutinin (HA) and neuraminidase (NA) and the integral matrix protein 2 (M2). HA, which represents approximately 80 % of the envelope proteins, forms trimeric spikes with receptor-binding sites and epitopes for antibody neutralization and contains a cleavage site. NA, which represents approximately 17 % of the envelope proteins, forms tetrameric spikes with enzyme activity cleaving sialic acid moieties from the host cell receptors. The M2 protein, which is the rarest of the three envelope

proteins, has an ion channel activity and is capable to transport hydrogen ions into the virus particle (Nayak et al., 2009).

Underneath the lipid envelope a layer of matrix protein 1 (M1) encloses the virion core which contains the nuclear export protein (NEP) and the segmented viral genome. The viral genome comprises eight segments which are viral ribonucleoprotein (vRNP) complexes (Bouvier and Palese, 2008).

Genetics

Each of the eight vRNP segments consists of one linear negative strand of coiled viral RNA (vRNA) stabilized by nucleoproteins (NP) and associated with a heterotrimeric RNA-dependent RNA polymerase (RdRp) complex of polymerase basic 1 (PB1), polymerase basic 2 (PB2) and polymerase acidic (PA) (Figure 3-1) (Portela and Digard, 2002).

The coding region of each vRNA segment (negative sense open reading frame) is flanked by non-coding regions at the 5' and 3' ends, of which the terminal sequences are conserved among all IAV segments and the adjacent sequences are segment-specific. A partial complementarity between the 5' and 3' conserved non-coding regions causes the formation of a short duplex where the RdRp complex binds. The entire vRNA molecule is coiled into a panhandle structure coated with NP (Elton et al., 2006; Portela and Digard, 2002). The vRNA segments are numbered from 1 to 8 according to their lengths with segment 1 being the longest and segment 8 being the shortest one (Bouvier and Palese, 2008).

Table 3-1: Length of the eight vRNA segments of IAV and proteins encoded by them; adapted from Bouvier and Palese (2008).

Segment	vRNA length (nucleotides)	Encoded proteins
1	2341	PB2 polymerase basic 2
2	2341	PB1 polymerase basic 1
		PB1-F2 (open reading frame overlapping with PB1)
3	2233	PA polymerase acidic
4	1778	HA hemagglutinin
5	1565	NP nucleoprotein
6	1413	NA neuraminidase
7	1027	M1 matrix protein 1
		M2 matrix protein 2 (splice variant of M1)
8	890	NS1 nonstructural protein 1
		NS2 nonstructural protein 2 (splice variant of NS1)
		(NEP) (nuclear export protein)

The IAV genome is subjected to continuing evolution by different mechanisms which consequently has an impact on the protein expression and causes a huge diversity not only among individual virus strains but also among virus subpopulations. (Webster et al., 1992). Especially regarding the changes in the antigenic proteins HA and NA, this causes two specific effects called antigenic drift and antigenic shift. The antigenic drift is based on the error-prone nature of the viral RdRp complex lacking a proofreading function. Mutations lead to the emergence of many variants such as new H and N variants to which the (human) population has a limited immunity and as a result epidemics arise (Webster et al., 1992). The antigenic shift is based on the segmentation of the viral genome. It allows a recombination of entire vRNA segments between different strains co-infecting a host cell. The so called reassortment of different HA (H1-18) and NA variants (N1-N11) from the natural reservoir, especially among different hosts, causes the emergence of new strains to which the (human) population may have little or no immunity. This is how global pandemics may arise (Steinhauer and Skehel, 2002). Another mechanism that causes genetic variation in IAV is the occurrence of internal deletions, especially on the three vRNA segments encoding the RdRp complex. Such defective RNA can compete with the according standard RNA and thus is termed defective interfering RNA (DI RNA). Virus particles containing DI RNA are called defective interfering particles (DIPs). Since they lack genomic information, cells solely infected with DIPs are not able to replicate such viruses. In contrast, cells co-infected with DIPs and standard virus particles (acting as a helper virus) are able to replicate both, preferring the DIPs (Huang and Baltimore, 1970; Nayak et al., 1985). The role of DIPs in viral pathogenesis may be to maintain a chronic persistent infection in the host by reducing the cytopathic effect (Holland et al., 1980).

Replication

The replication of IAV is cyclical and depends on mammalian host cells. The replication cycle can be roughly divided into the following stages – the virus attachment and entry, the synthesis of viral RNA species and viral proteins (replication, transcription and translation), the virus assembly and the virus release (Bouvier and Palese, 2008; Shaw and Palese, 2013). A schematic overview of the intracellular replication cycle of IAV is provided in Figure 3-2.

The virus attachment is dependent on receptors on the surface of the host cell membrane which are sialic acid (neuraminic acid) residues α 2-3 or α 2-6 linked to glycoproteins or glycolipids. These moieties are specifically recognized and bound by the viral HA protein. (Whittaker and Digard, 2006). The HA protein originally exists as a precursor (HA0) but is cleaved into two portions HA1 and HA2 at the cleavage site by specific serine proteases. The *in vivo* presence of

such enzymes determines the pathogenicity whereas the addition of trypsin promotes the *in vitro* virus activation (Klenk et al., 1975; Steinhauer, 1999).

The thus attached virus particle then enters the cell by receptor-mediated endocytosis. A low pH is adjusted in the endosome which has two consequences. First, a fusion peptide of the previously cleaved HA protein is exposed. It mediates the fusion between the viral and the cell membrane of the intracellular vesicle. Second, hydrogen ions are transported into the virus particle by the M2 ion channel which weakens the internal protein-protein interactions and thus enables the release of the vRNPs into the cytoplasm (Bouvier and Palese, 2008).

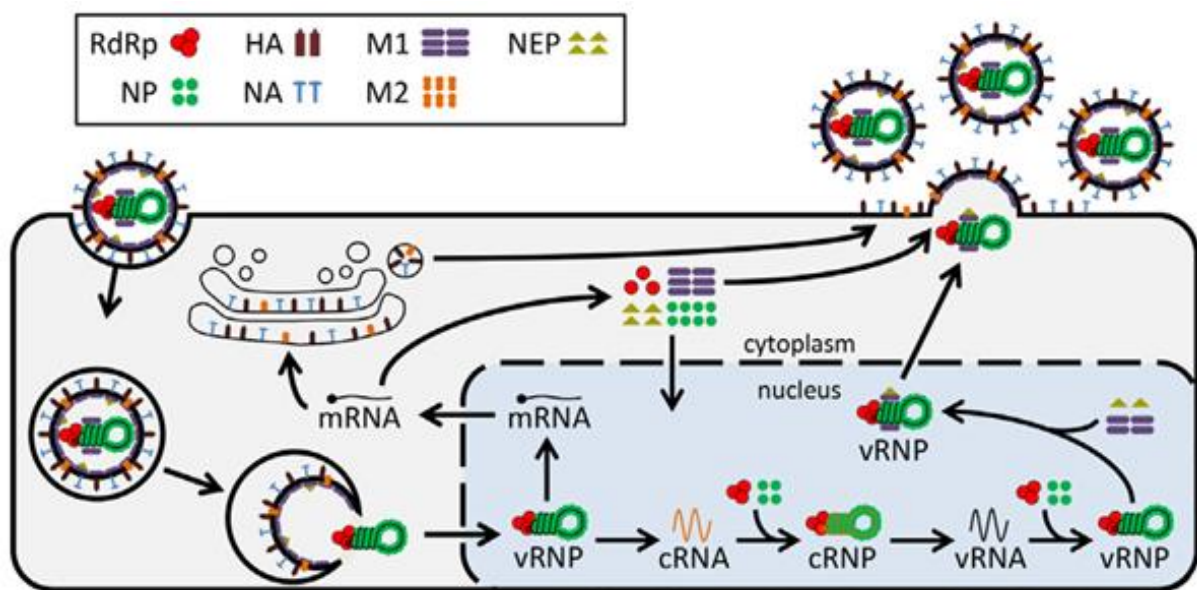


Figure 3-2: Intracellular replication cycle of influenza A virus; only one out of eight vRNP segments is depicted for simplicity; enzymes and structure proteins: RdRp RNA-dependent RNA polymerase, NP nucleoprotein, HA hemagglutinin, NA neuraminidase, M1 matrix protein 1, M2 matrix protein 2 NEP nuclear export protein; ribonucleic acid (RNA) types: vRNA viral RNA, vRNP viral ribonucleoprotein, mRNA messenger RNA, cRNA complementary RNA, cRNP complementary ribonucleoprotein; adapted from Heldt et al. (2013).

Mediated by NP carrying a nuclear localization signal (NLS), the vRNP complexes are then imported into the nucleus using a host cell mechanism. In the nucleus all viral RNA species are synthesized by the RdRp complex (Cros and Palese, 2003). First, the vRNA is transcribed into positive sense messenger RNA (mRNA). For initiation, 5'-capped RNA fragments are cleaved from host cell mRNAs by the viral polymerase and serve as a primer, which is called cap-snatching. The transcription is terminated by repetitively transcribing a short poly(U) stretch near the 5'-end of the vRNA template, resulting in a poly(A) tail (Portela and Digard, 2002; Resa-Infante, Jorba and Coloma et al., 2011). Second, the vRNA is transcribed unprimed into positive sense intermediate complementary RNA (cRNA) which is encapsidated by newly

synthesized NP and RdRps into cRNA containing ribonucleoprotein (complementary ribonucleoprotein, cRNP) complexes. The cRNA serves as a template for the unprimed synthesis of new negative sense vRNA molecules which are replicates of the original vRNA and are again encapsidated by newly synthesized NP and RdRps into vRNPs (Eisfeld et al., 2014; Portela and Digard, 2002).

The mRNA is exported into the cytoplasm. The translation of envelope proteins (HA, NA, M2) takes place at membrane-bound ribosomes followed by folding and posttranslational modifications in the Golgi apparatus and trafficking to the cell membrane for virus assembly (Bouvier and Palese, 2008). The translation of the other proteins takes place in the cytoplasm. The nuclear import of those proteins, triggered by NLS, allows the formation of cRNPs and vRNPs. To incorporate the vRNPs into new virus particles, they are exported from the nucleus into the cytoplasm. This is mediated by the binding of NEP and M1 carrying a nuclear export signal (NES) (Cros and Palese, 2003).

All viral components are assembled near the cell membrane of the host cell, each virus particle receiving a full complement of the eight vRNP segments (Fournier et al., 2011). New virus particles bud from the apical cell membrane of polarized host cells with the host membrane and the viral proteins as a coat (Nayak et al., 2009). The NA enzyme cleaves the α 2-3 or α 2-6 linked sialic acid moieties and thereby destroys the HA binding receptors on the host cell surface. This promotes the final release of individual virus particles (Bouvier and Palese, 2008).

Extensive studies of *in vitro* IAV replication in Madin-Darby canine kidney (MDCK) cells (see paragraph 0) have enabled the establishment and improvement of structured mathematical models, such as from Sidorenko and Reichl (2004), Heldt et al. (2012), Heldt et al. (2013), Heldt and Kupke et al., (2015) and Laske and Heldt et al. (2016). Such models help to understand complex mechanisms of cell growth and virus replication, can serve for the optimization of virus yields in vaccine production processes and may contribute to the development of antiviral drugs.

3.1.3 Influenza vaccines and vaccine production

Vaccination effectively prevents influenza virus infections and complications by immunization (Wright et al., 2013). Especially elderly people, children and immunocompromised individuals, which are most debilitated by influenza virus infections, benefit from vaccination (Genzel and Reichl, 2009).

Seasonal influenza vaccines comprise a yearly updated mixture of three (trivalent), four (quadrivalent) or more (multivalent) different influenza virus subtypes based on recommendations of the World Health Organization (WHO). These are usually two influenza A

virus strains and one influenza B virus strain (Genzel et al., 2013; WHO, 2017). Three types of influenza vaccines are produced. Live attenuated influenza vaccines (LAIV) contain cold adapted virus with an attenuated replication at body temperature. Inactivated influenza vaccines contain chemically treated non-replicable virus particles with a complete antigen presentation. Split or subunit influenza vaccines are restricted to the viral HA and NA proteins which are gained either by isolation from complete virus particles or by recombinant production in suitable expression systems (Genzel et al., 2013; Ulmer et al., 2006). An upcoming strategy is the insect cell and baculovirus expression vector system (BEVS) that has been extensively used for recombinant protein production (Milián and Kamen, 2015).

The production of influenza vaccines has been carried out in embryonated chicken eggs since the 1940s. After isolation from a clinical specimen, the virus is grown in the allantoic cavity of the eggs, harvested, purified, concentrated and inactivated (Audsley and Tannock, 2008). But even if the production process is well established and high yields are obtained, it is labour intensive and limited to the availability of large amounts of eggs. Especially in case of coming up epidemics or pandemics associated with a high demand for vaccines it is not expandable in a short term. Furthermore, the use of eggs as a substrate bears the risk of contamination and also the allergenicity of residual egg proteins (Hegde, 2015). Avoiding eggs, all these problems can be faced by using continuous cell cultures for vaccine production. Additionally, virus replication in cell cultures does not select a variant but preserves the initial viral variability which implicates a high vaccine efficiency (Gregersen et al., 2011). Among others, basically two prominent cell lines, Madin-Darby canine kidney (MDCK) cells and Vero cells (African monkey kidney epithelial cells), have become apparent to be suitable for influenza vaccine production due to their high virus yields and the high vaccine safety (Genzel et al., 2013; Hegde, 2015). The adherent cell lines are expandable in a large scale growing on microcarriers in stirred tank reactors. Alternatively, suspension cell lines established by the adaptation to serum-free media are available (Genzel et al., 2013). Though the cell lines and vaccines have been authorized/approved and passed several safety requirements the cell culture based vaccine production is still in its early stages and lots of studies are conducted. Several cell culture based influenza vaccines have been licensed (Genzel and Reichl, 2009; Milián and Kamen, 2015) but the majority of influenza vaccines is still produced in eggs (Buckland, 2015; Milián and Kamen, 2015).

3.2 Madin-Darby canine kidney (MDCK) cells

The MDCK cell line was established by Madin and Darby in 1958 (Madin and Darby, 1958). Originally isolated from a normal adult Cocker Spaniel, the renal cells have been transformed into a continuous cell line in an unknown way (Liu et al., 2010). The first characterization was done by Gaush et al. (1966).

3.2.1 Properties and applications

Due to the epithelial origin, MDCK cells adhere on surfaces forming a monolayer of apico-basolateral polarity. The formation of tight junctions and the presence of polarity-specific ion channels and pumps make them an appropriate model of renal distal tubule to study trafficking and polarized sorting as well as physiological functions, such as transport mechanisms (Arthur, 2000; Cao et al., 2012; Simmons, 1981).

Overall, the MDCK cell line is exhaustively investigated, well characterized and functionally stable (Gregersen et al., 2011). The cells are robust concerning the culture conditions as they grow in a wide pH range, are adaptable to different culture media and resist mechanical stress. They grow rapidly and are easy to handle (Genzel and Reichl, 2009; Merten et al., 1996; Oh et al., 2008). Due to the presence of $\alpha 2-6$ and $\alpha 2-3$ linked sialic acid receptors on their surface, the cells are highly susceptible to influenza virus infections (Lugovtsev et al., 2013; Oh et al., 2008). Taken all together, this makes the cell line a highly relevant object for basic research on influenza virus replication as well as for influenza virus isolation, propagation and characterization (Lugovtsev et al., 2013). Compared to other cell lines, the MDCK cell line yields high quantities of influenza virus and thus has been evolved as favorable for vaccine production (Genzel and Reichl, 2009; Liu et al., 2009). Safety issues for the use of the cell line as a substrate for virus cultivation are well-investigated as reviewed by Gregersen et al. (2011).

3.2.2 Heterogeneity within the cell population

The MDCK cell population is a non-clonal population meaning that it is not derived from a common ancestry cell and not constituted of identical (clonal) cells. Instead, it is constituted of geno- and phenotypically different cells with a large heterogeneity amongst them (Dukes et al., 2011; Nakazato et al., 1989). Currently, there are fourteen MDCK cell strains available from the most significant suppliers of cell lines (ATCC, 2016; ECACC, 2016; JCRB, 2016). As discussed by Dukes et al. (2011), they provide multiple parental populations as well as subpopulations isolated from any parental MDCK cell population which are geno- and phenotypically different and thus can serve for various purposes.

The first evidence for the presence of distinct cell types in an MDCK strain was found by Valentich (1981) who differentiated between low-passage and high-passage cells according to their specific morphology including the intercellular space, the cell size and the presence of cilia which are filiform sensory organelles on the cell surface. Besides morphological differences there was also found functional variability in subpopulations of a common progenitor population. Functions, such as electrophysiological or transport properties and hormonal response were found to differ between low-passage and high-passage cells (Barker and Simmons, 1981; Husted et al., 1986; Richardson et al., 1981).

The non-clonal nature of the MDCK cells makes it difficult to compare the results obtained from different research groups using different cell lines. Moreover, in many research cases it is desirable to obtain cell lines with more homogeneous properties and to select the most suitable one. This is done by cellular cloning and a subsequent expansion of the henceforth called clonal populations. The most prominent and conventional cloning procedure is the limiting dilution technique (small volumes of a diluted cell suspension are seeded on a microtiter plate aiming one cell per well (Clarke et al., 2011)).

There are numerous studies on (the characteristics of) distinct clonal MDCK cell populations which figure out the similarities and differences between the parental cell line and the descendent clonal cell lines. Mostly, the cells are classified into two types or strains, commonly designated strain I (derived from low passage numbers) and strain II (derived from high passage numbers) according to their morphological characteristics (the terms strain I and strain II were first used by Richardson et al. (1981)). They are associated with physiological functions or compositions and the probable origin of different renal locations (Arthur, 2000; Gekle et al., 1994; Hansson et al., 1986; Kersting et al., 1993; Nakazato et al., 1989; Nichols et al., 1986; Webb et al., 1996). However, the classification is not consistent throughout the studies as there are different strains designated according to their properties (such as motile and nonmotile (Nakazato et al., 1989)) or given numbers such as MDCK-1 and MDCK-2 (Kersting et al., 1993), type-1 and type-2 cells (Lugovtsev et al., 2013) or not named at all. Lugovtsev et al. (2013) further introduced type-3 cells which are characterized by the formation of domes (liquid-filled structures of the monolayer). Since most of the studies were based on different clonally derived MDCK cell lines they are not necessarily comparable even if properties are tried to be associated to each other. The high variability of the chromosome content of MDCK II cells obtained from different laboratories accounts for that (Cassio, 2013). The same study points out the effect of long term culture on the chromosome content and thus provides evidence for a limited genotypic stability of MDCK cell lines.

The clonal heterogeneity of the MDCK cell line can rather be considered a chance by cloning and selecting promising clonal cell populations. This is especially relevant for the application for influenza vaccine production. Instead of using the non-clonal cell population with an average virus yield, Liu et al. (2010) demonstrated that there are at least 15-fold differences in virus yields among 1228 clonally derived MDCK cell populations. After multiple rounds of cloning, the group derived a benefit from the seven highest yielding clones, adapted them to serum-free media and assessed their safety as a potential cell substrate for influenza vaccine production (Liu et al., 2010). Moreover, Lugovtsev et al. (2013) also used clonal MDCK cell population to analyze their specific susceptibility for different influenza virus strains. The infectivity titers of reference viruses as well as the virus yields produced by the individual clones could partly be associated to the morphological characteristics (type-1, type-2 and type-3; see above). In particular, using a specific IAV strain for infection, the type-2 cell clones produced a roughly 10-fold higher virus titer than the type-1 cell clones in the presence of trypsin but were nonproductive in the absence of trypsin (Lugovtsev et al., 2013). These two studies indicate the usable aspect of clonal heterogeneity.

3.3 Single-cell analysis

Cellular states and functions are commonly accessed by bulk measurements at the population level. But those averaging techniques are not capable of revealing cellular heterogeneity within a population and may even obscure relevant minor subpopulations. Single-cell analysis (SCA) therefore is a promising approach enabling the characterization of individual cells of a population (Di Carlo et al., 2012). There are numerous scenarios of cellular heterogeneity that can only be revealed by SCA. Some examples are illustrated in Figure 3-3.

First, SCA can reveal the extent of cell-to-cell variability in general (Figure 3-3 A). Cell-to-cell variability is the natural phenomenon that the individual cells of a population may vary in any characteristic, including morphology, biochemical properties, composition, function and behavior (Arriaga, 2009). With the help of SCA, the group of Elowitz et al. (2002) was able to measure and distinguish two stochastic effects (noise) leading to cell-to-cell variability in protein expression: intrinsic noise (stochasticity inherent in gene expression) and extrinsic noise (fluctuations in cellular components).

Second, SCA can reveal the occurrence of subpopulations within a cell population. The population average may even be completely misleading (Figure 3-3 B). Such a case was shown by Toriello et al. (2008) who with the help of single-cell analysis identified two cell

subpopulations with an either mediate or complete silencing instead of a bulk measured average silencing after the knockdown of a specific gene.

Similarly, SCA can reveal the occurrence of rare subpopulations which are discriminated by averaging population measurements (Figure 3-3 C). Often, such rare subpopulations are of special interest and their characterization depends on single-cell approaches (Di Carlo et al., 2012).

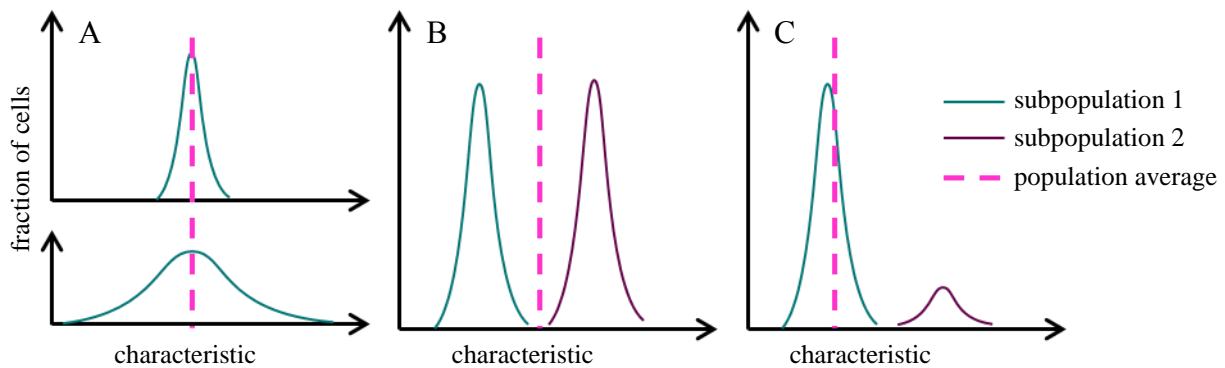


Figure 3-3: Examples for heterogeneity of cellular characteristics masked by population average; single-cell analysis is capable to reveal the extent of cell-to-cell variability (distributional dispersion) (A) and the occurrence of subpopulations (multimodal distributions) (B,C); population average can be misleading (B) or discriminate rare subpopulations (C); partly adapted from Di Carlo et al. (2012).

Apart from the possible endpoint based outcomes described above, SCA is capable of revealing dynamic heterogeneity in a cell population with the help of temporal (time-lapse) measurements at the single-cell level. For the average temporal trajectory based on population measurements may fail to represent single-cell activity (Muzzey and van Oudenaarden, 2009; Spiller et al., 2010). Overall, SCA comprises a powerful tool to investigate heterogeneity within a cell population and variability among single cells.

A critical point of SCA is the number of cells to be analyzed, especially given the fact that intrinsic noise particularly occurs when molecules are present in low quantities (Chen et al., 2016). Thus, depending on the preconditions, a reliable statistical evaluation must be ensured including the number of cells being assayed and the number of replicates to be performed (Chen et al., 2016). The miniaturization and establishment of automated high-throughput approaches therefore is a major topic in SCA (Fritzsche and Dusny et al., 2012; Weaver et al., 2014).

3.3.1 Approaches: Chances and limitations

Single-cell approaches in general combine two key competences, which are the separation of single cells (Gross, Schöndube and Zimmermann et al., 2015) and the analysis of specific features, such as nucleic acids, proteins, metabolites or other products (Wang and Bodovitz, 2010). Some frequently used methods are summarized in the following.

A very common technique for the separation or the separation and simultaneous analysis of single cells from a cell suspension is the fluorescence activated cell sorting (FACS), also called flow cytometry. Based on fluorescence signals of single cells passing a capillary, they are automatically sorted according to pre-defined characteristics and can optionally be used for further analysis. Single cells can also be isolated from cell suspensions by the limiting dilution technique (similar to the cloning approach mentioned in paragraph 3.2.2), by microfluidic devices, by manual cell picking (micromanipulator) or by microdissection (Gross, Schöndube and Zimmermann et al., 2015). These techniques depend on a previous dissociation of the cell population. However, the behavior of isolated cells may be considered to differ from the behavior of particular cells in a population context (Pelkmans, 2012) and the experimental approach should be confirmed not to interfere with the object of investigation. Fading this uncertainty, in some cases modern approaches allow the direct analysis of single cells in a population context (*in situ*) (Avital et al., 2014) or even in a living organism (*in vivo*) (Vinegoni et al., 2015).

The analysis of single cells is strongly limited by the amount of input material (extremely low sample volume and analyte concentration) to analytical techniques (Chen et al., 2016). This has at least three consequences. First, highly sensitive analytical methods are required, of which the availability depends on the object of investigation. Nucleic acids, for instance, can be amplified specifically using special polymerase chain reaction (PCR) protocols and further subjected to standard bulk methods modified for a lower detection limit, such as realtime PCR (qPCR) and sequencing. Proteins, lipids and metabolites, in contrast, cannot be amplified and the adaption of standard bulk methods is more challenging. Basically, protein measurements at the single-cell level rely on the specific binding of antibodies and the detection of fluorescence signals on platforms like flow cytometry, microfluidic devices or arrays. But also the miniaturization of electrophoresis and chromatography or mass spectrometry setups provides tools for the analysis of proteins derived from single cells (Wang and Bodovitz, 2010; Wu and Singh, 2011). Since either method is restricted to definite outputs, there is obviously no analytical method that allows an overall analysis of single-cell parameters.

Second, the analysis of multiple parameters is challenging. The application of multiple methods relies on a previous fractionation and secure handling of the small sample volume derived from a single cell (Haselgrübler et al., 2014). In other cases, the parallel analysis of intra- and extracellular features is included in the SCA approach (Heldt and Kupke et al., 2015)

Third, the analysis of low analyte concentrations is exceedingly prone to errors. This is not just because the methods are operated at the lower detection limit (low signal-to-noise ratio) but also because minor effects such as nonspecific adsorption of the analyte to surfaces and the loss of extremely small volumes during liquid handling gain in significance. This is why SCA approaches preferentially forego initial enrichment or purification steps, such as cell lysis and the extraction of nucleic acids (Svec et al., 2013).

The ongoing technological progress is bearing a manifold range of either existing approaches adapted from population analytics or completely new approaches meeting the needs of SCA. Despite there are still challenges remaining, recent and future SCA developments are very promising (Haselgrübler et al., 2014; Macaulay and Voet, 2014; Tsioris et al., 2014; Weaver et al., 2014).

3.3.2 Applications

The application of SCA is suitable whenever variability among individual cells of a heterogeneous population is to be analyzed. It can thus conduce the understanding of processes like the regulation of gene expression, the cellular differentiation and the development of organisms (Combe et al., 2015). Especially genetical and pharmaceutical perturbations can have various effects when exposed to a heterogeneous or even homogeneous tissue or cell population (Pelkmans, 2012). As a result, the most relevant application fields are derived from medicine, such as cancer biology, stem cell biology and hematology (Di Carlo et al., 2012).

Cancer is a highly heterogeneous disease as tumors are composed of multiple clonal subpopulations of cancer cells with different properties (Heppner and Miller, 1983). With the help of SCA, these can be differentiated functionally or based on genomics which can promote the understanding of tumor initiation, progression and metastasis. Furthermore, SCA enables the recording of the therapeutic response of different cancer cells and thus is a useful tool for the analysis of drug targets (Wang and Bodovitz, 2010; Wills and Mead, 2015). Stem cells, such as embryonic, adult or induced pluripotent stem cells, are heterogeneous populations with the particular ability to self-renew and to differentiate. Their investigation is of high interest in regenerative medicine as specific populations can be targeted to elucidate signaling pathways and networks (Graf and Stadtfeld, 2008; Wang and Bodovitz, 2010). The differentiation of

hematopoietic stem cells is a particular interesting field that can be assessed by SCA. Especially the isolation of rare blood cells is of high interest to determine their specific roles (Di Carlo et al., 2012). Immunological applications of SCA also base on the variability of blood cells. It can, for instance, help to better understand the immune response (Galler et al., 2014). Finally, cell-to-cell heterogeneity and the manifestation of different biologically and clinically significant phenotypes revealed by SCA provides valuable information on regulatory mechanisms (Li and You, 2013).

The heterogeneous behavior of cells is also of interest in drug discovery. The complex response of single cells can be accessed by SCA, analyzing gene expression, metabolic states or the cellular phenotype. In this way, new drug targets can be revealed and mechanisms can be understood (Galler et al., 2014).

Apart from biological research issues, SCA can also serve for diagnostics, such as preimplantation genetic diagnosis. It tests a single cell from a biopsy of an embryo after *in vitro* fertilization for genetic diseases and chromosome aneuploidies. Analyzing single cells requires a minimal biopsy sample and may in the future become feasible for point-of-care use (Galler et al., 2014; Wang and Bodovitz, 2010).

Another field that benefits from SCA is bioprocess engineering. Heterogeneity in a microbial production strain, for instance, can affect the bioprocess robustness. Monitoring the microbial population heterogeneity in the context of (micro)environmental conditions can help to understand its role and thus be used to improve the bioreactor performance (Delvigne and Goffin, 2014; Fritsch and Dusny et al., 2012). Further, the identification of non-productive subpopulations can help to make the production process more efficient (Haselgrübler et al., 2014).

3.3.3 Application for virus replication studies

According to a market survey on single-cell technologies amongst German universities, research institutes and industry conducted in 2014, immunology and oncology are the most common applications whereas in the research field of virology application is (still) very rare (Gross, Schöndube and Zimmermann et al., 2015). Yet, the presence of a viral component makes cell-to-cell variability getting even more complex. Variability is then not only driven by the individual host cell but also by the specific infecting virus particle and the interactions between viral and cellular components (Warrick and Timm et al., 2016).

Yet, the application of SCA for virus infection studies has evolved in recent years. Some pioneer work was done by Delbrück (1945) who measured the virus yield from single infected bacteria

and was able to depict a broad burst size distribution of different bacterial viruses. Also the release of Western equine encephalomyelitis virus from single cells was found to vary largely an additional kinetic aspect (gradual release) was considered (Dulbecco and Vogt, 1954). Such early findings contributed to the awareness of large cell-to-cell variability in virus replication and helped to unravel viral growth characteristics (Ackermann and Maassab, 1954).

Recent studies analyze not only the distributions of virus yields but also encounter nucleic acid analyses at the single-cell level. Apart from variability within the host cell population, aspects like the heterogeneity of the viral genome itself (including DIPs) and the viral fitness are pointed out and appear relevant for the understanding of viral diversity, adaption and evolution (Akpınar et al., 2016; Combe et al., 2015; Heldt and Kupke et al., 2015; Schulte and Andino, 2014; Zhu et al., 2009). These studies agree in intrinsic or extrinsic biological noise playing a crucial role for cell-to-cell variability since SCA allows to control or exclude environmental influences.

The analysis of virus-host cell interaction is nowadays facilitated by modern SCA approaches (Warrick and Timm et al., 2016). SCA of virus infected cells is complemented by stochastic models helping to explain the origin of cell-to-cell variability in virus replication (Heldt and Kupke et al., 2015; Hensel et al., 2009).

As the biological meaning of cell-to-cell variability in virus replication is to be seen in the context of virus spread and evolution overcoming bottlenecks (Combe et al., 2015), research is directed to how a minority of infected cells may deviate from the average behavior and lead to the rising of drug-resistant viruses or latent infections (Timm and Yin, 2012).

Apart from answering such research questions, figuring out the origin of cell-to-cell variability in virus replication using SCA potentially may lead to strategies to overcome bottlenecks of biotechnological virus production processes aiming high virus yields.

4 Material and methods

The practical approaches used for the present thesis are pointed out providing first the material and second the methods.

4.1 Material

In the following, the technical equipment and plastic ware, chemicals and reagents, buffers and media, primers, cell lines and virus strains used for the present thesis are given.

4.1.1 Technical equipment and plastic ware

Aside from standard technical laboratory equipment and plastic ware, the specific items used for the present thesis are listed in Table 4-1 and Table 4-2.

Table 4-1: List of technical equipment used for the present thesis; specific software is provided.

Technical equipment	Producer	Type
cell culture and virus incubators	Heraeus	Hera cell, Hera cell 240
inverted microscope, camera, software	Zeiss	Axio Observer.A1, AxioCam MRm, AxioVs V 4.8.2.0 (2010)
cell counting device, software	Beckman Coulter	Vi-Cell™ XR cell viability analyzer, Vi-Cell™ XR cell viability analyzer 2.03 (2003)
pH meter	WTW	inoLab pH7110
waterbath	Fisher Scientific	Isotemp 202
microwave oven	Bosch	HMT812B
centrifuges	Thermo Scientific	Heraeus Multifuge 35R+, Heraeus Biofuge promo R
thermocycler	biometra	T Professional Thermocycler
pipetting robot, software	Qiagen	QIAgility, QIAgility 4.15.1 (2012)
heat sealer	Qiagen	Rotor-Disc® Heat Sealer
qPCR machine, software	Qiagen	Rotor-Gene Q, Rotor-Gene Q 2.0.2

Table 4-2: List of plastic ware used for the present thesis.

Plastic ware	Supplier	Catalog number
centrifuge tubes	greiner bio-one	
- 15 mL		188271
- 50 mL		227261
reaction tubes	greiner bio-one	
- 1.5 mL		616201
- 2 mL		623201

Table 4-2: List of plastic ware used for the present thesis. (continued)

Plastic ware	Supplier	Catalog number
cryovials, 2 mL	greiner bio-one	126279
freezing container	Sigma-Aldrich	C1562
filter cup cell culture flasks	greiner bio-one	
- 25 cm ²		690175
- 75 cm ²		658175
- 175 cm ²		660175
tissue culture dishes 35 mm	Sarstedt	83.3900
cell culture multiwell plates	greiner bio-one	
- 6-well		657160
- 24-well		662160
cell culture microplates	greiner bio-one	
- 96-well		655180
- 96-well, U-bottom		650160
- 384-well		781182
- 384-well, non-binding		781901
adhesive seal sheets	Thermo Scientific	AB1170
96-well PCR plate, 0.2 mL	Thermo Scientific	AB0900
8 cap strips	Thermo Scientific	AB0783
conductive filter-tips, 50 µL	Qiagen	990512
Rotor-Disc [®] 100	Qiagen	981311
Rotor-Disc [®] heat sealing film	Qiagen	981601

4.1.2 Chemicals and reagents

Aside from standard chemicals and reagents which were obtained from Roth or Merck, the specific commercial chemicals and reagents used for the present thesis are listed in Table 4-3.

The chemicals and reagents were stored as specified by the suppliers.

Table 4-3: List of commercial chemicals and reagents used for the present thesis.

Substance	Supplier	Catalog number
GMEM, powder	Gibco	22100093
lab-M-peptone	idg	MC 33
fetal bovine serum (FBS)	Gibco	10270106
trypsin, 1:250	Gibco	27250018
dimethyl sulfoxide (DMSO)	Sigma	D2650
gentamicin reagent solution, 10 mg/mL	Gibco	15710064
standard count agar	Merck	101621
trypan blue solution, 0.4 %	Sigma-Aldrich [®]	93595
crystal violet, powder	Sigma-Aldrich	C0775
Coulter Cleanz [®] cleaning agent	Beckman Coulter	8448222
isopropanol	Roth	6752
methanol	Roth	4627
acetone	Roth	9372

Table 4-3: List of commercial chemicals and reagents used for the present thesis. (continued)

Substance	Supplier	Catalog number
RNase-free water	Qiagen	1073291
bovine serum albumin (BSA), 20 mg/mL	Thermo Scientific	B14
RiboLock RNase inhibitor, 40 U/ μ L	Thermo Scientific	EO0381
dNTP mixture (10 mM each)	Thermo Scientific	R0193
Maxima H Minus reverse transcriptase (200 U/ μ L), 5x RT buffer	Thermo Scientific	EP0752
QuantiTect SYBR Green PCR master mix (2x)	Qiagen	204145
influenza anti A/Puerto Rico/8/34 (H1N1) serum	National Institute for Biological Standards and Control (NIBSC)	03/242
donkey anti-sheep IgG (H+L) cross-adsorbed secondary antibody Alexa Fluor 488	Invitrogen	A11015

Ultra-pure water was obtained from a Milli-Q water purification system (Advantage A10 and Q-POD[®], Millipore). Further, the following non-commercial reagents were used which were available in the lab of the Bioprocess Engineering group at Max Planck Institute for Dynamics of Complex Technical Systems. Total MDCK RNA (350 ng/ μ L) was obtained by isolating RNA from untreated Madin-Darby canine kidney (MDCK) cells. Standards (5 ng/ μ L) of segment 5 and segment 8 vRNA for real-time reverse transcription quantitative PCR (RT-qPCR) were derived from plasmids. Red blood cells (RBC) (approximately $2 \cdot 10^7$ RBC/mL) were isolated from chicken blood obtained from Wiesenhof Möckern.

4.1.3 Buffers and media

Buffers and media that were not obtained readily were prepared and stored as described below.

Phosphate buffered saline (PBS) for washing purposes

8 g NaCl, 0.2 g KCl, 0.2 g KH_2PO_4 and 1.15 g Na_2HPO_4 per liter were dissolved in ultra-pure water. The pH was checked to be in a range of 7.4-7.6. PBS for sterile use was autoclaved. The buffer was stored at room temperature.

Trypsin/EDTA solution for passaging

1.25 g trypsin (1:250; activity in a range of 600-800 BAEE U/mL) and 0.5 g EDTA were dissolved in 250 mL PBS to obtain a 10-fold stock solution. Sterilization was carried out by vacuum sterile filtration. Working solutions (1-fold) were made by diluting the 10-fold stock solution with sterile PBS. The enzyme solutions were stored at 4 °C.

Trypsin solution as a supplement for virus amplification

Trypsin (1:250; activity in a range of 600-800 BAEE U/mL) was diluted to an activity of 500 BAEE U/mL with PBS. Sterilization was carried out by vacuum sterile filtration. The enzyme solution was stored at -20 °C.

Basic Glasgow's Minimum Essential Medium (GMEM)

62.5 g GMEM powder, 20.0 g NaHCO₃ and 5.00 g glucose were dissolved in 4.5 L ultra-pure water at 37 °C. The pH was adjusted to 6.7 using NaOH or HCl. Sterilization was carried out by pressure sterile filtration. The medium was stored at 4 °C.

GMEM complete medium for cell culture (hereafter referred to as Z-medium)

Basic GMEM was supplemented with 100 mL fetal bovine serum (FBS) and 10 mL of sterile a 200 g/L Lab-M-peptone solution per liter. The medium was stored at 4 °C.

GMEM for virus amplification (hereafter referred to as V-medium)

Basic GMEM was supplemented with 10 mL of a sterile 200 g/L Lab-M-peptone solution per liter. The medium was stored at 4 °C.

Freezing medium

Z-medium was supplemented with 10 % (v/v) DMSO. The freezing medium was freshly prepared prior to cryopreservation.

Infection medium

V-medium was supplemented with 1 % (v/v) trypsin solution as a supplement for virus amplification. The infection medium was freshly prepared prior to use.

Lysis buffer for lysis of single cells

50 µL of a 20 U/mL BSA solution and 25 µL of a 40 mg/mL solution of RiboLock were added to 925 µL RNase-free water. The lysis buffer was freshly prepared or stored at 4 °C.

Agar stock solution for overlay mixture

3 % (w/v) agar was dissolved in PBS and the mixture was autoclaved. The solid gel was stored at room temperature. Before use, the gel was liquefied by heating and boiling in a microwave oven and kept at a temperature of 45 °C in a waterbath.

Overlay mixture

Preheated agar stock solution (45 °C) was diluted with preheated V-medium (45 °C) to a final 1 % (w/v) agar concentration and kept at this temperature in a waterbath to avoid solidification. Immediately prior to use, the overlay mixture was supplemented with 1 % (v/v) trypsin solution.

Crystal violet solution

200 mg crystal violet powder was dissolved in 50 mL ethanol. 1 mL methanol and 49 mL ultra-pure water were added. The staining solution was stored in the dark at room temperature.

4.1.4 Primers

The primers for reverse transcription (RT) of vRNA (Table 4-4) and for realtime PCR (qPCR) of the RT products (Table 4-5) were adapted from Heldt and Kupke et al. (2015) and obtained from Invitrogen. The primers for RT were diluted to 1 µM working solutions in RNase-free water. The primers for qPCR were diluted to 10 µM working solutions in RNase-free water.

Table 4-4: List of primers used for reverse transcription (RT); underlined letters indicate tag sequence; 100 µM stock solutions were prepared in RNase-free water.

Name	Target	Sequence (5' - 3')
Seg 5 tagRT for	Segment 5	<u>ATTTAGGTGACACTATAGAAGCGAGTGATTATGAGGGACGGTTGAT</u>
Seg 8 tagRT for	Segment 8	<u>ATTTAGGTGACACTATAGAAGCGGATAGTGGAGCGGATTCTG</u>

Table 4-5: List of primers used for realtime PCR (qPCR); underlined letters indicate tag sequence; 100 µM stock solutions were prepared in RNase-free water.

Name	Target	Sequence (5' - 3')
vRNA tagRealtime for	introduced tag sequence	<u>ATTTAGGTGACACTATAGAAGCG</u>
Seg 5 Realtime rev	Segment 5	<u>CGCACTGGGATGTTCTTC</u>
Seg 8 Realtime rev	Segment 8	<u>CACTTCTGCTTGGGTATGA</u>

4.1.5 Cell line and virus strain

The MDCK cell line was obtained from European Collection of Authenticated Cell Cultures (ECACC; catalog number 84121903, lot number 05G029) and a master cell bank was set up. A working cell bank at passage 4 upon receipt is kept in liquid nitrogen (-196 °C).

The human influenza virus A/Puerto Rico/8/34 (H1N1) was obtained from Robert Koch Institute (RKI; catalog number 3138) and a seed virus stock is kept at -80 °C. The virus stock had an infectious virus titer of $1.1 \cdot 10^9$ virus particles/mL according to 50 % tissue culture infection dose (TCID₅₀) assay.

4.2 Methods

In the following, the methods used for the present thesis are described. The complete names, specifications and suppliers of the materials are provided in paragraph 4.1 and thus not again mentioned below.

4.2.1 MDCK cell culture

Adherent MDCK cells were routinely cultivated as a static culture in Z-medium (GMEM complete medium for cell culture) and incubated at 37 °C in a 5 % CO₂ atmosphere.

4.2.1.1 Maintenance and expansion

For maintenance or expansion, the cells were passaged weekly in 75 cm² or 175 cm² culture flasks up to a limit of 20 passages.

Before passaging, the medium was checked for a clear red color and the cells were inspected microscopically to detect an unwanted pH shift or a contamination. The passaging was performed according to the volumes given in Table 4-6. Therefore, the exhausted medium was poured off and the cells were washed three times with phosphate buffered saline (PBS). Then trypsin/EDTA solution was added and the flask was incubated at 37 °C for 20-30 min and carefully jolted every 6-7 min to detach the cells. After complete detachment, Z-medium was added to stop the enzymatic reaction and the cells were suspended by pipetting the liquid up and down several times. An aliquot of the suspension was used for checking the cell count. The remaining suspension served as a seed for the inoculation of cell culture flasks filled with fresh medium for cultivation. The cells were then homogeneously distributed by wave movements and the flasks were put into the incubator.

Table 4-6: Volumes of buffers and media for passaging of MDCK cells for maintenance or expansion in different cell culture vessels.

Cell culture vessel	Trypsinization			Inoculation	
	PBS	Trypsin/EDTA	Z-medium	Cell suspension	Z-medium
75 cm ² flask	5-10 mL	3 mL	3 mL	1 mL	50 mL
75 cm ² flask	10-15 mL	6 mL	6 mL	2 mL	100 mL

4.2.1.2 Measurement of cell count, viability and cell diameter

The total and viable cell count as well as the viability and the cell diameter were determined using the Vi-Cell XR cell viability analyzer (Beckman Coulter) which performs a trypan blue staining and deploys an image recognition software to detect and count living (unstained) and dead (blue stained) cells. Therefore, 0.5-1 mL of sample cell suspension in the range of

$1 \cdot 10^4$ - $1 \cdot 10^7$ cells/mL was applied to the system. The single cells from 100 images were analyzed by the automated system set to the characteristics of MDCK cells. The total and viable cell count as well as the average viability and diameters were displayed. The diameters were additionally displayed as distribution data for total and viable cells.

4.2.1.3 Calculation of the cell volume

The cell volume of a sample cell suspension was approximated using the binned distribution data on the cell diameters for viable cells obtained from the Vi-Cell XR cell viability analyzer. The cell volume of the cells in each bin was calculated based on the respective average cell diameter assuming a spherical cell shape. The total cell volume V_{total} is the cumulative cell volume in each bin V_i and the total cell count c_{total} is the cumulative cell count in each bin c_i . The average cell-specific cell volume V_s is calculated by the total cell volume divided by the total cell count (Equation 1). The cell volume in the well of a 6-well plate V_{well} was calculated by multiplying the average cell-specific cell volume and the cell number in the particular well c_{well} (Equation 2).

$$V_s = \frac{V_{\text{total}}}{c_{\text{total}}} = \frac{\sum V_i}{\sum c_i} = \frac{\sum c_i \cdot \frac{1}{6} \cdot \pi \cdot d_i^3}{\sum c_i \cdot 10^9} \quad (1)$$

$$V_{\text{well}} = V_s \cdot c_{\text{well}} \quad (2)$$

c_i	cell count in the i^{th} bin	[-]
c_{total}	total cell count	[-]
c_{well}	cell number per well	[cells/well]
d_i	cell diameter in the i^{th} bin	[μm]
i	bin index	[-]
V_i	cell volume in the i^{th} bin	[μL]
V_s	average cell-specific cell volume	[$\mu\text{L}/\text{cell}$]
V_{total}	total cell volume	[μL]
V_{well}	cell volume per well	[$\mu\text{L}/\text{well}$]

4.2.1.4 Harvesting of conditioned medium

The medium of MDCK cells grown for three or four days in a 75 cm^2 cell culture flask was collected and passed through a $0.2 \mu\text{m}$ syringe filter to remove cells, cell debris and extracellular matrix. Aliquots were stored at $-20 \text{ }^\circ\text{C}$.

4.2.1.5 Cloning and expansion of subclones

The cloning of MDCK cells was carried out by limiting dilution followed by microscopic identification of single cells. The clones were expanded by stepwise passaging in culture vessels of increasing growth area up to a T75 flask.

The cloning procedure described below is the outcome of cloning experiments whereby selected parameters were varied (see paragraph 5.1.1).

For the limiting dilution technique, an MDCK preculture was grown by inoculating a T75 flask with $3.5 \cdot 10^6$ cells and incubated for three days to obtain cells in exponential growth phase. A $0.5 \cdot 10^6$ cells/mL dilution of these cells was then used to seed $1 \cdot 10^6$ cells in 35-mm dishes. Keeping the cells exponentially growing, those were incubated for another 24 h in a humidified atmosphere preventing evaporation of the medium. Two dishes were used to measure the cell count. Therefor, the supernatant was first discarded and the cells were washed with 1 mL PBS. Then 0.5 mL trypsin/EDTA solution was added and the dishes were incubated at 37 °C for up to 15 min and carefully jolted in appropriate intervals to detach the cells. After complete detachment, 0.5 mL Z-medium was added to stop the enzymatic reaction and the cells were suspended by pipetting the liquid up and down several times. The complete cell suspension was applied to the cell count device (paragraph 4.2.1.2) and the obtained cell counts were averaged. The cells in a third dish served for the actual cloning procedure. For that purpose, they were first trypsinized as described above and then serially diluted in 2 mL microcentrifuge tubes (to $3 \cdot 10^5$ cells/mL, $3 \cdot 10^4$ cells/mL and $3 \cdot 10^3$ cells/mL), in a 15 mL centrifuge tube (to $3 \cdot 10^2$ cells/mL) and in a 50 mL centrifuge tube up to a final concentration of $3 \cdot 10^2$ cells/mL which corresponds to an average of 1.5 cells per 50 μ L. The Z-medium used for dilution (conditioned medium was optionally used to improve communication in low cell density scenarios) as well as a non-binding 384-well plate were prewarmed to 37 °C before. The cell suspension was then quickly dispensed to 50 μ L per well onto the 384-well plate with the help of a multichannel multistep pipet in order to isolate single cells. The plate was then optionally incubated in a humidified atmosphere preventing evaporation of the medium until the phase contrast microscopic examination.

Directly or up to 24 h post seeding, the wells of the plate were screened for the presence of single cells by phase contrast microscopy. To promote the cells to settle down, the plate was briefly centrifuged at 150 g for 30 s before. Positive wells were recorded and monitored during the following days to exclude faulty detected ones.

The proliferation and colony formation originating from single cells was documented by taking photos and noting observations like the cell morphology, the confluency and the color of the medium. The medium was exchanged at least once a week to prevent exhaustion. To improve communication in low cell density scenarios conditioned medium was optionally used. When the cells reached a medium to high confluency of 30-70 % and the medium started to shift the color to orange, they were passaged to a larger culture vessel and again grown under the same conditions. This procedure was repeated using a 96-well plate, a 24-well plate (optionally), a 6-well plate and finally a T75 flask as culture vessels. The passaging was performed according to the volumes given in Table 4-7.

Table 4-7: Volumes for passaging of clonal MDCK cells for expansion in different cell culture vessels; arrows indicate the transfer of the cells to the next cell culture vessel; 24-well plate optionally skipped.

Cell culture vessel	Trypsinization			Inoculation	
	PBS	Trypsin/EDTA	Z-medium	Cell suspension	Z-medium
384-well plate	50 μ L	10 μ L	40 μ L		
96-well plate	200 μ L	30 μ L	170 μ L	50 μ L	150 μ L
24-well plate	1 mL	150 μ L	850 μ L	200 μ L	800 μ L
6-well plate	1 mL	500 μ L	500 μ L	200 μ L or 1 mL	1.8 mL or 2 mL
75 cm ² flask	10-15 mL	6 mL	6 mL	1 mL	50 mL

Therefore, the supernatant was first discarded and the cells were washed with PBS. Then trypsin/EDTA solution was added and the plate was incubated at 37 °C for 15-30 min and carefully jolted every 6-7 min to detach the cells. After complete detachment, Z-medium was added to stop the enzymatic reaction and the cells were suspended by pipetting the liquid up and down several times. Without checking the cell count the complete suspension served as a seed for inoculation of plates or flasks prefilled with fresh Z-medium. The cells were then homogeneously distributed by wave movements and put into the incubator.

In case of a limited proliferation due to the formation of tight discrete colonies, the cells were trypsinized as described above and then reseeded into an equivalent cell culture vessel.

When cells reached confluency in the 75 cm² cell culture flask, they were grown at least one more day until cryopreservation (paragraph 4.2.1.6). In case the cell number was not sufficient, the cells were reseeded in a 75 cm² cell culture flask to further expand them and cryopreserved subsequently.

4.2.1.6 Cryopreservation and thawing

The clonal MDCK cell populations were cryopreserved in liquid nitrogen (-196 °C) for long-term storage. Dimethyl sulfoxide (DMSO) served as a cryoprotectant.

Cryopreservation

Confluent cells were trypsinized (paragraph 4.2.1.6) and the cells were diluted by adding Z-medium to a total volume of 50 mL in a 50 mL centrifugation tube. After taking 1 mL of the cell suspension to measure the cell number (paragraph 4.2.1.2), it was centrifuged at 500 g for 5 min. The supernatant was discarded. The cell number in the remaining cell pellet was calculated and a final cell concentration of approximately $1.3\text{-}1.9 \cdot 10^6$ cells/mL was set by adding the respective amount of freezing medium (Z-medium supplemented with 10 % DMSO). The cells were resuspended gently and aliquots of 1.6 mL containing $2\text{-}3 \cdot 10^6$ cells were dispensed into at least three cryovials. The cryovials were placed into a freezing container filled with isopropanol and precooled to 4 °C. The freezing container was set into a -80 °C freezer allowing a slow cooling down at a rate of approximately 1 °C/min. After one to three days, the cryovials were shifted into a liquid nitrogen tank.

Thawing

Thawing of parental or clonal MDCK cells was performed quickly due to the toxicity of the cryoprotectant DMSO. The cryovial was taken from the liquid nitrogen tank and put into a 37 °C waterbath. As soon as the content was thawed, it was transferred into a 15 mL centrifugation tube filled with 10 mL of prewarmed (37 °C) Z-medium. After centrifugation (300 g, 7 min), the supernatant was discarded and the cells were gently resuspended in 5 mL of prewarmed Z-medium. The cell suspension was then transferred into a 75 cm² cell culture flask (parental MDCK cells for general purposes) or a 25 cm² cell culture flask (clonal MDCK cells for experiments) filled with 50 mL or 10 mL of prewarmed Z-medium. The cells were then homogeneously distributed by wave movements and the flask was put into the incubator.

4.2.1.7 Maintenance of clonal MDCK cell populations

After synchronous thawing in 25 cm² cell culture flasks and growing to confluency for 6 d, the clonal MDCK cell populations were passaged weekly in 6-well plates. Before passaging, the medium was checked for a clear red color and the cells were inspected microscopically to detect an unwanted pH shift or a contamination.

For passaging the cells from the 25 cm² cell culture flasks to the 6-well plate, the cells were washed two times with 5 mL PBS. Then, 1.5 mL trypsin/EDTA solution was added and the flask was incubated at 37 °C for 15-60 min and carefully jolted every 7-10 min to detach the cells. After complete detachment, 1.5 mL Z-medium was added to stop the enzymatic reaction and the cells were suspended by pipetting the liquid up and down several times. An aliquot of the

suspension was used for checking the cell count. The remaining suspension served as a seed for the inoculation of 6-well plates. In each well, a volume equaling $0.5 \cdot 10^6$ cells was dispensed and a general volume of 3.75 mL Z-medium was added. The cells were then homogeneously distributed by wave movements and the plates were put into the incubator.

For passaging the cells from one 6-well plate to another, the cells were washed once with 1 mL PBS. Then, 1 mL trypsin/EDTA solution was added and the flask was incubated at 37 °C for 60 min and carefully jolted every 15 min to detach the cells. After complete detachment, 2 mL Z-medium was added to stop the enzymatic reaction and the cells were suspended by pipetting the liquid up and down several times. An aliquot of the suspension was used for checking the cell count. The remaining suspension served as a seed for the inoculation of 6-well plates. In each well, a volume equaling $0.5 \cdot 10^6$ cells was dispensed and a general volume of 3.75 mL Z-medium was added. The cells were then homogeneously distributed by wave movements and the plates were put into the incubator.

4.2.2 Influenza A virus (IAV) infection of MDCK cells

Infection experiments comprised the seeding of the cells, the infection with influenza A virus (IAV) and the sampling. Adherent MDCK cells were infected as a static culture in infection medium (V-medium supplemented with 1 % trypsin) and incubated at 37 °C in a humidified, 5 % CO₂ atmosphere.

4.2.2.1 Population level

Infection experiments at the population level were performed on 6-well plates. All clonal MDCK cell populations were analyzed simultaneously, along with the parental MDCK cell population in triplicate. Two different infection protocols were applied, using preset or altered infection conditions.

Infection conditions

The infection conditions were for reference adapted from Heldt and Kupke et al. (2015). Initially, exponentially growing cells were harvested from 6-well plates. For each population, two wells were seeded with $1 \cdot 10^6$ cells and a general volume of 1.75 mL of Z-medium was added. Forming a monolayer at 24 h post seeding, the cells in one of the two wells were trypsinized and counted. The cells in the other well were washed once with 1 mL of PBS and subsequently infected with IAV. A multiplicity of infection (MOI) of 10 was aimed for each individual population, meaning an average of 10 virus particles (based on TCID₅₀ titer) were

present per cell (based on the current cell count). Therefore, 250 μL of an infection mixture ($V_{\text{infection mixture}}$) of freshly thawed virus stock ($V_{\text{virus stock}}$) and infection medium ($V_{\text{infection medium}}$) according to Equations 3 and 4 were dispensed evenly onto the monolayer.

$$V_{\text{virus stock}} = \frac{\text{MOI}}{t_{\text{TCID}_{50}, \text{virus stock}}} \cdot c_{\text{well}} = \frac{10 \frac{\text{virus particles}}{\text{cell}}}{1.1 \cdot 10^9 \frac{\text{virus particles}}{\text{mL}}} \cdot c_{\text{well}} \cdot 10^3 \quad (3)$$

$$V_{\text{infection medium}} = V_{\text{infection mixture}} - V_{\text{virus stock}} = 250 \frac{\mu\text{L}}{\text{well}} - V_{\text{virus stock}} \quad (4)$$

c_{well}	cell number per well	[cells/well]
MOI	multiplicity of infection	[virus particles/cell]
$t_{\text{TCID}_{50}, \text{virus stock}}$	virus titer of the virus stock based on TCID ₅₀ assay	[virus particles/mL]
$V_{\text{infection medium}}$	volume of infection medium per well	[μL /well]
$V_{\text{infection mixture}}$	volume of infection mixture per well	[μL /well]
$V_{\text{virus stock}}$	volume of virus stock per well	[μL /well]

The 6-well plates were put into the incubator. Every 20 min, the infection mixture was homogeneously distributed in the wells by wave movements. After 1 h, the infection mixture was removed and the infected cells were washed once with 1 mL of PBS. Each well was filled with 2 mL of infection medium and the 6-well plates were placed back into the incubator.

At 12 h post infection (hpi), the wells were sampled. Therefore, the supernatant of each individual population was collected for the determination of the virus titer by three virus quantification assays: hemagglutination (HA) assay, TCID₅₀ assay and plaque assay (see paragraph 4.2.3). The plaque assay was performed immediately using the fresh supernatant whilst the remaining supernatant was aliquoted and kept at -80 °C for HA and TCID₅₀ assay. The cells were washed with 1 mL of PBS and then trypsinized and counted. The cell count at 12 hpi was used as a basis for the calculation of cell-specific virus titers.

Alternative infection conditions

The previously described infection conditions were altered in respect of the following aspects. For each population, stationary growing cells were harvested and seeded with $0.5 \cdot 10^6$ cells and a general volume of 3.75 mL of Z-medium was added. The cells were infected with MOI 10 four days post seeding when they were supposed to be in the stationary growth phase. The sampling

time point was chosen in accordance with the occurrence of the cytopathic effect which was confirmed by phase contrast microscopy (cell detachment and morphological changes). A common sampling time point of 48 hpi was chosen for all populations. The sampling included only the harvest of the supernatant from each well. The supernatant was centrifuged at 400 g and 4 °C for 10 min to remove the cells and stored at -80 °C, solely for HA assay. The cell count at infection time point was used as a basis for the calculation of the cell-specific virus titer.

4.2.2.2 Single-cell level

Infection experiments at the single-cell level were performed in 35 mm (8 cm²) tissue culture dishes. The parental and two clonal MDCK cell populations (clone 8 and clone 26) were analyzed in three independent experiments, respectively. The infection conditions were adapted from Heldt and Kupke et al. (2015)

Initially, exponentially growing cells were harvested from a 75 cm² cell culture flask. Three dishes were seeded with 1·10⁶ cells (0.5·10⁶ cells in case of clone 26) at a total volume of 2 mL. Forming a monolayer at 24 h post seeding, the cells in two of the dishes were trypsinized for maximum 15 min, carefully jolting in appropriate intervals. The cells were counted and the average cell number per dish was calculated. The cells in the third dish were washed once with 1 mL of PBS and subsequently infected with IAV. A multiplicity of infection (MOI) of 10 was aimed. Therefor, 250 µL of an infection mixture of freshly thawed virus stock and infection medium according to Equations 3 and 4 were dispensed evenly onto the monolayer in the dish.

The dish was put into the incubator. Every 20 min, the infection mixture was homogenously distributed in the dish by wave movements. After 1 h, 1.75 mL of infection medium was added to the infection mixture to obtain a total volume of 2 mL. The dish was placed back into the incubator for another 1.5 h.

After that (at 2.5 hpi), the single cell isolation was carried out using the limiting dilution technique (the same technique used for the cloning described in paragraph 4.2.1.5). Therefor, the infection mixture was removed and the infected cells were washed once with 1 mL of PBS. The infected cells were trypsinized for maximum 15 min, carefully jolting in appropriate intervals. Taking into account the average cell number per dish obtained prior to infection, the cells were serially diluted in 2 mL microcentrifuge tubes (to 3·10⁵ cells/mL, 3·10⁴ cells/mL and 3·10³ cells/mL), in a 15 mL centrifuge tube (to 3·10² cells/mL) and in a 50 mL centrifuge tube up to a final concentration of 3·10² cells/mL which corresponds to an average of 1.5 cells per 50 µL. The infection medium used for dilution as well as a non-binding 384-well plate were prewarmed to 37 °C before. The cell suspension was then quickly dispensed to 50 µL per well onto the

384-well plate with the help of a multichannel multistep pipet in order to isolate single infected cells. The plate was then put into the incubator.

At 12 hpi, the wells of the plate were screened for the presence of single cells by phase contrast microscopy. To promote the cells to settle down, the plate was briefly centrifuged at 150 g for 30 s before. Approximately 40 wells containing exactly one cell were recorded and subsequently sampled. The sampling included the determination of the virus titer by plaque assay and the preparation of the cell lysate for the determination of the vRNA content. For the plaque assay, the complete supernatant (50 μ L) was used (see paragraph 4.2.3.4). The cell was subsequently washed with approximately 80 μ L of PBS and 5 μ L of lysis buffer for the lysis of the single cell was added. The plate was then stored at -80 °C which allowed the cell lysis by the freezing and thawing process. The cell lysate was then further used for the determination of the vRNA content of specific IAV genome segments (see paragraph 4.2.4).

4.2.3 Virus quantification assays

The IAV titer was quantified using different assays. For each assay, the detection principle is described shortly.

Virus samples derived from population based experiments were analyzed by HA assay, TCID50 assay and plaque assay (paragraphs 4.2.3.1 to 0) whereas virus samples derived from single-cell experiments were analyzed by a dedicated plaque assay protocol (paragraph 4.2.3.4).

4.2.3.1 Hemagglutination (HA) assay

The HA assay was used to detect the number of total (infectious and non-infectious) virus particles per mL in the supernatant of IAV infected cells. The assay is based on the ability of IAV to bind to receptors on the surface of red blood cells (RBC) of certain animal species which is called hemagglutination. In the presence of virus particles, the red blood cells cross-link preventing the cells to sediment. In the absence of virus particles, the red blood cells sediment forming a clearly visible dot. The virus containing sample is serially diluted and subjected to RBC. A critical dilution with no detection of virus particles is taken as an endpoint. The negative decadic logarithm of that concentration is defined as the logarithmic HA titer per 100 μ L (\log_{10} HAU/100 μ L) and determines the concentration of virus particles in the sample.

The HA assay was carried out according to SOP V/05, version 2.2 (20.01.2011) *Hemagglutination assay (HA assay)* which is currently used in the Bioprocess Engineering group at Max Planck Institute for Dynamics of Complex Technical Systems. The SOP is provided in

the Appendix (A 1.1) and is based on the method described by Kalbfuss et al. (2008). The analysis was done photometrically and the results were checked by visual evaluation.

The concentration of virus particles per mL (t_{HA}) was obtained based on the logarithmic HA titer using Equation 5. Therefore, the concentration ($n_{RBC, well}$) and the volume ($V_{RBC, well}$) of the red blood cell suspension were accounted assuming a ratio of one virus particle per RBC in the critical dilution (Burlison et al., 1992).

$$t_{HA} = \frac{n_{RBC, well}}{V_{RBC, well}} \cdot 10^{-\log_{10} HAU/100 \mu L} \quad (5)$$

$-\log_{10} HAU/100 \mu L$	logarithmic HA titer per 100 μL	[-]
$n_{RBC, well}$	number of RBC per well	[RBC/well]
t_{HA}	virus titer based on HA assay	[virus particles/mL]
$V_{RBC, well}$	volume of RBC suspension per well	[mL/well]

4.2.3.2 50 % Tissue culture infection dose (TCID₅₀) assay

The TCID₅₀ assay was used to detect the number of infectious virus particles per mL in the supernatant of IAV infected cells. The assay is based on the ability of the virus particles to infect cells of a monolayer and cause the cytopathic effect. The virus containing sample is serially diluted and subjected to the cells. After incubation and fixation, viral antigens produced by the cells are captured by a specific primary antibody and detected by a fluorescent secondary antibody. A critical dilution with the last detection of virus particles is taken as a 50 % endpoint. The TCID₅₀ is thus defined as that dilution of a virus sample required to infect 50 % of a given batch of cells. It is calculated according to the Spearman Kärber method (Genzel and Reichl, 2007; Hierholzer and Killington, 1996).

The TCID₅₀ assay was carried out according to SOP V/08, version 2.1 (02.06.2008, 09.01.2013) *TCID₅₀ Assay* which is currently used in the Bioprocess Engineering group at Max Planck Institute for Dynamics of Complex Technical Systems. The SOP is provided in the Appendix (A 1.2).

4.2.3.3 Plaque assay

The plaque assay was used to detect the number of propagable infectious virus particles per mL in the supernatant of IAV infected cells. The assay is based on the local spread of the virus infection from initially infected cells of a monolayer to neighboring cells when immobilized. The virus containing sample is serially diluted and subjected to the cells. The local cytopathic effect can be observed as countable plaques after fixation and staining of the otherwise healthy monolayer. One plaque is assumed to be caused by one propagable infectious virus particle, that is a plaque forming unit (PFU) in the sample (Hierholzer and Killington, 1996).

The plaque assay was carried out according to Heldt and Kupke et al. (2015) as follows. In advance, MDCK cells were seeded on 6-well plates at a density of $1 \cdot 10^6$ cells per well. The plates were incubated at 37 °C and 5 % CO₂ for approximately 40 h to form a uniform monolayer.

Virus samples from population based experiments were serially diluted in infection medium up to a 10^{-10} dilution. The supernatant of the MDCK cells on the 6-well plates was removed and the monolayers were washed twice with PBS. 250 µL of six dilutions of the virus samples (10^{-5} to 10^{-10}) were dispensed evenly onto the monolayer in either of the six wells of the plates. The 6-well plates were put back into the incubator. Every 20 min, the infection mixture was homogenously distributed in the wells by wave movements. After 1 h, the infection mixture was removed and 2 mL of a freshly prepared agar containing overlay mixture (45 °C) were dispensed in each well. After solidification of the agar overlay, the 6-well plates were incubated for 4 d.

The remaining MDCK cell monolayers were fixated by adding 2 mL of chilled (4 °C) methanol on top of the agar overlay and incubation for 15 min. The supernatant and the agar overlay were then removed carefully using a spatula without damaging the monolayer. For staining, the bottom of each well was covered with crystal violet solution and incubated for 10 min. The residual staining solution was removed and after drying, the plates were stored at room temperature until analysis.

For analysis, where possible, the plaques in each well were counted with the naked eye or using a microscope. For each well with a given dilution factor D (for instance 10^{-7}), the number of PFU per mL of a virus sample derived from a population based experiment (t_{PFU}) was calculated according to Equation 6. In case more than one dilution resulted in a countable number of plaques, first the number of PFU was calculated for each dilution and second the arithmetic mean was calculated.

$$t_{\text{PFU}} = \frac{n}{D \cdot V_{\text{sample}}} = \frac{n}{D \cdot 0.25 \text{ mL}} \quad (6)$$

D	dilution factor	[-]
n	number of plaques	[plaques]
t_{PFU}	virus titer based on plaque assay	[PFU/mL]
V_{sample}	volume of sample	[mL]

4.2.3.4 Plaque assay for single cells

In contrast to the plaque assay protocol described above (paragraph 4.2.3.3) which suits for the analysis of virus samples derived from population based experiments, a dedicated protocol was used for the analysis of virus samples derived from single-cell experiments. The plaque assay for single cells was carried out according to Heldt and Kupke et al. (2015). This allows the detection of the number of propagable infectious virus particles produced by a single cell coping with a very small sample volume.

Monolayers of MDCK cells were seeded in 6-well plates as described previously (paragraph 4.2.3.3). After removing the supernatant and washing the cells, the wells were prefilled with 250 μL of infection medium. The complete sample volume of 50 μL for each cell derived from the single-cell experiment was applied to one well of a 6-well plate and the total content of 300 μL was mixed well. From that mixture, a 30 μL aliquot was taken and applied to a second well. The infection mixtures were distributed homogeneously by wave movements. Thus two dilutions were present, representing a 9/10 fraction and a 1/10 fraction of the virus sample. The 6-well plates were put back into the incubator. Every 20 min, the infection mixture was homogeneously distributed in the wells by wave movements. After 1.5 h, the infection mixture was removed and 2 mL of a freshly prepared agar containing overlay mixture (45 °C) were dispensed in each well. After solidification of the agar overlay, the 6-well plates were incubated for 4 d. The fixation and staining was carried out as described previously (paragraph 4.2.3.3).

For analysis, where possible, the plaques in each well were counted with the naked eye or using a microscope. For each well with a given dilution factor (1/10 or 9/10), the number of PFU per cell in a virus sample derived from a single-cell experiment (PFU_{cell}) was calculated according to Equation 7. In case more than one dilution resulted in a countable number of plaques, first the number of PFU was calculated for each dilution and second the arithmetic mean was calculated.

$$PFU_{\text{cell}} = \frac{n}{D} \quad (7)$$

D	dilution factor	[-]
n	number of plaques	[plaques]
PFU _{cell}	number of PFU per single cell	[PFU/cell]

4.2.4 Absolute intracellular vRNA quantification in single cells by RT-qPCR

Intracellular vRNA of segment 5 and segment 8 in single cells was quantified by real-time reverse transcription quantitative PCR (RT-qPCR) directly without an intermediate purification step. The reverse transcription (RT) reaction specifically amplifies vRNA of a distinct segment synthesizing complementary DNA (cDNA) copies using a gene-specific tagged primer. These provide templates for the specific amplification of double stranded DNA fragments by realtime quantitative PCR (qPCR) with intercalating SYBR green fluorescent dye enabling a signal recording. Employing a vRNA standard of each segment at various concentrations allows the transformation of the signal recordings into a the number of vRNA molecules per cell in the original sample based on a calibration curve (Kawakami et al., 2011).

The method used here is dedicated for single-cell analysis with very low vRNA concentrations and was adapted from Heldt and Kupke et al. (2015). Within one run, 40 lysed single cells could be analyzed. The samples and reagents were handled on ice under a PCR hood.

Reverse transcription (RT)

The RT was carried out on 96-well PCR plates in a PCR cycler with a separate reaction cavity for each cell and each standard dilution to be analyzed.

An RT mastermix was prepared as given in Table 4-8 using one of the segment-specific primers given in Table 4-4. Each cavity of the PCR plate was filled with 3.5 μL of the RT mastermix.

Table 4-8: Composition of the RT mastermix; one of the primers given in Table 4-4 was used; the mastermix was prepared in an excess of 10 %.

Reagent	Volume (μL) per reaction
primer (1 μM) (Seg 5 tagRT for or Seg 8 tagRT for)	0.5
dNTP mixture (10 mM each)	0.5
RNase-free water	2.5
total	3.5

Table 4-9: Composition of the RT hot start mastermix; Maxima H Minus Reverse Transcriptase (40 U/ μL) was used as the enzyme with the respective buffer; the mastermix was prepared in an excess of 25 %.

Reagent	Volume (μL) per reaction
RT buffer (5x)	2
reverse transcriptase	0.25
RNase-free water	1.25
total	3.5

1 μL of the cell lysate from each previously sampled well of a 384-well plate (see paragraph 4.2.2.2) was pipetted into distinct cavities of the PCR plate. To obtain a total volume of 6.5 μL , 2 μL of RNase-free water was added into either of these cavities. The segment-specific vRNA standard (5 ng/ μL) was serially diluted in lysis buffer and eight dilutions (10^{-1} to 10^{-9}) equaling concentrations of $0.5 \cdot 5 \cdot 10^{-9}$ ng/ μL were prepared. 2 μL of these dilutions were pipetted in distinct cavities of the PCR plate. To resemble intracellular conditions, 1 μL of a 10^{-6} dilution ($3.5 \cdot 10^{-4}$ ng) of total MDCK RNA was added in either cavity, again obtaining a total volume of 6.5 μL . The yet incomplete RT reaction mixture was homogenized, centrifuged and set into the PCR cycler and the RT temperature program given in Table 4-10 was started, accounting for a hot start reaction.

Table 4-10: RT temperature program; a hot start was realized; the lid temperature was 99 °C.

Reaction step	Temperature (°C)	Time (min:s)
1 preheating / denaturation	65	05:00
2 initiation <i>addition of RT hot start mastermix</i>	55	05:00
3 cDNA synthesis	60	30:00
4 denaturation / termination	85	05:00
5 temporary storage	4	pause

Additionally, a RT hot start mastermix was prepared as given in Table 4-9 and preheated in the PCR cycler. During the second step of the RT temperature program, 3.5 μL of the RT hot start mastermix was added to each cavity of the PCR plate. The RT temperature program was continued according to Table 4-10. The RT products were then 1/2 diluted with 10 μL of RNase-free water.

Quantitative real time PCR (qPCR)

The qPCR was carried out on a Rotor-Disc 100 mold in a dedicated real time cycler with 100 separate reaction cavities. The RT products of each cell and each standard dilution as well as a no template control were analyzed as two technical replica.

A qPCR mastermix was prepared as given in Table 4-11 using the universal forward primer and one of the segment-specific primers given in Table 4-5.

Table 4-11: Composition of the qPCR mastermix; the commercial Quanti Tect SYBR Green PCR master mix (2x) contains polymerase, dNTP mix, fluorescent dye and buffer; one of the primer pairs given in Table 4-5 was used; the mastermix was prepared in an excess of 25 %.

Reagent	Volume (μL) per reaction
RNase-free water	1
Quanti Tect SYBR Green PCR master mix (2x)	5
primer (10 μM) (vRNA tagRealtime for)	0.5
primer (10 μM) (Seg 5 Realtime rev or Seg 8 Realtime rev)	0.5
total	7

A pipetting robot was employed to fill each cavity of the Rotor-Disc 100 with 7 μL of the qPCR mastermix and 3 μL of the diluted RT product or RNase-free water. The Rotor-Disc 100 was sealed and set into the real time cycler. The qPCR temperature and signal recording program given in Table 4-12 was started recording an amplification curve and a melting curve for each cavity.

Table 4-12: qPCR temperature and signal recording program; # indicates recording of signal intensity.

Reaction step	Temperature ($^{\circ}\text{C}$)	Time (min:s)
1 initial denaturation	95	5:00
2 denaturation	95	0:10
3 primer annealing and elongation	62	0:20 #
4 final denaturation	95	0:15
5 melting curve recording	65	1:30
	ramp $\downarrow \Delta=1$	0:05 #
	90	each step

The melting curves were considered to evaluate the specificity of the qPCR product. The melting curves of fragments derived from segment 5 vRNA had a maximum slope at 80-81 $^{\circ}\text{C}$ whereas those of fragments derived from segment 8 vRNA had a maximum slope at 83-84 $^{\circ}\text{C}$. The amplification curves were slope corrected and a threshold was set at a normed fluorescence signal of 0.05. The threshold cycle (c_T) values were outputted for each cavity and the average mean was calculated for the duplicates. Samples with unusual amplification curves, associated with very high c_T values were excluded and categorized as not detected.

The actual quantification was based on the following considerations. The mass of standard vRNA present in the RT reaction cavities (m_{RT}) was calculated (Equation 8). The coefficient for the dilution of the RT reaction in the qPCR reaction (F_{qPCR}) was defined (Equation 9) and used to calculate the mass of standard cDNA present in the qPCR reaction cavities (m_{qPCR}) (Equation 10). The number of standard cDNA molecules present in the qPCR reaction cavities ($N_{\text{molecules qPCR}}$) was calculated involving the molar mass of the cDNA molecule ($k \cdot N_{\text{bases}}$) and

the Avogadro constant (N_A) (Equation 11). The c_T values were then plotted against the decadic logarithm of the number of standard cDNA molecules present in the qPCR reaction cavities ($\log_{10} N_{\text{molecules qPCR}}$) resulting in a negative linear correlation (Figure 4-1). The according linear equation is given in Equation 12 with the negative slope a and the positive intercept b .

$$m_{\text{RT}} = c_{\text{standard}} \cdot V_{\text{standard}} = c_{\text{standard}} \cdot 2 \mu\text{L} \quad (8)$$

$$F_{\text{qPCR}} = \frac{V_{\text{RT}}'}{V_{\text{RT/qPCR}}} = \frac{20 \mu\text{L}}{3 \mu\text{L}} = \frac{20}{3} \quad (9)$$

$$m_{\text{qPCR}} = \frac{m_{\text{RT}}}{F_{\text{qPCR}}} = \frac{c_{\text{standard}} \cdot 2 \mu\text{L}}{\frac{20}{3}} = c_{\text{standard}} \cdot 0.3 \quad (10)$$

$$N_{\text{molecules qPCR}} = \frac{m_{\text{qPCR}} \cdot N_A}{k \cdot N_{\text{bases}} \cdot 10^9} \quad (11)$$

c_{standard}	concentration of standard dilution applied for RT ($0.5 \cdot 10^{-9} \text{ ng}/\mu\text{L}$)	$[\text{ng}/\mu\text{L}]$
c_T	threshold cycle	$[-]$
F_{qPCR}	coefficient for dilution of RT reaction in qPCR reaction	$[-]$
k	average mass of one nucleotide (340 g/mol)	$[\text{g/mol}]$
m_{qPCR}	mass of cDNA in qPCR reaction	$[\text{ng}]$
m_{RT}	mass of vRNA in RT reaction	$[\text{ng}]$
N_A	Avogadro constant ($6.02 \cdot 10^{23} \text{ molecules/mol}$)	$[\text{molecules/mol}]$
N_{bases}	number of nucleotides (fragment length) of qPCR product (segment 5: 1571; segment 8: 893)	$[-]$
$N_{\text{molecules qPCR}}$	number of standard cDNA molecules in qPCR reaction	$[\text{molecules}]$
V_{RT}'	volume of RT reaction after dilution	$[\mu\text{L}]$
$V_{\text{RT/qPCR}}$	volume of diluted RT reaction aliquot in qPCR reaction	$[\mu\text{L}]$
V_{standard}	volume of standard dilution in RT reaction	$[\mu\text{L}]$

Reversely, the number of standard cDNA molecules present in a qPCR reaction cavity after amplification of vRNA of a sample single-cell lysate was calculated using Equation 13.

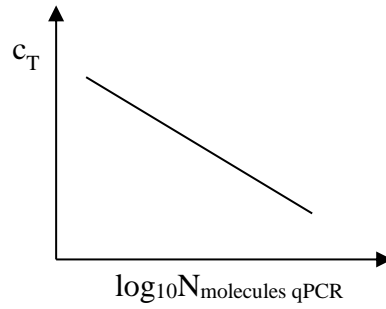


Figure 4-1: Linear correlation between the decadic logarithm of the number of standard cDNA molecules present in a qPCR reaction cavity ($\log_{10} N_{\text{molecules qPCR}}$) and the threshold cycle (c_T) value; the according linear equation is given in Equation 12.

Further, Equation 14 was used to calculate the number of vRNA molecules present in the RT reaction containing a sample single-cell lysate ($N_{\text{molecules RT}}$). Finally, Equation 15 resulted in the number of vRNA molecules (copies) per cell.

$$c_T = a \cdot \log_{10} N_{\text{molecules qPCR}} + b \quad (12)$$

$$N_{\text{molecules qPCR}} = 10^{\frac{c_T - b}{a}} \quad (13)$$

$$N_{\text{molecules RT}} = N_{\text{molecules qPCR}} \cdot F_{\text{qPCR}} \quad (14)$$

$$N_{\text{molecules cell}} = N_{\text{molecules RT}} \cdot \frac{V_{\text{lysate total}}}{V_{\text{lysate qPCR}}} = N_{\text{molecules RT}} \cdot \frac{5 \mu\text{L}}{1 \mu\text{L}} = N_{\text{molecules RT}} \cdot 5 \quad (15)$$

a	slope of the linear regression (Figure 4-1)	[-]
b	intercept of the linear regression (Figure 4-1)	[-]
$N_{\text{molecules cell}}$	number of vRNA molecules per cell	[-]
$N_{\text{molecules RT}}$	number of vRNA molecules in RT reaction	[-]
$V_{\text{lysate qPCR}}$	volume of sample single-cell lysate applied for RT	[μL]
$V_{\text{lysate total}}$	total volume of sample single-cell lysate	[μL]

4.2.5 Statistical analysis

Basic calculations were done using the software Microsoft Excel. The statistical analysis of data (Shapiro-Wilk normality test, two-sample *t*-test and Mann-Whitney *U* test) was carried out using the software OriginPro 9.1.0 (2013). The calculations for the Siegel-Tukey test (Siegel and Tukey, 1960) were done manually as described by Sheskin (2000).

The hypothesis tests (*t*-test and Mann-Whitney *U* test) and the normality test were based on a significance level α of 0.05 meaning a 5 % risk of concluding a false positive outcome (type I error). The outcome of the normality test was positive in case the p-value was greater than α ($p > 0.05 = \alpha$). The outcome of hypothesis tests was depicted in charts using asterisks according to the scheme given in Table 4-13, which was adapted from GraphPad Software (2015).

Table 4-13: Summary of possible outcomes of hypothesis tests; symbols (asterisks) and the respective p-values and meanings are given; α significance level; p probability of type I error; adapted from GraphPad Software (2015).

Symbol	p value	Meaning
ns	$p \geq 0.05 = \alpha$	not significant
*	$0.01 \leq p < 0.05$	significant
**	$0.001 \leq p < 0.01$	very significant
***	$0.0001 \leq p < 0.001$	extremely significant
****	$p < 0.0001$	extremely significant

5 Results

The present master thesis aims at identifying factors that contribute to variability of influenza A virus (IAV) replication in MDCK cells. The first section covers the cloning of MDCK cells in order to reduce heterogeneity in the non-clonal cell line (paragraph 5.1). Assuming that the resulting clones represent the heterogeneous character of MDCK cells they were used to study the contribution of the same to variability of IAV replication which is covered by the second section (paragraph 5.2).

5.1 Cloning and characterization of clonal MDCK cell populations

Clonal MDCK cell populations were generated by a cloning procedure that was established concomitantly. During cell expansion, different morphological characteristics were observed. A further distinction of the clonal MDCK cell populations was made based on the growth characteristics.

5.1.1 Cloning procedure

An MDCK cell line (ECACC 84121903) was present as a working cell bench in liquid nitrogen at passage number four upon receipt. This was used as the parental MDCK cell population for cloning (for exact passage numbers used for seeding see Table A-1 in the appendix 0). Cloning was performed by a limiting dilution technique on a 384-well plate which allows the separation of individual cells followed by the expansion of the clonal cell populations in culture vessels of increasing growth area. The lack of a ready-to-use cloning protocol made it necessary to establish a set of suitable parameters. Finally, 31 clonal MDCK cell populations were generated and cryopreserved.

Limiting dilution

Two types of 384-well plates were tested of which the surfaces were either physically treated to improve cell adhesion (hereafter referred to as binding plate) or chemically modified to reduce non-specific biomolecule binding (hereafter referred to as non-binding plate). For limiting dilution, preliminarily cells were used that have reached confluency in a 75 cm² cell culture flask after growing for three days. In each well of the binding and non-binding plate 50 µL of a 30 cells/mL dilution in fresh Z-medium were seeded to obtain an average 1.5 cells per well. 20 h post seeding the plates were centrifuged briefly to allow the settling of the cells and single cells were identified by phase contrast microscopy. On both, the binding and the non-binding plate the proportion of wells containing one single cell was half of that expected according to Poisson

distribution (33.5 %). One reason for that was the presence of quite high amounts of adverse particles (Figure 5-1 A,B) which interfered with the identification of single cells. They were considered to be a fraction of the extracellular matrix of the cell culture used for seeding. Thus, for the subsequently performed cloning experiments, instead a preculture of the MDCK cells was prepared in a 9.6 cm² tissue culture dish and used for seeding the next day. However, the proportion of wells containing one single cell still did not exceed 20 %.

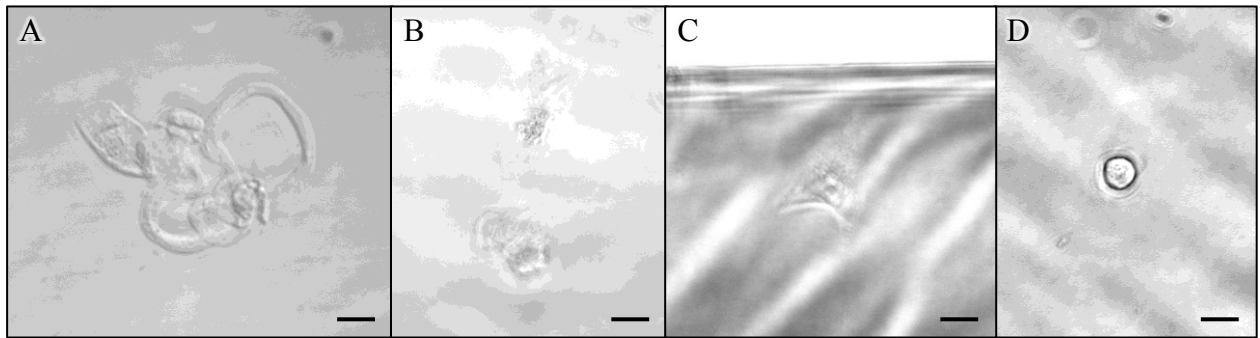


Figure 5-1: Examples for adverse particles (A,B) and single cells (C,D) on a 384-well plate; single cells were either adherent (C) or round shaped (D); phase contrast microscopic images taken with 40-fold magnification; scale bars equal 20 μ m.

Another obstacle with microscopy, regardless of the type of plate, was that more than half of the cells were adherent and thus difficult to identify in contrast to the otherwise round shaped cells which were clearly definable (Figure 5-1 C,D). To overcome this, in the subsequently performed cloning experiments the plates were centrifuged and microscopically examined either immediately or 16 h post seeding. By reducing the time for the cells to adhere to 16 h, still half of the cells were adherent. In contrast, the immediate examination was suitable to catch the round shaped cell state before adherence, leading to an almost solely occurrence of round shaped cells. Regarding the type of plates, there were only slightly differences observed. A disadvantage of the binding plates was the sporadic adherence of difficult to recognize cells on the vertical wall of the wells which was a source of misjudgment concerning the identification of single cells. On the other hand, the non-binding plates were prone to the formation of small air bubbles while seeding the cell suspension in the wells. Those which did not disappear even after centrifugation also hindered the identification of single cells. Since the latter was easier to control (exclude wells containing bubbles), the non-binding plates were preferred. Nevertheless, the identification of single cells is the most critical step of the cloning procedure since the resulting populations can only be called clonal, if they arose from the propagation of one single cell. This clearly requires some experience. Checking the positive wells (marked as containing one single cell) the following days helped to ensure that no hidden cell is contaminating the

clonal cell. Also the monitoring of the propagating clonal cell populations enabled the assessment of their growth state and their morphological characterization.

The final cloning protocol is provided in paragraph 4.2.1.5.

Propagation and expansion

The propagation of one single cell to a colony in the well of a 384-well plate is exemplarily shown in Figure 5-2 (clone 1). The single cells typically started to divide within the first two to three days post seeding. In the following days, the frequency of cell division differed strongly from clone to clone. As a conclusion, the approximate cell number on the eighth day post seeding spanned from one or two cells over groups of 10-30 cells to colonies of more than 50 cells which equals an approximate 5 % confluency.

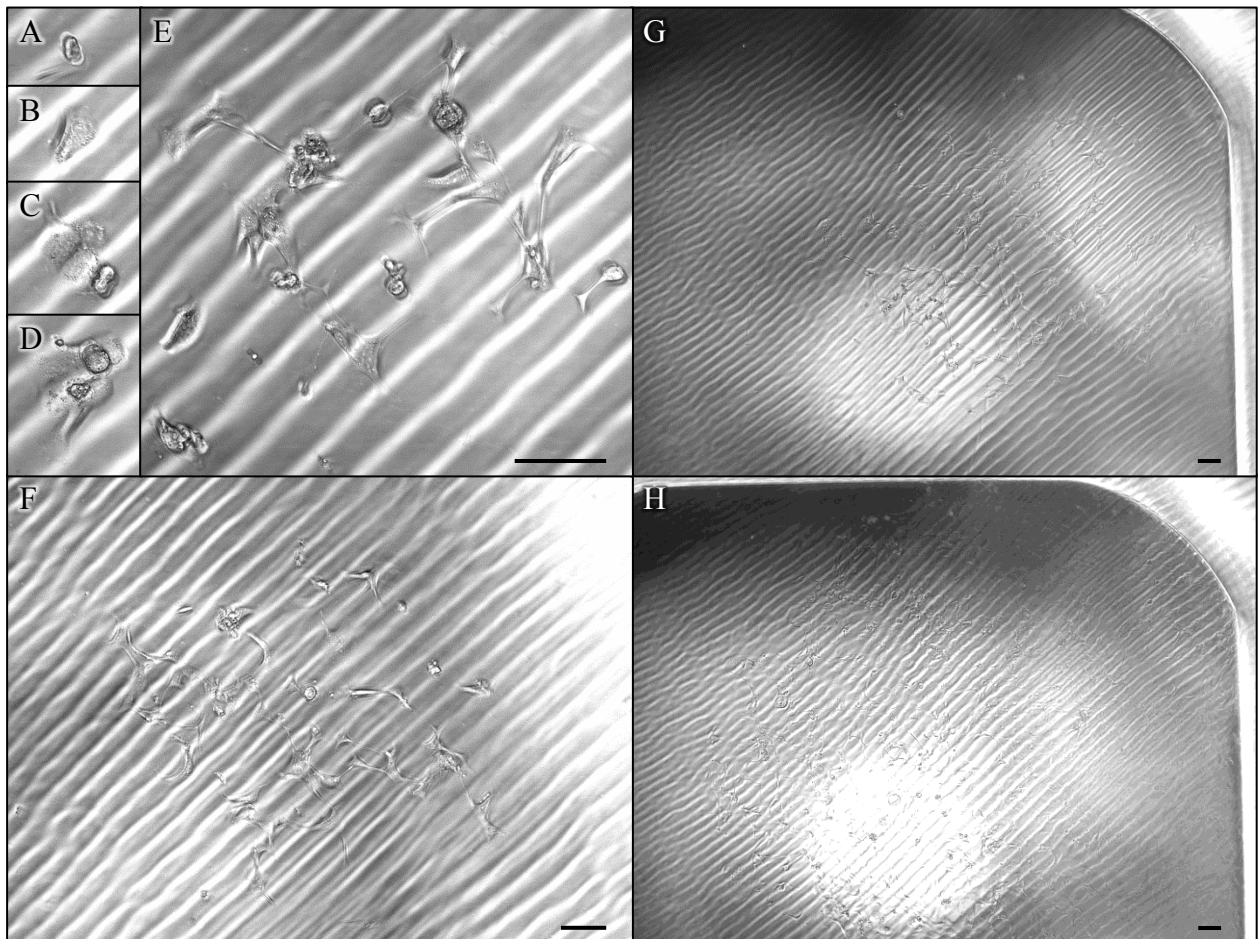


Figure 5-2: Propagation of a clonal MDCK cell population (clone 31) from one single cell on a 384-well plate; phase contrast microscopical images taken at 0 (A), 1 (B), 2 (C), 3 (D), 5 (E), 6 (F), 9 (G) and 13 (H) days post seeding on a 384-well plate with 20-fold (A-E), 10-fold (F) and 5-fold (G-H) magnification; scale bars equal 100 μm .

An approximate 20 % fraction of the clones did not even survive until this time point. Dead cells were distinguishable from living cells by their high contrasts and dark appearance. Until two weeks post seeding, another 40 % fraction of the clones died at a low cell number state. In contrast, there were sixteen clones that had reached a medium or high confluency of 30-80 % at this time point. Additionally, the color of their culture medium was shifted from red to orange indicating a pH shift due to the release of lactate. These observations were considered as criteria for the passaging of the clonal colonies to a cell culture vessel with an increased growth area, which is a 96-well plate. The remaining clones were at a multi-cell state with differing portions of dead cells among them or reached a confluency of up to 30 % until two weeks post seeding. In order to maintain the nutrient supply, the cell culture medium of these remaining clonal colonies was completely exchanged, even if a preliminary testing of either none or partial or total culture medium replacement did not show a tendential improvement of growth. Since the communication between cells at very low densities is in general challenging, a fraction of 25 % of conditioned culture medium was added when replacing the culture medium. However, a positive effect was not observed. Instead, a high fraction of the monitored clones (another approximate 20 % of the clones from the beginning) did not even exceed a colony size of ten cells at three weeks post seeding but kept a stagnant state or even lost vitality. In the following, the medium of the remaining clones was exchanged weekly. Additionally, some of the stagnating clonal cells were tried to rearrange and thus vitalize by trypsinizing and reseeding them in a well of the 384-well plate. But this strategy also did not succeed. Whenever a clone met the criteria mentioned before, it was passaged onto a 96-well plate. A total number of 35 clones (which is less than 20 % of the clones from the beginning) did reach this state within four weeks post seeding while the remaining clones were not able to further propagate until six weeks post seeding.

The expansion of the clonal cell populations proceeded from the 384-well plate to a 96-well plate, then to a 6-well plate and finally to a 75 cm² cell culture flask. Generally, a population was passaged whenever a confluency of at least 60 % was reached. The parameters for passaging of the propagating clonal cell populations to cell culture vessels of increasing growth area were determined within a preliminary experiment. For instance, the amount of trypsin was chosen according to the complete covering of the bottom of the plate. The time for trypsinization was chosen on the basis of microscopical control of the cell detachment. The final volume in the subsequent cell culture vessel was chosen in accordance with the filling volume recommended by the supplier. For the expansion protocol, see the method (paragraph 4.2.1.5).

An overview of the temporal aspect of each successfully expanded clone is shown in Figure 5-3. As mentioned before, the originally single cells needed two to four weeks to overcome the state in a 384-well plate. Once passaged onto a 96-well plate, the clonal cell populations reached an almost 100 % confluency after two to four days of propagation. An intermediate step on a 24-well plate was skipped since confluency again was reached after only one day as tested with the first clone. The clones 15 and 16 spent an especially long time in the 96-well plate state because of an initially very slow growth. When propagating, the cells formed very dense colonies that were not expanding in size. This is why a trypsinization and reseeding was carried out (indicated by a solid line between two identical culture vessels). Three clones were lost at the 96-well plate state due to a too low cell density (not listed in the timeline). On the 6-well plate most of the clonal cell populations grew three to six days while some exceeded two or three weeks. In those cases, the culture medium was at least weekly replaced by fresh Z-medium.

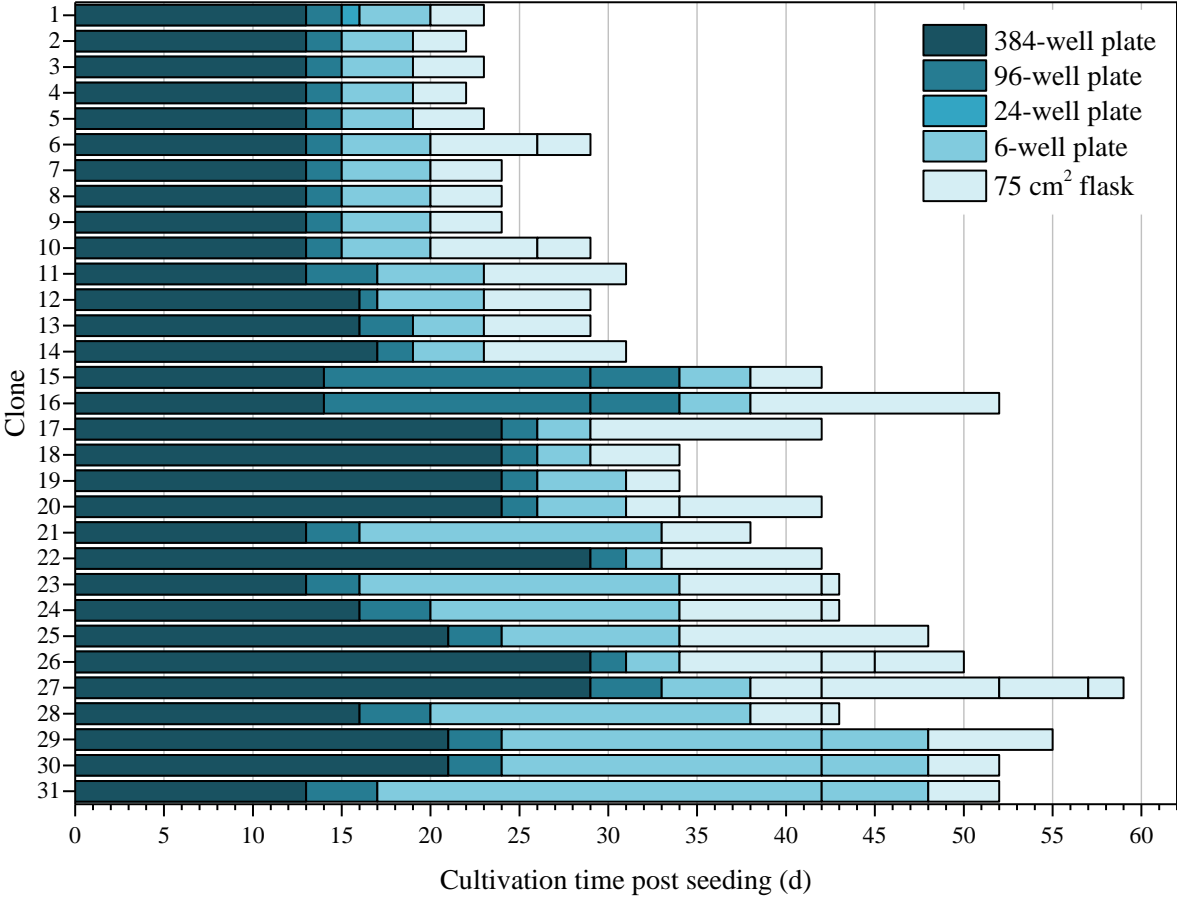


Figure 5-3: Timeline of the expansion of 31 clonal MDCK cell populations in culture vessels with increasing growth area; different colors indicate different culture vessels; solid lines between different or identical culture vessels indicate trypsinization and (re)seeding; except for clone 1, the 24-well plate was skipped.

Trypsinization and reseeding was necessary in case the cells formed dense focal points. One more clone was lost at the 6-well plate state due to a too low cell density (not listed in the timeline). The final expansion step in a 75 cm² cell culture flask was mostly terminated after less than one week. For cryopreservation, at least 7·10⁶ cells were needed. As long as the according cell number was not achieved, the cells were reseeded in a 75 cm² cell culture flask. During a period of about three to eight weeks from the seeding of single cells to the cryopreservation, overall 31 clonal MDCK cell populations were obtained

5.1.2 Morphological characteristics

During the expansion of the clonal MDCK cell populations their morphological characteristics were observed by phase contrast microscopy. On the 384-well plate, the cells were challenged by a very low cell density. Their spread was clearly visible done by the formation of elongated cells (indicated by solid lined arrows in Figure 5-4). Additionally, there were occurring strongly flattened cells with no definite cell boundary that seemed to move in a flowing manner (indicated by dashed lined arrow in Figure 5-4). Also there were round cells detaching from the growth surface which are suspected to move and adhere at another site (indicated by dotted lined arrows in Figure 5-4). In general, the cells were dynamically changing their constellations. When spreading, there were initially large spaces between the cells which were subsequently filled when further propagating which is exemplary shown in Figure 5-4. These morphological characteristics of spreading cells were observed with each clonal MDCK cell population.

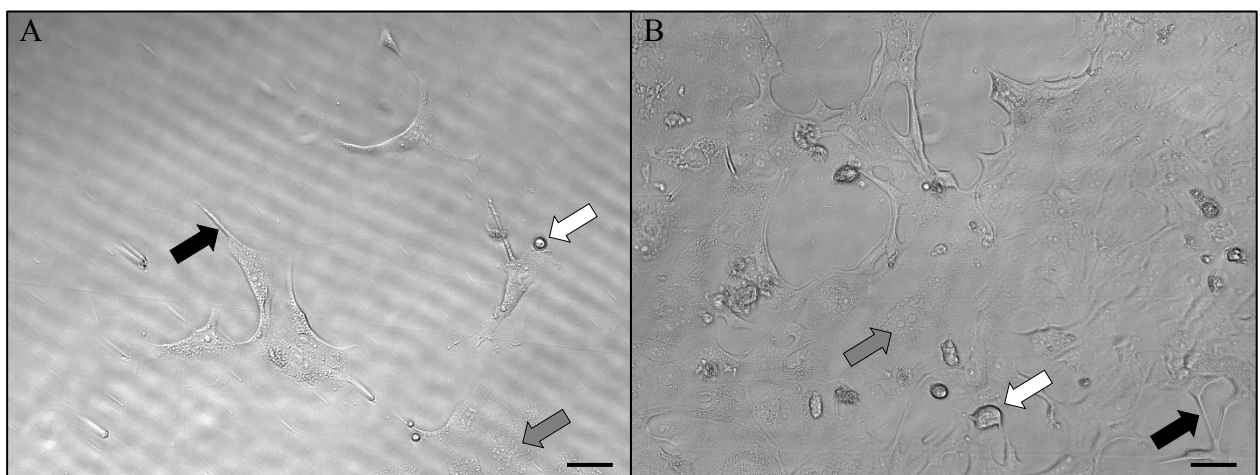


Figure 5-4: Morphological characteristics during the spread of a clonal MDCK cell population; black arrows: elongated cells, grey arrows: flattened cells, white arrows: detaching round cells; phase contrast microscopical images taken at 5 (A) and 20 (B) days post seeding on a 384-well plate with 20-fold magnification; scale bars equal 100 μ m.

Even if there were differences in the colony boundary and density among the propagating clonal MDCK cell populations on the 384-well plate, these were not definite distinguishable. But with passaging the populations to new culture vessels the cells were in general not confronted with such low cell densities as they were in the initial phase. From then, some clone-specific morphological characteristics were observed. The clonal MDCK cell populations did roughly match one of the typical morphologies (types A-D) summarized in Table 5-1 (Figure 5-5).

Table 5-1: Morphological characteristics of subconfluent clonal MDCK cell populations; Types A-D were distinguished according to cell shape, colony formation, motility and propagation; generic images are provided in Figure 5-5)

	Type A	Type B	Type C	Type D
cell shape	round to fusiform individual cells	mainly round to fusiform or elongated individual cells; scatteredly flattened cells	scatteredly flattened scrubby cells; few dense focal points of round to fusiform cells	tight polygonal cells
colony formation	loose colonies	loose colonies	few focal points of increasing density	dense, clearly edged clusters
motility	motile	highly motile	nonmotile focal points	nonmotile
propagation	homogeneous propagation	homogeneous propagation	very heterogeneous propagation (focal point-dependent)	propagation mainly within the edges of the clusters
clones	1,3,4,6,7,8,9,13, 18,21,22,27	5,10,11,12,14	15,16,17,19,20,23, 24,28,29,30,31	2,25,26

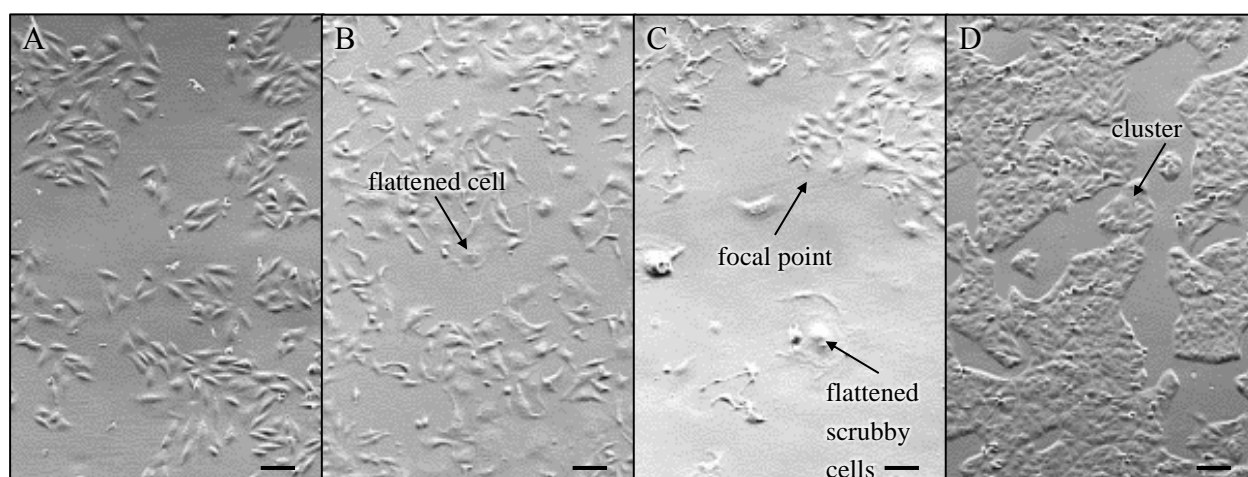


Figure 5-5: Morphological characteristics of subconfluent clonal MDCK cell populations; A-D depict types A-D which are described in Table 5-1; phase contrast microscopical images taken on 75 cm² flasks with 2.5-fold magnification; scale bars equal 100 μ m.

The morphological types described above were mostly based on the growth in 75 cm² flasks and were roughly consistent with the observations on the 96-well and 6- well plates. Nevertheless, the assignment of the clones to these types was vague in some cases, especially because some features were rarely occurring mixed.

In contrast to the characterization at a subconfluent state, the distinguishment of the clonal MDCK cell populations was not at all possible at a confluent state. The cells were shaped polygonally due to their tight neighbouring. Indeed the morphology of the cells forming the monolayer seemed to differ in the visibility of the cell boundaries and the nuclei and in the three dimensional appearance. These differences have been used by several groups to classify MDCK cells for example in type I and type II (Gekle et al., 1994; Lugovtsev et al., 2013; Nakazato et al., 1989; Valentich, 1981) (see discussion). But in this case, it turned out not to be a clone-specific matter but a matter of the location within the monolayer. In Figure 5-6 this is exemplary shown by a panorama view of a clonal MDCK cell population (clone 20) grown to confluency on a 6-well plate three days after seeding approximately half a million cells. The cells in the center of the well (on the right), which are suspected to be the oldest cells, are flat and irregularly shaped with a clearly visible nucleus. Their intercellular space is almost indistinguishable. In contrast, the peripheral cells (on the left), which are suspected to be the youngest cells, appear high and polygonal but their nucleus is almost invisible. Instead, their intercellular space is clearly distinguishable. Overall, the morphological characteristics of the clonal MDCK cell populations were not considered a substantial feature.

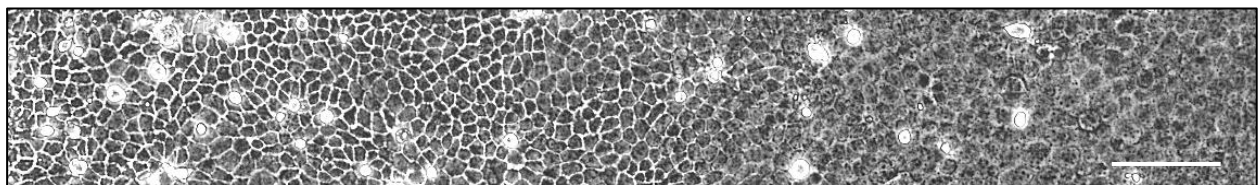


Figure 5-6: Morphological characteristics of a confluent clonal MDCK cell population (clone 20); phase contrast microscopical image taken on 6-well plate with 10-fold magnification; scale bar equals 100 μm.

5.1.3 Growth characteristics

The expansion process of the clonal MDCK cell populations already demonstrated a differing growth characteristic regarding the time to reach confluency (Figure 5-3). Since the conditions such as the seeding density were not constant during cloning, a more suitable method was needed to characterize the growth of the individual clonal MDCK cell populations. The recording of growth curves, which would be the first choice for that purpose, was not part of the present thesis but was carried out by a different examiner (results not shown). Nevertheless, the

weekly passaging of the populations under defined conditions, accompanied with the measurement of the cell count and the cell diameter was used to collect data and to draw conclusions on the growth characteristics. (Virtually, the cells were assumed to be in the stationary growth phase at the point of analysis.) Three data sets were available (n=3) for three parental as well as all 31 clonal MDCK cell populations except for six ones (n=2). All populations have been thawed simultaneously in 25 cm² cell culture flasks before and subsequently been cultured in 6-well plates with a seeding density of 0.5·10⁶ cells per well.

In Figure 5-7 the resulting average cell diameters and the respective average cell counts per well are plotted, each dot representing one population. The non-clonal MDCK cell populations can be clustered into two distinct groups (list in Figure 5-7): these which grow to high cell densities (4.2-6.7·10⁶ cells/well) forming small cells (12.2-13.2 μm) – in the following referred to as small cells – and those which grow to low cell densities (2.4-4.1·10⁶ cells/well) forming big cells (14.4-15.8 μm) – in the following referred to as big cells. It should be remarked that the average cell diameters were derived from cell size distributions as exemplary shown in Figure A-1 (Appendix).

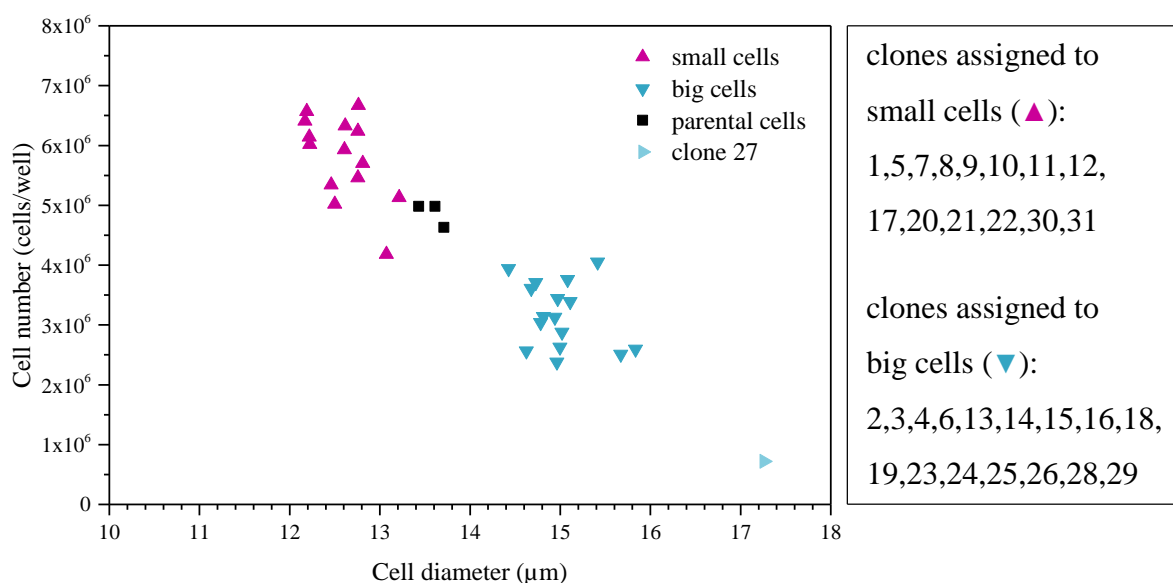


Figure 5-7: Correlation between average cell number and diameter of cells grown to confluency from clonal and non-clonal MDCK cell populations; colors and shapes of the dots indicate the distinct clusters containing populations with similar growth characteristics (respective clones listed above); 0.5·10⁶ cells were seeded in 6-well plates 7 d prior to measurement; n=2-3 (independent experiments).

The population of clone 27 does not fit the formerly defined clusters but forms an exceptional population which grows to a very low density (0.7·10⁶ cells/well) forming very big cells (17.3 μm). The average cell count and diameter of the cells of the parental MDCK cell

population, of which three independent cultures were prepared, are lying in between those of the small cells and the big cells.

Regarding the distributions of the cell diameter and the cell number among the clonal MDCK cell populations (Figure 5-8 A,B), the two groups are clearly separated and the parental cells are positioned in between both. Similarly, the cell volume of the individual cells allows the distinction of small cells (average cell volume of 0.94 to 1.21 pL) and big cells (1.57 to 2.69 pL). Overall, the average cell count per well and the cell size seem to be associated to each other. This agrees well with the limitation of growth area in the stationary growth phase, so that either the cell size (growth) or the number of cells (division) is promoted. The areal limitation leads to a limitation of the total cell volume which is the volume formed by the whole amount of cells in a well. This is confirmed by the average total cell volume per well calculated for each population. It is more homogeneously distributed than the average cell count and diameter. This means that the total cell volume of small cells and big cells is quite similar (Figure 5-8 C).

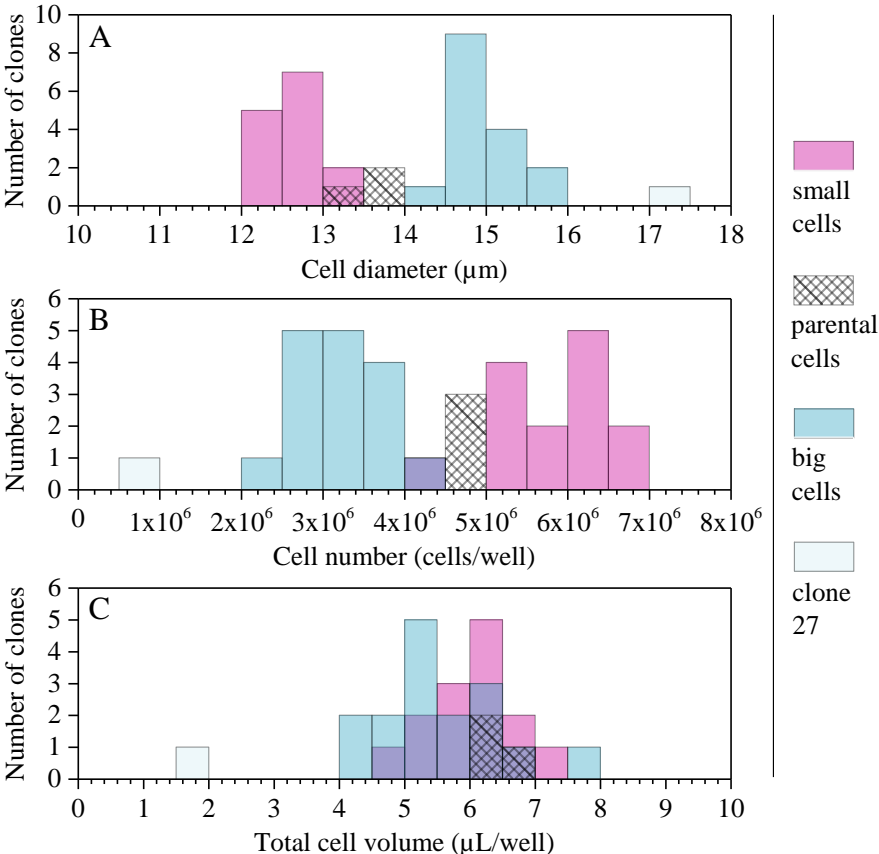


Figure 5-8: Distribution of the average cell diameter (A), cell number (B) and cell volume (C) per well at confluency among the clonal and non-clonal MDCK cell populations; $0.5 \cdot 10^6$ cells were seeded in 6-well plates 7 d prior to measurement; average means are used for binning; $n=2-3$ (independent experiments)

5.2 IAV infection of clonal and parental MDCK cell populations

The clonal MDCK cell populations were compared to the non-clonal (parental) MDCK cell population regarding virus titers produced at the population level after infection with influenza A virus (paragraph 5.2.1). This screening provided the basis for performing single-cell experiments comparing the cell-to-cell variability of influenza A virus replication in terms of virus yields and intracellular vRNA levels among the parental and selected clonal MDCK cell populations (paragraph 5.2.2).

5.2.1 Screening at the population level

The clonal MDCK cell populations were screened for the average virus titer they are capable to produce after infection with influenza A virus in 6-well plates in order to identify potential high- and low-producer clonal MDCK cell populations and thus to distinguish between them.

5.2.1.1 Analysis of the virus yield

The infection protocol was for reference adapted from Heldt and Kupke et al. (2015). It determines a multiplicity of infection (MOI) of 10 and the harvest at 12 hours post infection (hpi). The cells were infected one day post seeding of $1 \cdot 10^6$ cells when confluency was reached (exponential growth phase expected). The resulting virus titers were measured by three independent methods which deploy different principles and thus enable the distinction of total virus particles (HA assay), infectious virus particles (TCID₅₀ assay) and infectious virus particles that are able to propagate, also called plaque forming units (PFU) (plaque assay). Three independent experiments (n=3) were carried out with three parental as well as all 31 clonal MDCK cell populations except for four ones (n=2).

Virus titers per mL

In Figure 5-9 the resulting virus titers per mL are shown for each population and for each virus titration method. The average (avg) of the 31 clonal as well as that of the three replicated parental MDCK cell populations is shown in additional columns.

Among the clonal MDCK cell populations the total virus titers ranged from $5.7 \cdot 10^9$ (clone 27) to $1.6 \cdot 10^{10}$ (clone 16) virus particles per mL (equaling 2.42 to 2.87 log₁₀ HAU/100 μL) which is a less than three-fold difference. The amount of infectious virus particles was one magnitude smaller and ranged from $4.9 \cdot 10^8$ (clone 27) to $1.6 \cdot 10^9$ (clone 28) virus particles per mL which is a 3.2-fold difference. A still lower titer of $2.7 \cdot 10^8$ (clone 27) to $1.0 \cdot 10^9$ (clone 15) virus particles per mL, which is a 3.7-fold difference, was provided by the plaque forming units.

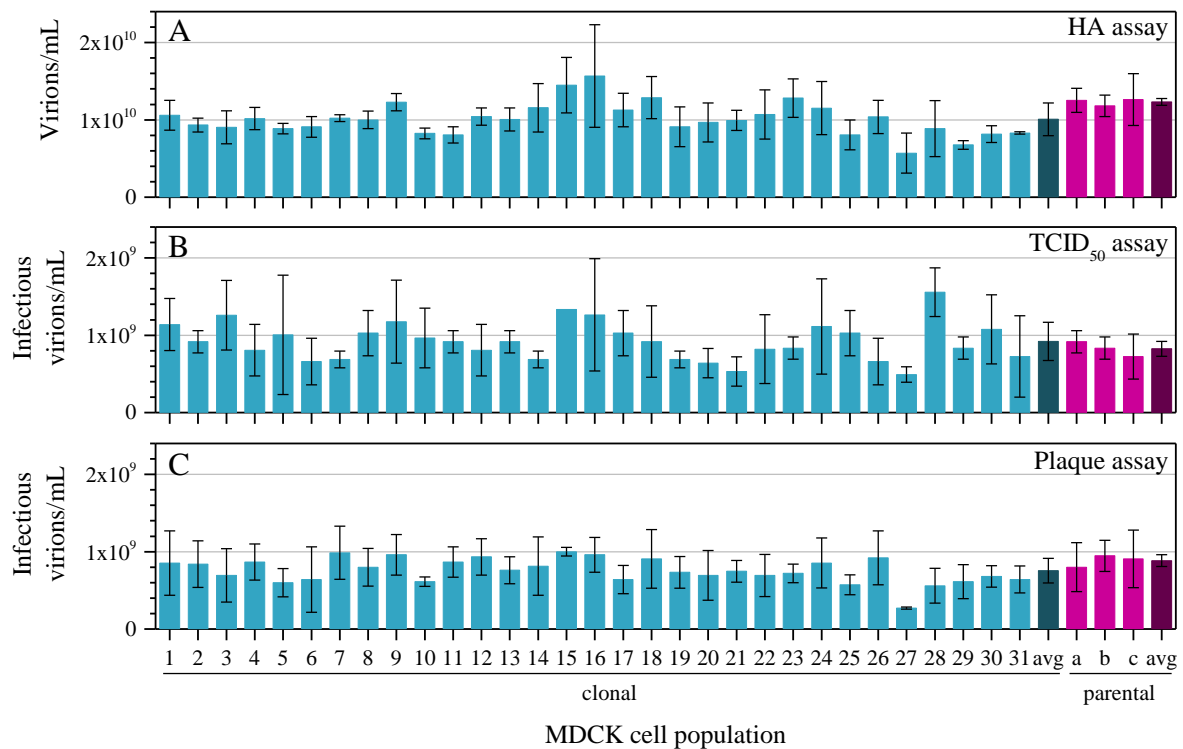


Figure 5-9: Virus titers per mL produced by IAV-infected clonal (1-31) and parental (a-c) MDCK cell populations (MOI 10, 12 hpi) measured by HA assay (A), TCID₅₀ assay (B) and plaque assay (C); n=2-3 (independent experiments); avg: average; error bars indicate SD.

The differences in virus titers among the clonal MDCK cell populations are quite small and appear insignificant, especially given the fact that virus replication is proceeding over several orders of magnitude. Thus none of the clonal MDCK cell population can be called a high- or low-producer. Above all, the data collected over the three independent experiments did not consistently bring about the clonal MDCK cell populations in the same order of precedence regarding their virus titers. Similarly, the virus titration methods themselves did not. Instead, there were fluctuations occurring which can be attributed to random errors of the experimental setup on the one hand and to the errors of the virus titration methods on the other hand. This is why the error bars are partially quite high for the different populations.

Compared to the average virus titer produced by the three parental MDCK cell populations (total $1.0 \cdot 10^{10}$ virus particles per mL, equaling $2.68 \log_{10}$ HAU/100 μ L; dark pink column), the virus titer averaged over all 31 clonal MDCK cell populations (total $1.2 \cdot 10^{10}$ virus particles per mL, equaling $2.78 \log_{10}$ HAU/100 μ L; dark blue column) is similar, regardless of the virus titration method. But the fluctuations among the individual average virus titers of each clonal MDCK cell population are higher than that among the individual average virus titers of the replicated non-clonal/parental MDCK cell populations which seems not solely to occur due to the different number of analyzed objects (31 versus three).

Cell-specific virus titers

Knowing that the individual clonal MDCK cell populations tend to grow to higher or lower cell densities within a given period of time, as shown in paragraph 5.1.3, this does inevitably lead to different cell numbers after uniformly seeding $0.5 \cdot 10^6$ cells per well of a 6-well plate. This indeed was observed during this experiment. At the time point of infection, the cell counts of the clonal MDCK cell populations ranged from $1.0 \cdot 10^6$ (clone 27) to $2.2 \cdot 10^6$ (clone 5) cells per well, while the cell count of the non-clonal/parental MDCK cell population was averagely $1.7 \cdot 10^6$ cells per well. At 12 hpi, the cell counts were further increased to a range of $1.1 \cdot 10^6$ (clone 27) to $2.7 \cdot 10^6$ (clone 9) cells per well for the clonal MDCK cell population and to averagely $2.3 \cdot 10^6$ cells per well for the non-clonal/parental MDCK cell population. Both at the time point of infection and at 12 hpi the average cell counts differed by the factor two among the clonal MDCK cell populations while the average over the 31 clonal MDCK cell populations matched well with the average over the three replicated non-clonal/parental MDCK cell population.

The cell counts at 12 hpi were used to normalize the virus titers per mL to the cell-specific virus titer which is a common way to express virus yields. In Figure 5-10 the resulting cell-specific virus titers are shown for each population and for each virus titration method. The average (avg) of the 31 clonal as well as that of the three replicated parental MDCK cell populations is again shown in additional columns.

Among the clonal MDCK cell populations the total cell-specific virus titers ranged from $6.0 \cdot 10^3$ (clone 30) to $1.4 \cdot 10^4$ (clone 16) virus particles per cell which is a 2.3-fold difference. The amount of infectious virus particles was again one magnitude smaller and ranged from $4.1 \cdot 10^2$ (clone 21) to $1.6 \cdot 10^3$ virus particles per cell (clone 28) which is a 3.9-fold difference. Again, a still lower titer of $4.7 \cdot 10^2$ (clone 5) to $1.0 \cdot 10^3$ (clone 26) virus particles per cell, which is a 2.1-fold difference, was provided by the infectious virus particles that are able to propagate.

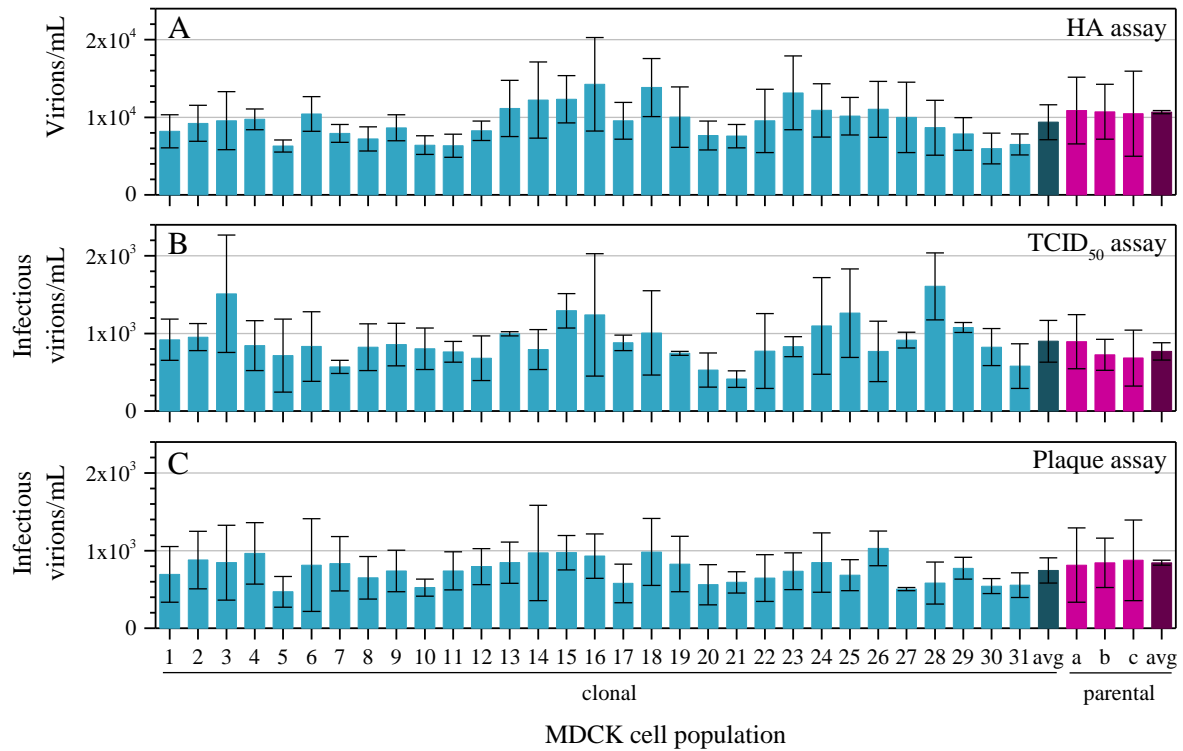


Figure 5-10: Cell-specific virus titers produced by IAV-infected clonal (1-31) and parental (a-c) MDCK cell populations (MOI 10, 12 hpi) measured by HA assay (A), TCID₅₀ assay (B) and plaque assay (C); avg: average; cell counts at 12 hpi were used for calculation of cell-specific titers; n=2-3 (independent experiments); avg: average; error bars indicate SD.

As shown with the virus titers per mL before, the differences in cell-specific virus titers among the clonal MDCK cell populations are similarly small regardless of the virus titration method used. In accordance with the relevance of magnitudes for virus replication, a presentation of the data on a logarithmic scale was considered (Figure 5-11). This points out the similarity of the cell-specific virus titers even more. Nevertheless there is still a fluctuation among the individual average cell-specific virus titers of each clonal MDCK cell populations which is higher than among the individual average cell-specific virus titers of the replicated parental MDCK cell populations. Indeed, small differences in cell-specific virus titers are apparent among the clones but they lack reproducibility as indicated by the relatively large errors obtained from three independent experiments. Considering this, the differences are regarded as insignificant.

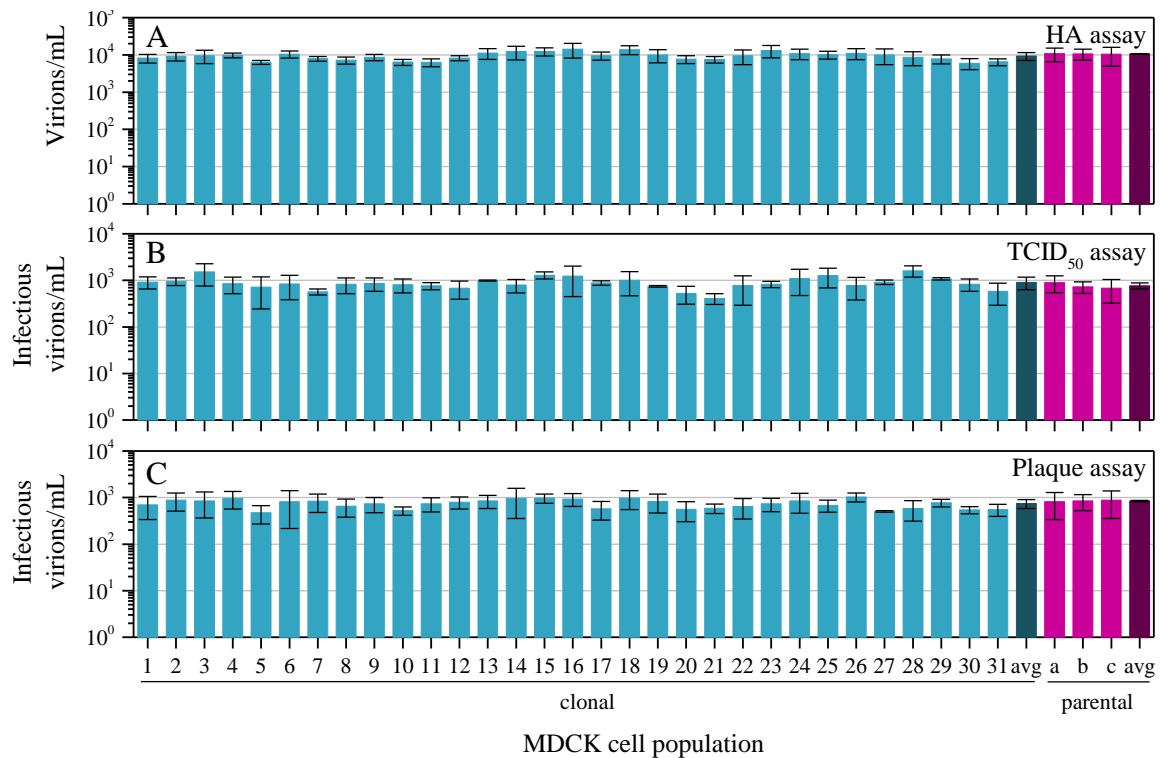


Figure 5-11: Cell-specific virus titers produced by IAV-infected clonal (1-31) and parental (a-c) MDCK cell populations plotted on a log₁₀ scale (MOI 10, 12 hpi) measured by HA assay (A), TCID₅₀ assay (B) and plaque assay (C); avg: average; logarithmic scale; cell counts at 12 hpi were used for calculation of cell-specific titers; n=2-3 (independent experiments); avg: average; error bars indicate SD.

Assumptions on scalability of cell-specific virus titer

So far it was on the one hand shown that the virus titers per mL as well as the cell-specific virus titers produced by the individual clonal MDCK cell populations hardly differ from each other under preset infection conditions. On the other hand, it was shown that the clonal MDCK cell populations consistently grow to clearly distinguishable cell numbers (that negatively correlate with the cell size) when cultured in 6-well plates up to the stationary growth phase (paragraph 5.1.3). Combining these information it was of interest, whether the similar cell-specific virus titer is scalable in terms of obtaining a multi-fold increase of the virus titer per mL when infecting a multi-fold cell number. In case this assumption applies, it would be advisable to use any clonal MDCK cell population that is growing to high densities in order to achieve the highest possible virus titer.

5.2.1.2 Analysis of the virus yield under alternative infection conditions

To answer this question, an alternative infection protocol was applied. The cells were infected with an MOI of 10 four days post seeding of $0.5 \cdot 10^6$ cells when the stationary growth phase was considered and thus the highest difference in cell numbers among the clonal MDCK cell populations was expected. A later harvest time point was employed, where the maximum total virus titer was expected to be achieved. This time point was defined by the occurrence of the cytopathic effect, whereby the cells were almost completely detached. Surprisingly, the cytopathic effect occurred quite simultaneously among the clonal MDCK cell populations at 48 hpi. For quantification, the total virus titer was measured (HA assay). The measurement of the infectious virus titer was not suitable because of the virus particles instability and loss of infectivity during the 48 hpi. This endpoint determination was also promising to reveal the highest possible differences in virus titers among the clonal MDCK cell population.

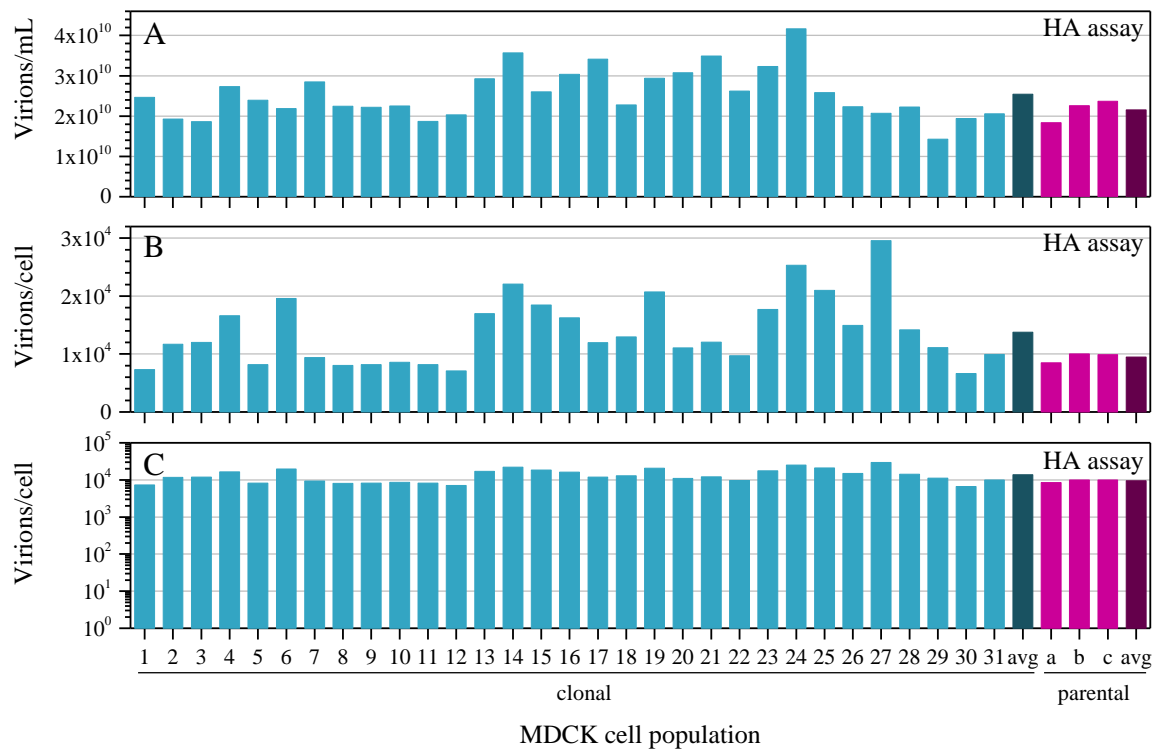


Figure 5-12: Virus titers produced by IAV-infected clonal (1-31) and parental (a-c) MDCK cell populations (MOI 10, 48 hpi) measured by HA assay; virus titers are shown per mL on a linear scale (A) and per cell (cell-specific virus titers) on a linear scale (B) as well as on a logarithmic scale (C); n=1; avg: average.

In Figure 5-12 A the virus titers per mL are shown for each population. The average (avg) of the 31 clonal as well as that of the three replicated parental MDCK cell populations is shown in additional columns. Compared to the virus titers per mL under preset infection conditions, the cells produced an average 2.5-fold higher total amount of virus particles under modified

infection conditions. This is probably both due to the higher cell numbers and to the later harvest time point. The virus titers spanned from $1.4 \cdot 10^{10}$ (clone 29) to $4.2 \cdot 10^{10}$ (clone 24) virus particles per cell (equaling 2.85 to 3.31 \log_{10} HAU/100 μ L) which is interestingly still an only three-fold difference. Based on that, still there cannot be drawn any conclusion about high- or low producer clones. To examine the previously made assumption, the total virus titer per mL produced by the individual clonal and parental/non-clonal MDCK cell populations was plotted against their respective cell number per well at the infection time point (Figure 5-13). The two groups of clonal MDCK cell populations which were already defined due to their growth characteristics earlier (paragraph 5.1.3) are also recognizable in this depiction (indicated by different colors/symbols). Obviously, the total virus titer per mL does not depend on the cell number per well at infection time point. Instead, both groups produce a similar average of $2.6 \cdot 10^{10}$ (low density) or $2.5 \cdot 10^{10}$ (high density) virus particles per mL (equaling 3.09 or 3.08 \log_{10} HAU/100 μ L).

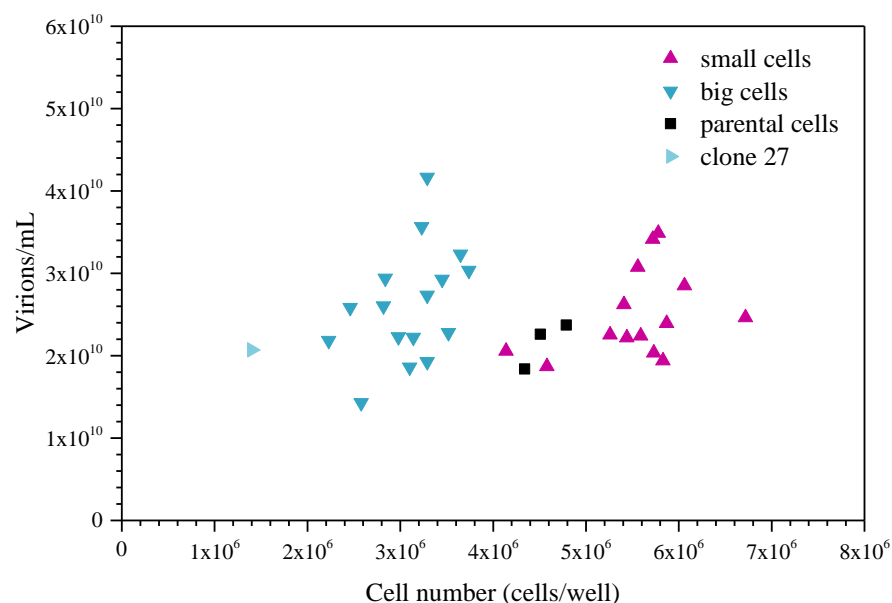


Figure 5-13: Relation between cell number and virus titer per mL produced by IAV-infected clonal and parental MDCK cell populations (MOI 10, 48 hpi) measured by HA assay; colors and shapes of the dots indicate the distinct clusters containing populations with similar growth characteristics (see paragraph 5.1.3); n=1.

This apparent contradiction to the previously made assumption that the cell-specific virus titer is scalable can be clarified when looking at the cell-specific virus titers again. These, gained under the alternative infection conditions, are shown in Figure 5-12 B (linear scale) based on the cell number at the infection time point. Basically, they are comparable to those, gained under preset infection conditions based on the 12 hpi time point (Figure 5-10 A and Figure 5-11 A). But, however, there is now a 4.4-fold difference among the cell-specific virus titers of the individual

clonal MDCK cell populations instead of a previous 2.4-fold difference. This implies that the cell-specific virus titers among the individual MDCK cell populations are not as indifferent as expected even if they are still in the same order of magnitude (Figure 5-12 C, logarithmic scale). This can be highlighted when linking the cell-specific virus titer to the two groups of clonal MDCK cell populations according to their growth characteristics (Figure 5-14). The alternative infection protocol was designed so that the cells were infected when being in the stationary growth phase. This allows a more precise distinguishment of the cell diameters of small cell and big cell clones compared to the infection at exponential growth phase where the cell diameters were more similar.

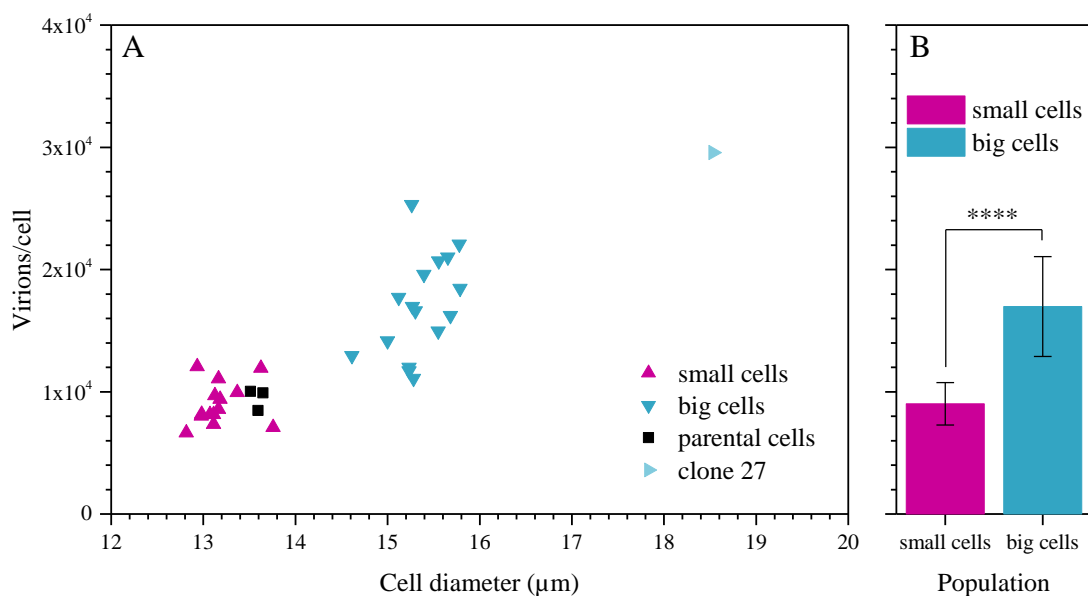


Figure 5-14: Cell-specific virus titers produced by IAV-infected clonal and parental MDCK cell populations (MOI 10, 48 hpi) measured by HA assay; A Correlation between average cell diameter and cell-specific virus titer; colors and shapes of the dots indicate the distinct clusters containing populations with similar growth characteristics (see paragraph 5.1.3); $n=1$; B arithmetic mean of the cell-specific virus titers of either cluster: populations of small cells ($n = 14$) and populations of big cells ($n = 16$); error bars indicate SD; arithmetic means of the cell-specific virus titers of the two clusters is extremely significantly different according to t -test (**** $p \leq 0.0001$).

The clonal MDCK cell populations are again clearly distinguishable forming the two clusters mentioned before (Figure 5-14 A). Interestingly, the smaller cells (cell diameter 12.8-13.8 μm at infection time point) turn out to be characterized by a lower cell-specific virus titer (averagely $0.9 \cdot 10^4$ virus particles per cell at 48 hpi) whereas the bigger cells (14.6-15.8 μm) produce a roughly two-fold higher cell-specific virus titer (averagely $1.7 \cdot 10^4$ virus particles per cell). This difference was confirmed extremely statistically significant by the t -test (indicated by asterisks in Figure 5-14 B). The cell-specific virus titers produced by the individual clonal MDCK cell

populations in either cluster were previously confirmed to be normally distributed by Shapiro-Wilk normality test. Overall, the cell-specific virus titer seems to be associated with or even depend on the cell diameter.

To close the circle, the findings from Figure 5-13 can be easily explained by bringing in the cell volume (see also Figure 5-8). The smaller cells occur in a higher cell number (their lower cell-specific virus titer is multiplied by a higher factor) whereas the bigger cells occur in a lower cell number (their higher cell-specific virus titer is multiplied by a lower factor), both leading to a similar total cell volume and an indistinguishable total virus titer per mL (Figure 5-15).

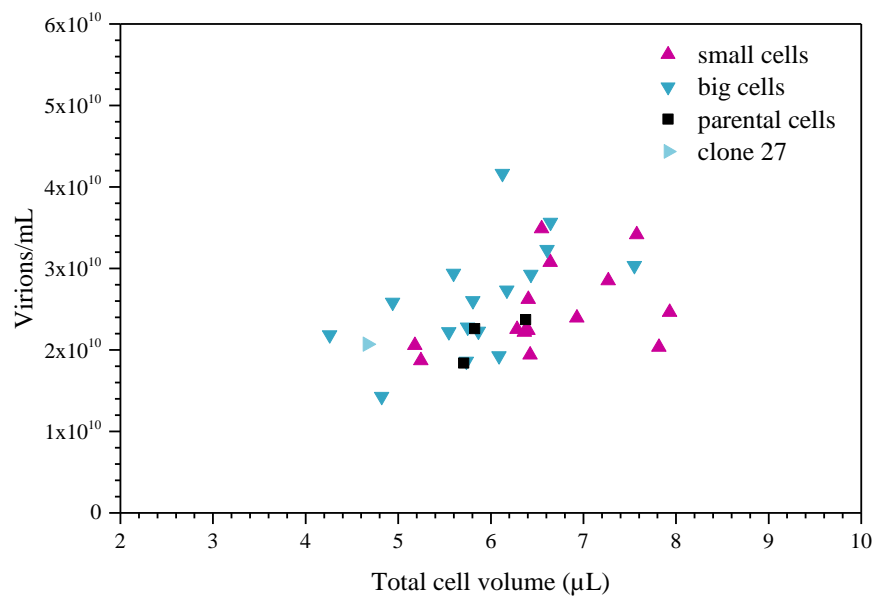


Figure 5-15: Relation between total cell volume and virus titer per mL produced by IAV-infected clonal and parental MDCK cell populations (MOI 10, 48 hpi) measured by HA assay; colors and shapes of the dots indicate the distinct clusters containing populations with similar growth characteristics (see paragraph 5.1.3); n=1.

5.2.2 Single-cell analysis

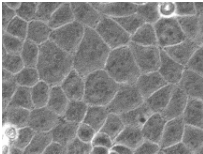
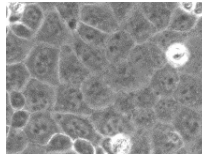
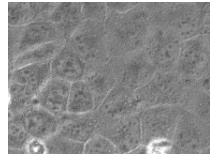
Compared to the population based experimental setup which is an averaging technique, the single-cell based experimental approach allows an insight into the distribution of parameters among individual cells.

5.2.2.1 Selection of clonal MDCK cell populations

Performing single-cell experiments for each clonal MDCK cell population was no option. Nevertheless, it was necessary to analyze more than one clonal MDCK cell population in order to see tendencies. The limited temporal throughput of single-cell experiments (paragraph 4.2.2.2) on the one hand, and the requirement to run three independent experiments to obtain a high sample size on the other hand led to the selection of two clonal MDCK cell populations.

To select these two clonal MDCK cell populations, neither there were outstanding clonal MDCK cell populations identified in terms of virus titers nor did the cell morphology provide a substantial criterion (lacking a linkage to the virus titers). In contrast, the individual clonal MDCK cell populations could be divided into two groups according to their cell number and cell diameter when cultivated in 6-well plates (these growing to high cell densities forming small cells and those growing to low cell densities forming large cells) (paragraph 5.1.3). This correlation was consistently observed during passaging (Figure 5-7) and within the infection experiments. Additionally, the two clusters of clonal MDCK cell populations could be recovered when plotting the cell-specific virus titer against the cell diameter (small cells producing a low cell-specific virus titer and large cells producing a high cell-specific virus titer) (Figure 5-15 A). Thus, the two clonal MDCK cell populations to analyze at the single-cell level were picked from each of the two clusters, namely one of those forming the smallest cells (clone 8) and one of those forming the largest cells (clone 26). Their features and those of the parental MDCK cell population obtained so far are summarized in Table 5-2.

Table 5-2: Features of clone 8, clone 26 and the parental MDCK cell population. All features obtained on 6-well plates; photos for morphology taken after 2 d of growth (40x magnification); cell diameter and density measured after 7 d of growth; n=3 (independent experiments); cell-specific virus titers produced by IAV-infected cell populations (MOI 10, 12 hpi, $1 \cdot 10^6$ cells were seeded in 6-well plates 24 h prior to infection; cell counts at 12 hpi were used for calculation of cell-specific titers) (paragraph 5.2.1.1); PFU: plaque-forming units.

Feature	Population		
	Clone 8	Parental	Clone 26
morphology at confluency			
average cell diameter [μm]	12.2	13.6	15.7
average cell density [cells/well]	$6.57 \cdot 10^6$	$4.9 \cdot 10^6$	$2.51 \cdot 10^6$
average cell-specific virus titer [PFU/cell]	650	844	1029

Each of the three MDCK cell populations were infected with influenza A virus using the same preset infection parameters as in population studies (MOI 10, 12 hpi) according to Heldt and Kupke et al. (2015). The cells were infected one day post seeding of $1 \cdot 10^6$ cells when confluency was reached (exponential growth phase expected) As an exception, the clone 26 population was seeded at a density of $0.5 \cdot 10^6$ cells since it otherwise would reach the stationary growth phase. The clonal and parental populations were analyzed at the single-cell level. Therefore, the infected cells were diluted and seeded on a 384-well plate. The virus yield was determined by plaque assay which counts the number of infectious virus particles released into the supernatant. Furthermore, the intracellular vRNA levels (copies per cell) of two genome segments (segment 5 and segment 8) were determined by vRNA- and segment-specific reverse transcription and quantitative realtime PCR. For each population the results of three independent experiments (n=3), each analyzing about 40 single cells were pooled.

5.2.2.2 Analysis of the virus yield

The frequency distributions of virus yields produced by the single cells of each population are shown in Figure 5-16 A-C. There is also a proportion of non-productive cells in each population as shown by the extra bars on the left of the histograms. Each of the distributions roughly spans three orders of magnitude and can be considered as broad distributions. Indeed their shapes are similar as they are positively skewed displaying many low-productive but few high-productive cells and thus resembling a lognormal distribution.

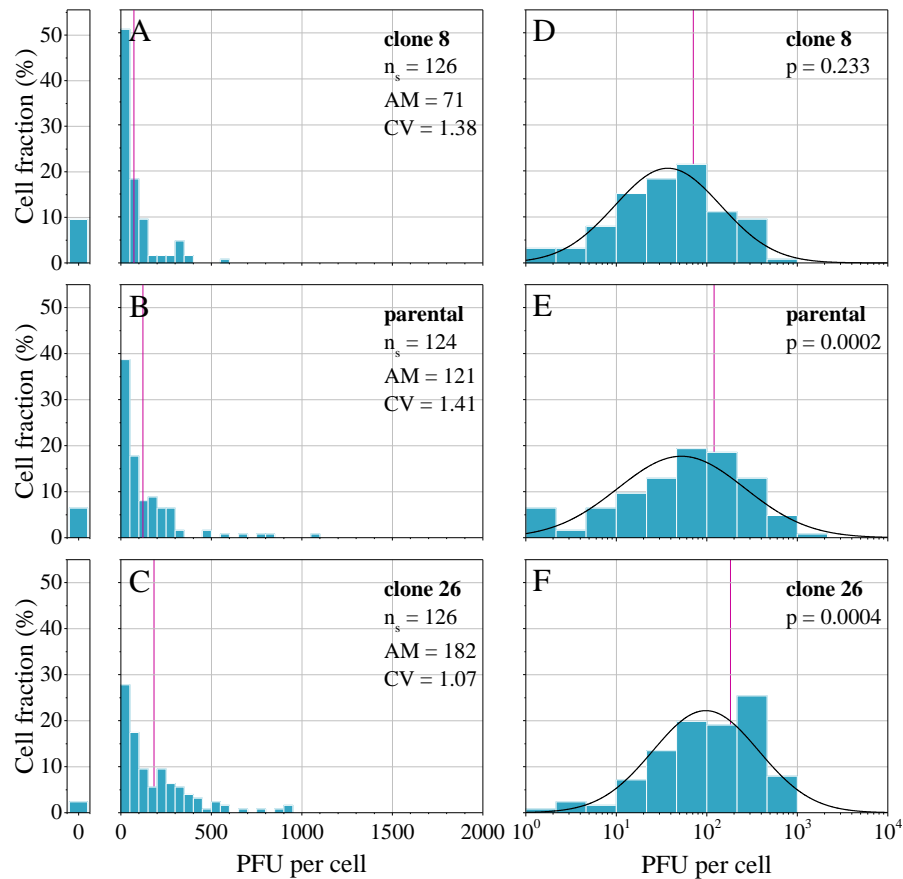


Figure 5-16: Distribution of the virus yield expressed as plaque-forming units (PFU) per cell on a linear (A-C) and logarithmic (D-F) scale produced by IAV-infected (MOI 10, 12 hpi) single cells of different MDCK cell populations: clone 8 (A,D), parental (B,E) and clone 26 (C,F); the first bar on the left indicates the number of non-productive cells (0 PFU); data were pooled from independent experiments ($n=3$); the number of analyzed cells is indicated as n_s ; the vertical line indicates the arithmetic mean (AM); the coefficient of variation is indicated as CV; lognormal distributions are fitted to the data (solid lines in D,E,F); p -value indicates the result of Shapiro-Wilk normality test on logarithmized data.

However, the virus yield distributions of the distinct populations are distinguishable by several features that can be shown by reference to the particular results (Figure 5-16). For instance, the fraction of cells producing less than 50 PFU is increased when using the clone 8 population (51 %) and is decreased when using the clone 26 population (28 %) in comparison to the non-clonal population (39 %). The same tendency can be obtained with the fraction of unproductive cells. Conversely, the fraction of cells producing at least 500 PFU is decreased when using the clone 8 population (0.8 %) and is increased when using the clone 26 population (8 %) in comparison to the parental population (4 %).

Distributional location

The indications mentioned above contribute to the value of the arithmetic mean of the virus yield per cell as a distributional location parameter (vertical lines in Figure 5-16). By reference to the particular results, the arithmetic mean is lower when using the clone 8 population (71 PFU/cell) and higher when using the clone 26 population (182 PFU/cell) in comparison to the parental population (121 PFU/cell). These trends are supported by the location of the frequency distributions of virus yields on a logarithmic scale shown in Figure 5-16 D-E. The distributions resemble normal distributions. Using the clone 8 population shifts the distribution of the parental population to the left while using the clone 26 population shifts it to the right.

In Figure 5-17 the virus yield distribution data are presented as a box plot chart on a logarithmic scale. The box covers the interquartile range from the first quartile to the third quartile, divided by a solid line indicating the median. Additionally the arithmetic mean is indicated by a dashed line. The ends of the whiskers represent the minimum and maximum of the data, where the minimum is in any case 0 PFU/cell (not defined on logarithmic scale).

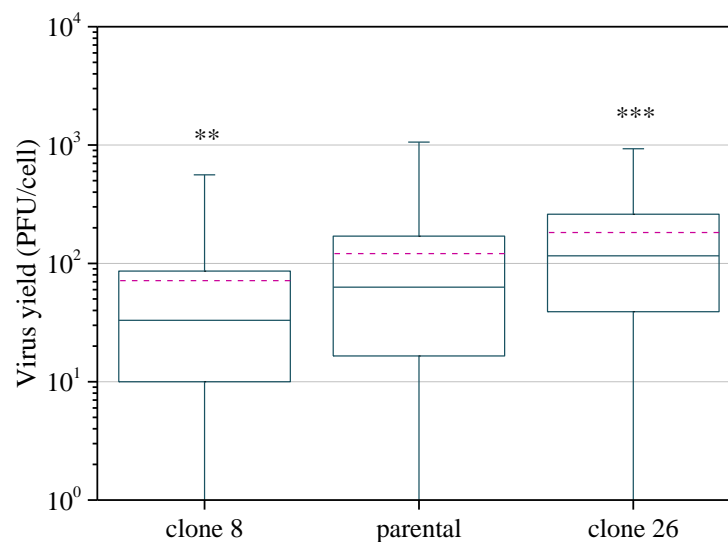


Figure 5-17: Boxplot of virus yield expressed as plaque-forming units (PFU) per cell produced by IAV-infected (MOI 10, 12 hpi) single cells of different MDCK cell populations; logarithmic scale; non-productive cells included; hinges cover 25 to 75 %, whiskers mark min-max range; lines within boxes show median (solid) and arithmetic mean (dashed); data were pooled from independent experiments (n=3); the median of clone 8 or clone 26 is significantly lower (** $p \leq 0.01$) or higher (***) $p \leq 0.001$) than the median of non-clonal cells according to Mann-Whitney U test.

The Mann-Whitney U test (one-tailed), a nonparametric hypothesis test comparing the median values of two samples, confirmed statistically significant the assumption that the cells of the clone 8 population produce a lower and that the cells of the clone 26 population produce a higher virus yield than the cells of the non-clonal population (indicated by asterisks in Figure 5-17).

This finding agrees well with the outcome of the population-based experiment which identified clonal populations of smaller cells as slightly lower and clonal populations of bigger cells as slightly higher cell-specific producer in comparison to the non-clonal MDCK cell population (Figure 5-14). A one-tailed two-sample t-test, retrospectively performed on the data from the former experiments (paragraph 5.2.1.1), confirmed statistically significant ($p < 0.05$) that the average cell-specific virus yield, expressed as PFU/cell, is lower than that of the non-clonal population when using the clone 8 population. However, there was no statistically significant confirmation that the reverse case applies when using the clone 26 population.

Strikingly, there is a huge difference (factor 6 to 9) between the average cell-specific virus yields obtained at the population level and the arithmetic mean cell-specific virus yields obtained at the single-cell level for each of the analyzed MDCK cell populations. Possible reasons for this are provided in the discussion. Nevertheless, comparing the analyzed populations with each other, there is factor 0.8 (population level) or factor 0.6 (single-cell level) between the non-clonal and the clone 8 population and factor 1.2 (population level) or factor 1.4 (single-cell level) between the non-clonal and the clone 26 population. The latter numbers stress the reproducibility of the relative cell-specific virus yields of different clonal MDCK cell populations in comparison to the non-clonal one, regardless of performing the analysis either at the population or at the single-cell level. Thus, the experimental setup for single-cell analysis can be considered valid for the analysis of different (clonal) MDCK cell populations.

Distributional dispersion

After having shown the differences in distributional location, that is the average virus yields produced by single cells of different MDCK cell populations, the next step is to analyze the distributional dispersion, which is the final aim of the present master thesis.

The distributions of virus yields produced by the single cells of each population appear not to be distinguishable regarding the histograms (Figure 5-16 D-F), since the shape of the histograms resembles each other. This is a first graphical hint, that the cell-to-cell variability in virus replication does not differ much among the two tested clonal MDCK cell populations in comparison to the parental one. Regarding the interquartile ranges on a logarithmical scale (Figure 5-17), there seems to be a slightly lower dispersion among the clone 8 cells and an even lower dispersion among the clone 26 cells, respectively compared to the parental cells. This tendency did also apply on the coefficient of variation (CV) given in Figure 5-16 A-C, which was considered as a measure of dispersion. There seems to be a high difference between the parental (1.41) and the clone 26 cell population (1.07). But, this difference fades knowing the

fluctuations within the three independent experiments. In particular, the CV values on the virus yield fluctuated between 0.94 and 1.31 within a single experiment, respectively, using the parental cell population.

To get a more reliable statement, the Siegel-Tukey test, a nonparametric hypothesis test comparing the variances of two samples, was employed. Using the original data, the variance of the virus yield within the clone 8 population was not confirmed statistically significant different from (or smaller than) that of the parental population at 5 % level. Similarly, it was not for the clone 26 population.

These results indicate, that the cell-to-cell variability in terms of the virus yield produced by influenza A virus infected single cells does not depend on the MDCK cell population used.

5.2.2.3 Analysis of the intracellular vRNA content

The frequency distributions of intracellular vRNA levels of segment 5 and segment 8 occurring in single cells of each population are shown in Figure 5-18 on a logarithmic scale. Since the qPCR method is limited in sensitivity, the distributions are left-censored at the values below the detection limit. The distributions of vRNA levels are even broader than that of the virus yields and span at least three orders of magnitude, whereby there are many cells containing a low amount of vRNA and few cells containing a high amount of vRNA (distributions on linear scale not shown). The thus positively skewed distributions appear to be deviated from lognormal behavior which was partially confirmed by Shapiro-Wilk normality test performed on the logarithmized data (p-values indicated in the boxes in Figure 5-18).

Distributional location

A first view to the distributions of the intracellular vRNA levels of either segment (Figure 5-18) does not indicate great differences of the central tendency among the tested populations: The distributions of the vRNA levels on logarithmic scale do not appear to be shifted to the left or to the right comparing the populations with each other. However, the shapes of the histograms are not identical. The arithmetic mean of the vRNA levels as a distributional location parameter, also does not allow any conclusion on differences among the populations.

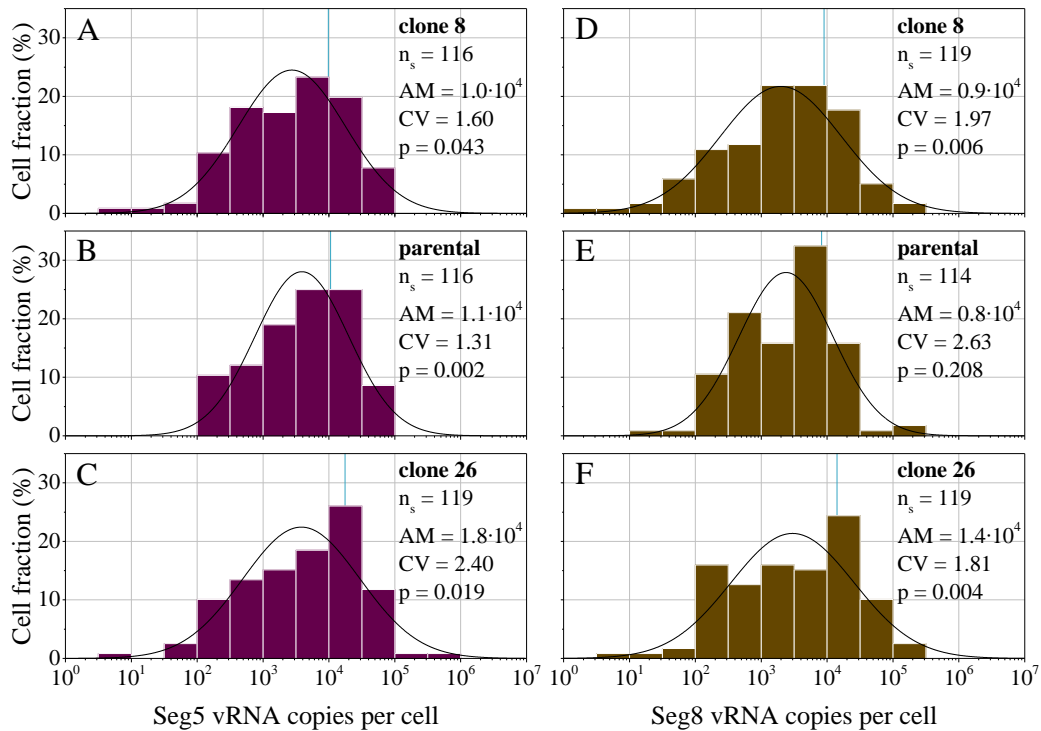


Figure 5-18: Distribution of the number of segment 5 (A,B,C) and segment 8 (D,E,F) vRNA copies per cell on a logarithmic scale produced by IAV-infected (MOI 10, 12 hpi) single cells of different MDCK cell populations: clone 8 (A,D), parental (B,E) and clone 26 (C,F); the vertical line indicates the arithmetic mean (AM); data were pooled from independent experiments ($n=3$); lognormal distributions are fitted to the data (solid lines); p -value indicates the result of Shapiro-Wilk normality test on logarithmized data.

By reference to the particular results, the cells of clone 8, the parental population and clone 26 averagely contained $1.0 \cdot 10^4$, $1.1 \cdot 10^4$ and $1.8 \cdot 10^4$ segment 5 vRNA copies per cell and $0.9 \cdot 10^4$, $0.8 \cdot 10^4$ and $1.4 \cdot 10^4$ segment 8 vRNA copies per cell, respectively. In comparison to the large broadness of the distributions these amounts are close to each other and in the same order of magnitude.

In Figure 5-19 the vRNA level distribution data are presented as a box plot chart on a logarithmic scale with the same specifications as described earlier. As well as the arithmetic means, the medians differ only slightly between the parental population and the clonal populations. The latter was confirmed by the Mann-Whitney U test to be a result of chance but not statistically significant at 5 % level (indicated by ns (not significant) in Figure 5-19). Thus, the differences in the average virus yield do not apply to the average vRNA content of the single cells of different populations.

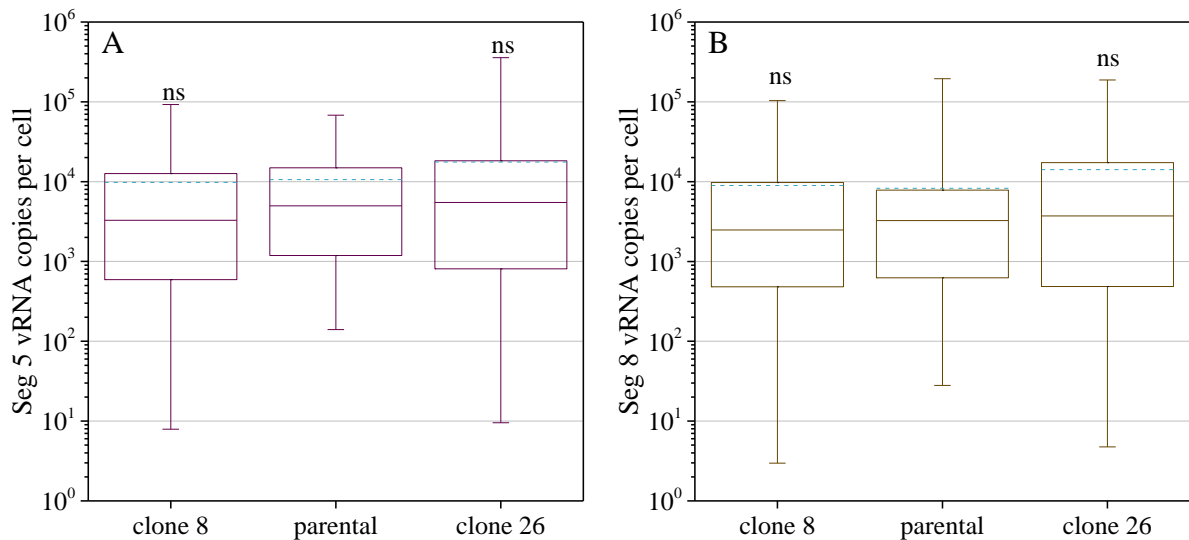


Figure 5-19: Boxplot of the number of segment 5 (A) and segment 8 (B) vRNA copies per cell produced by IAV-infected (MOI 10, 12 hpi) single cells of different MDCK cell populations; logarithmic scale; hinges cover 25 to 75 %, whiskers mark min-max range; lines within boxes show median (solid) and arithmetic mean (dashed); data were pooled from independent experiments (n=3); for both, segment 5 and segment 8 vRNA levels, the median of clone 8 and clone 26 is not significantly (ns) lower or higher than median of non-clonal cells according to Mann-Whitney U test ($p > 0.05$).

Distributional dispersion

As mentioned before, the distributions of intracellular vRNA levels span at least three orders of magnitude and can even exceed four orders of magnitude (Figure 5-18). Thereby, the distributions belonging to either clonal cells appear to be broader than those belonging to the parental cells for both, segment 5 and segment 8. The same tendency is shown by the box plot charts (Figure 5-19). The whiskers (absolute ranges) and the interquartile ranges belonging to the parental cells are shorter than those belonging to either clonal cells, implying a somehow lower dispersion of the former.

However, the CV values given in Figure 5-18 as a measure of dispersion for each distribution do not support this. The previously seemingly smallest distribution, which is the intracellular segment 8 vRNA content in parental cells, is characterized by the overall highest CV (2.63). In contrast, the CV of the equivalent segment 5 distribution is the overall lowest one (1.31). However, this discrepancy should not be overemphasized since the CV values obtained within each of three independent experiments of an individual setup were not found to be consistent. For example, the CV values on the segment 8 vRNA levels fluctuated between 1.53 and 2.77 within a single experiment, respectively, using the parental cell population (data not shown). Again, the Siegel-Tukey test was employed. It did not confirm significantly different variances on 5 % level based on the original data. According to that, the variances of the intracellular

segment 5 or segment 8 vRNA level distributions are similar between the clonal and the parental MDCK cell populations.

These results indicate, that the cell-to-cell variability in terms of the vRNA content in influenza A virus infected single cells does not depend on the MDCK cell population used.

6 Discussion

Influenza A virus infection of MDCK cells underlies a large cell-to-cell variability in terms of the production of vRNA and propagable virus particles (Heldt and Kupke et al., 2015). It is also known that the MDCK cell line comprises a heterogeneous pool of non-clonal cells that differ in morphological as well as functional features, such as influenza virus replication (Liu et al., 2010; Lugovtsev et al., 2013). The present study is the first to combine both phenomena by analyzing the cell-to-cell variability in IAV replication among clonal MDCK cells.

Originating from a non-clonal MDCK cell population, 31 clonal MDCK cell populations were generated. Apart from morphological differences, they were basically classified into populations of small cells growing to high cell densities and populations of big cells growing to low cell densities in the stationary growth phase (Figure 5-7).

At the population level, there were apparently no significant differences in the volumetric virus titers produced by the IAV infected (MOI 10) clonal MDCK cell populations at 12 hpi (Figure 5-9 to Figure 5-11). However, the populations of small cells yielded a significantly lower average cell-specific total virus yield than populations of big cells at 48 hpi when infected in the stationary growth phase (MOI 10) (Figure 5-14). By implication, the cell size and cell density of the respective cones in combination with their cell-specific virus titers result in similar total cell volumes producing similar volumetric virus titers.

At the single-cell level (MOI 10, 12 hpi), using two clonal MDCK cell populations that represented small cells and big cells, accordingly low and high virus yields were produced per cell (Figure 5-17). Though, the cell-to-cell variability in terms of the intracellular vRNA level and the virus yield was similar regardless of taking the parental or the non-clonal cell populations as a basis (Figure 5-16 and Figure 5-18). As a conclusion, the clonal heterogeneity of the MDCK cell population does not contribute to the large cell-to-cell variability in influenza A virus replication.

6.1 Clonal MDCK cell populations

The heterogeneity within the parental MDCK cell population should be represented by the individual clonally derived cell lines. The clones, in turn, should ideally comprise homogeneous cell populations. Therefore, the cloning procedure aimed to reducing heterogeneity of the cell line.

Cloning to reduce heterogeneity

The successively established cloning protocol included the limiting dilution technique, the propagation and the expansion. The limiting dilution technique enabled the isolation of single cells and owing to early and ongoing microscopic monitoring provided a very high certainty of clonality. The propagation from single cells to widespread colonies taking two to four weeks, however, implied a notable loss of clones. Indeed, the cloning efficiency was comparatively low (less than 20 %). The use of conditioned medium, which has been reported elsewhere to improve cell proliferation at low densities (Clarke et al., 2011; Maldonado and Meléndez-Zajgla, 2007; Zhu and Yang et al., 2012), did not show a positive effect. Alternatively, the cloning medium may be enriched with growth factors or other growth-enhancing substances or additional FBS but altered environmental conditions in turn may change the phenotype of the cells (Clarke et al., 2011). A reduced exposure time of the cells outside the incubator during microscopy should definitely advance the cells wellness, but the clonality must still be ensured. Even if a clonal cell population derived from a single cell is considered to consist of genetically identical cells, nevertheless, mutations and epigenetic changes may occur over time and potentially reintroduce heterogeneity (Clarke et al., 2011). This is why the cryopreservation of the clonal populations was done as early as possible. To obtain a population in an order of 10^7 cells (which is needed for cryopreservation) from a single cell, about 25 cell division rounds (generations) are necessary assuming an ideal geometric growth and the cells were passaged at least three times during propagation. Overall, the expansion of the clonal cell populations up to 75 cm² flasks took from barely two weeks up to more than five weeks, depending on the proceeding of propagation. Moreover, the time between thawing and carrying out the infection experiments was kept as short as possible. Indeed the short term genetic stability of clonal or non-clonal MDCK cells has, to the best of our knowledge, not been reported yet, but long term culture (several months) of different MDCK cell strains has been found to alter the chromosome content which illustrates the possible drift of the populations (Cassio, 2013). Nevertheless, the particular morphological and functional stability of selected clonal MDCK cell populations over several or more than 50 passages has been shown (Gekle et al., 1994; Meier et al., 1983). Multiple rounds of cloning (recloning) may help to eliminate the trait of recurring heterogeneity (Clarke et al., 2011). In some cases, such like ensuring the long term suitability of MDCK cell clones for vaccine production as investigated by Liu et al. (2010), this is a necessity. Unlike this, for the present thesis the approach was not followed since a basic understanding of variability in influenza virus replication in MDCK cells was aimed, nevertheless keeping the option of recloning candidates of particular interest.

Morphological characteristics

During the spread of the clonal MDCK cell populations in the early cloning phase, the cell morphology was predominated by different spreading strategies, such as elongated cells, flattened cells and detaching cells. The biological meaning of cell adhesion and motility includes morphogenesis, wound healing and tissue homeostasis (Pietuch and Janshoff, 2013). Since these characteristics were found in all clones in low cell density scenarios, the spread and the respective cell morphologies were not considered a clone-specific characteristic. In contrast, different morphological features were found among the clones at subconfluent conditions during the expansion of the clonal cell populations. According to the cell shape, the colony formation, the motility and the propagation, the clones were assigned to four types, A-D (Table 5-1 and Figure 5-5). Type A and B were similarly composed of round and fusiform individual cells forming loose and homogeneously propagating colonies. Type B additionally contained elongated cells with pseudopodial extensions and scatteredly some flattened cells in association with a highly motile phenotype. In contrast, type D had a completely different morphology as the cells formed dense, nonmotile clusters resulting in a tight arrangement of polygonal cells. Type C combined characteristics of both, type B (scatteredly flattened cells) and type D (focal points of increasing density). The parental MDCK cell population, in turn, displayed morphological features of either type defined before, mainly comprising a type A like morphology. This morphological heterogeneity inherent in the parental population therefore could be represented by the clones of distinct types.

Overall, similar morphological types of subconfluent clonal MDCK cells have been described in the literature earlier. Type A and B resemble the motile clones with flattened cells (such like R and D) whereas type D resembles the nonmotile clones with cuboidal cells (such like L and M) described by Meier et al. (1983) who examined the expression of cell surface receptors by different clonal MDCK cell populations. The parental MDCK cell line used for that study (obtained from ATCC) displayed both, a motile and a nonmotile phenotype. Since the clones were observed to be morphologically stable for more than 50 passages, the authors concluded that various cell types are inherent in the parental MDCK cell line rather than they have arisen by dedifferentiation or mutation (Meier et al., 1983). The same parental MDCK cell line has been used by Nakazato et al. (1989) to obtain clonal cell lines for biochemical and hormonal investigations. Accordingly, two similar morphological types were described, first motile clones with an extended and flattened cells (resembling type A and B) and second nonmotile clones with cuboidal cells (resembling type D). Using a different parental MDCK cell line, Webb et al.

(1996) found the same to form tight, discrete colonies (resembling type D) whereas the therefrom clonally derived MDCK-1 cell line displayed a semi-scattered morphology (resembling type A and B). The authors showed the response of both cell lines on the hepatocyte growth factor inducing the cell scattering (Webb et al., 1996). As the literature cited here does not attribute the specific clones to MDCK strain I or strain II cells, the clones of type A-D of the present thesis cannot be definitely classified according to this nomenclature. Nevertheless, consulting the morphological characteristics described by Richardson et al. (1981) and Nichols et al. (1986), type A and B were assumed to match strain I and type D to match strain II, whereas type C remains an intermediate type that most resembles type D and thus strain II after the initial formation of focal points.

Strikingly, the previously made attribution of the 31 clones to type A-D or strain I and II under subconfluent conditions did not apply to confluent cultures lacking a distinguishable morphology. A similar observation was made by Nakazato et al. (1989) as the morphological differences between motile and nonmotile clones became indistinct. However, in the literature, strain I and II or resembling MDCK cells have been clearly distinguished according to their morphology, especially at confluency. MDCK strain I or type-1 cells are described as flat and polygonal with small intercellular spaces and clearly visible nuclei. MDCK strain II or type-2 cells, in contrast, are described as high and cuboidal with clearly distinguishable intercellular spaces and almost invisible nuclei (Gekle et al., 1994; Lugovtsev et al., 2013). Contrary to these distinct strain-specific characteristics, both phenotypes were present in one and the same clone in the framework of the present thesis. Since this was observed for each of the 31 clones as well as for the parental MDCK cell population, it was not considered an exception but was found to follow a pattern with a strain I-like morphology in the center of the cultivation vessel and a strain II-like morphology in the peripheral regions (Figure 5-6). This specific phenomenon has, to the best of our knowledge, not been described before. One possible explanation may be the effect of light scattering in phase contrast microscopy which also depends on the focal plane. In this case, a physical artifact would be responsible for the (mis)judgment. Otherwise, the coexistence of both phenotypes in one and the same monolayer of any clone would challenge the hitherto opinion of clone-specific morphologies. Rather, the morphology may depend on the cell aging and density. For instance, the oldest cells may be located in the center whereas the peripheral cells may keep on proliferating. This concept is related to the various population contexts (Snijder et al., 2009), such as sparsely or densely populated areas of the culture vessel, but regarding the complete monolayer. Nevertheless, it remains unclear, why pure phenotypes have been observed for clonally derived MDCK cell strains before.

In conclusion, the particular observations made in the context of the present thesis would prefer the morphological classification of MDCK cell lines based on subconfluent rather than confluent conditions. Nevertheless, classifying specific (clonal) MDCK cell populations according to their morphology should be done with caution. As discussed before, the features are not consistently found in the cell lines over time and local differences occur. Yet, evidence for the differentiation of (clonal) MDCK cells over time and depending on the cell culture conditions has been shown in the study of Kersting et al. (1993). As a result, the morphology was not considered a specific and substantial criterion for the classification of clonal MDCK cell populations in the present study.

Growth characteristics

Instead of morphological characteristics, growth characteristics turned out to suit for distinguishing the clones. Admittedly, dynamic parameters were not recorded in the framework of the present thesis but by a different examiner (results not discussed here). Instead, the simple endpoint analysis of cells allowed a classification of the MDCK cell clones. To base this classification on the measurements at 7 d post seeding was accounted to be the most indiscriminating way as the clonal MDCK cell populations were very likely to be all in the stationary growth phase. This is deduced from the growth kinetics data of the parental MDCK cell line performed under similar conditions in this lab which displayed a stationary growth phase at three to eight days post seeding (Rehberg et al., 2013). In the stationary growth phase, the cell count and the cell size are assumed to be constant which allows a reliable measurement of these parameters and thus makes the individual populations comparable in this respect.

The classification of the MDCK cell clones resulted in two clusters: these clones which grow to high cell densities forming small cells and those clones which grow to low cell densities forming big cells. An outstanding growth characteristic was found for clone 27 which grew to the lowest cell density forming the biggest cells. (Figure 5-7).

In most studies of MDCK cell clones the cell size has not been provided but Barker and Simmons (1981) stated a significantly different cell volume between clones derived from low passages (1.3 pL) and high passages (1.7 pL) after trypsinization. By indirect inference, assigning low passage clones to strain I and high passage clones to strain II (Richardson et al., 1981), the clones of small cells may preferentially belong to the strain I and the clones of big cells may preferentially belong to the strain II MDCK cells.

The parental MDCK cell population displayed an intermediate position regarding both, the cell diameter and the cell density. This means that the two subpopulations within the parental population lead to an average cell density and cell diameter. Therefore, the clones reflect the heterogeneous character of the parental population not just in terms of the subconfluent morphology (see morphological characteristics) but also in terms of the growth characteristics. However, both did not emerge to be linked to each other as the morphological types and the clusters derived from the growth characteristics comprised different sets of clones.

Reflecting the presence of small cells and big cells (capable to grow to high or low cell densities, respectively) in the heterogeneous parental MDCK cell population, it seems to be contradictory. Virtually, one would expect the small cells at high cell densities to overgrow the big cells at low cell densities. Indeed, both coexist, though. The missing link is the total cell volume. As the low volume of small cells multiplies with a high cell number and the high volume of the big cells multiplies with a low cell number, the resulting total cell volume of either type is similar preventing a unidirectional overgrowth. This coherence is shown in Figure 5-8.

A correlation between the cell number and the average cell diameter or cell volume is obvious during the growth of the cells and has been shown by Erlinger and Saier (1982) with MDCK cells. More precisely, the cell volume of MDCK cells has been shown to decrease as the cells passed from a sparse to a highly confluent state (Erlinger and Saier, 1982). In contrast to that dynamic consideration, in the context of the present thesis the cells were finally analyzed solely at the stationary growth phase where the cell size and number were assumed to be dynamically constant due to the limited growth area. Indeed, it is not unusual that the final cell numbers might differ among cultivations inoculated under the same conditions (Rehberg et al., 2013). But the two clusters of MDCK cell clones with either small cells or big cells were consistently found over several passages and were even met after freezing and thawing. Thus, the maximum cell density or minimum cell size seems to be a clone-specific parameter and therefore an interesting phenomenon. The *in vivo* physiological regulation of the cell size of renal collecting duct cells, despite the cell cycle, occurs by a special mechanism. The cilia on the apical cell surface detect the urine flow and subsequently negatively regulate the cell size. As a result, abnormal non-ciliated cells are bigger than normal ciliated cells (Boehlke and Kotsis et al., 2010; Lloyd, 2013). But as this cell size regulation depends on a liquid flow, and static cultures are used for the culture of MDCK cells, this does not explain the preferential formation of small or big cells *in vitro*. Nevertheless, non-ciliated cells have been observed among the heterogeneous MDCK cell population in the past and were assigned the strain I MDCK cells but were not necessarily bigger than strain II MDCK cells (Hansson et al., 1986; Nichols et al., 1986; Valentich, 1981).

However, the presence or lack of cilia was not analyzed for the 31 clonal MDCK cell populations of the present study. The dynamical constancy of the cell size in the stationary growth phase (as, for instance, shown by Rehberg et al. (2013)) can be dedicated to the physiological homeostasis of the cell size. Since the cell size regulation in asynchronous mammalian cell populations and size regulators inherent in the cells are not completely understood yet (Tzur and Kafri et al., 2009) it is not further discussed here. Studying the growth kinetics of the clones could help to understand the differences among both clusters of clones and therefore the underlying principle.

Number of clonal MDCK cell populations to be investigated

The number of clonal MDCK cell populations to be investigated is critical in order to see and evaluate differences in their characteristics. Even if the group of Liu et al. (2010) was able to generate 2500 MDCK cell clones whereas the group of Lugovtsev et al. (2013) isolated as little as 10 MDCK cell clones, both for influenza virus infection studies, a total number of 31 clonal MDCK cell populations was considered sufficient for the screening purpose within the framework of the present thesis. Inevitably, there is a fraction of clones that failed to propagate (low cloning efficiency) and thus there happened an unwanted selection of clones that are able to cope with low cell density scenarios. This fraction was not included in the subsequent investigations and its characteristics remain unknown. On the one hand, this may lead to an incomplete representation of the heterogeneity within the MDCK cell population regarding the characteristics and the average virus yield on population based virus infection experiments (for a closer look see paragraph 6.2.1). On the other hand, this apparently does not affect the outcome of the single-cell experiments which aim to reveal the cell-to-cell variability. Generally, either the cell-to-cell variability in virus replication is reduced when using clonal cells for virus infection (in this case, the clonal heterogeneity of the MDCK cell population contributes to the cell-to-cell variability) or it is not (in this case, other factors than the clonal heterogeneity account for it). That should not depend on which clone to be regarded. This is also why as little as two clonal MDCK cell populations were selected for the comparison of their virus yield distributions among single cells with that of the non-clonal population (for a closer look see paragraph 6.2.2).

6.2 IAV infection of clonal and parental MDCK cell populations

The clonal MDCK cell populations provide a valuable source to analyze the contribution of the clonal heterogeneity of the MDCK cell population to the cell-to-cell variability in IAV

replication. Performing screening experiments at the population level was not only a necessary milestone for this, but also showed the (low) potential of clonal populations to increase the virus yield in virus production processes. The single-cell approach finally revealed the largely remaining cell-to-cell variability in spite of the supposed reduction in heterogeneity in the MDCK cell population.

6.2.1 Screening at the population level

MDCK cells are known to produce high yields of IAV in comparison to other animal cell lines (Genzel and Reichl, 2009; Liu et al., 2009). As a possible strategy to further increase the virus yield, Liu et al. (2010) have demonstrated that the heterogeneity inherent in the MDCK cell population provides a large variation in the ability to produce progeny viruses among more than one thousand clones. This allows the selection of high productive clones for vaccine production. Additionally, evidence for a large variability in IAV replication among single cells of the MDCK cell population has been shown by Heldt and Kupke et al. (2015) and might be a result of clonal heterogeneity.

At the population level, IAV infection and screening for the virus yield of the 31 clones obtained from the same MDCK cell line as used by Heldt and Kupke et al. (2015) revealed a lesser variability in virus titers than expected. Indeed, the virus titers in the supernatant as well as the cell-specific virus yields of the clonal MDCK cell populations infected at MOI 10 at 12 hpi spanned a two- to four-fold range depending on the virus detection method (Figure 5-9 to Figure 5-11). This by far does not reflect the range of three orders of magnitude differences in PFU yielded by single cells of the parental MDCK cell population under similar infection conditions (Heldt and Kupke et al., 2015). In fact, a different virus stock of the same IAV strain (obtained from NIBSC) was used for the aforesaid study but the results of the single-cell experiments with the virus stock obtained from RKI revealed a similar cell-to-cell variability as shown in the present thesis. It is thus concluded that the relatively small clone-to-clone differences in virus yields cannot be the reason for the large cell-to-cell variability observed at the single-cell level. To prove this, single-cell experiments were performed with clonal MDCK cell populations (see paragraph 6.2.2).

Variability in virus titers across clonal MDCK cell populations

The total virus titers obtained from populations of the clonal MDCK cells IAV infected at exponential growth with MOI 10 and analyzed at 12 hpi were around $1 \cdot 10^{10}$ virus particles per mL (equaling approximately $2.7 \log_{10}$ HAU/100 μ L) and cell specific virus titers of around

$1 \cdot 10^4$ virus particles per cell were achieved. Infectious virus titers as well as titers of propagable virus amounted to approximately one tenth of the total virus titers (Figure 5-9 to Figure 5-11). All together, these are more or less typical quantities compared to titers obtained by other research studies and under production conditions (Frensing, Kupke and Bachmann et al., 2016; Genzel and Reichl, 2009).

The average total virus titer of all 31 clones was found to resemble the total virus titer averagely obtained from the parental MDCK cell population. This implies that the parental MDCK cell population is constituted of cells with slightly different virus yields which finally contribute to a stable average virus yield.

The more than 15-fold variability of infectious virus titers among more than 1200 clonal MDCK cell populations described by Liu et al. (2010) could, however, not be reproduced. Despite the fact that this group used a different strain of MDCK cells (obtained from ATCC) and different IAV strains, this is certainly a matter of the number of clones which were investigated (only one fortieth as much clones were investigated in the present thesis) as well as the infection conditions and the time point of analysis. A very low MOI of 0.001 was employed and the infectious virus titers were not analyzed until 3 days post infection in that study. These parameters, which were based on production conditions, allow not only multiple rounds of infection but also the further growth and afterwards apoptosis of the cells (making cell specific virus titers an uncertain parameter) and the loss of infectious virus yield (due to degradation). This is why for the present study, in accordance with the experimental approach used by Heldt and Kupke et al. (2015), the infection was realized at MOI 10 and virus yields were analyzed at 12 hpi which is also a time point of maximum cell specific virus production (Heldt et al., 2013).

The heterogeneity of the MDCK cell population has furthermore been investigated by Lugovtsev et al. (2013) regarding the applicability of clonal populations to influenza virus research. Studying, among others, the susceptibility of ten clonal MDCK cell populations to influenza different influenza virus strains revealed that not all clones were equivalent in supporting efficient multicycle replication of different H1N1 viruses. The group evaluated the permissiveness of the clones by comparative TCID₅₀ titration of reference viruses. The type-1 cells (resembling the strain I mentioned in paragraph 6.1) and the type-3 cells (segregated by the authors due to the formation of domes on the monolayer) mainly resulted in infectious virus titers in the same order as the parental population (Lugovtsev et al., 2013). Such large differences were possible since the TCID₅₀ titration included a period of seven days. A comparable experiment was not done with the clonal MDCK cell populations obtained in the framework of the present thesis. In contrast to the results of the permissiveness experiments, the

type-2 cells (resembling the strain II mentioned in paragraph 6.1) displayed significantly lower infectious virus titers of approximately one hundredth in the study of Lugovtsev et al. (2013). Conversely, representative type-1 cells produced lower infectious virus titers than type-2 clones when infected with an H1N1 virus strain at MOI $1 \cdot 10^{-6}$ in the presence of trypsin, but no virus titers were obtained with type-2 clones in the absence of trypsin (Lugovtsev et al., 2013). Such detailed studies were not performed with the clonal MDCK cell populations obtained in the framework of the present thesis but nevertheless, here again two groups of clones could be identified when consulting the growth characteristics described earlier.

Two clusters of clones

The screening of the clonal MDCK cell populations for the virus titers they produce when infected at exponential growth indicated similar cell-specific virus titers among the clones. The cell densities at infection time point were similar among the clones. By characterization of the clones at stationary growth phase, the occurrence of high cell densities (small cells) and low cell densities (big cells) was shown. Thus it was hypothesized that, when infected at stationary growth phase, these clones with high cell densities would produce higher volumetric virus titers than those clones with low cell densities, assuming a scalable cell-specific virus titer.

However, this hypothesis was not confirmed valid. Instead, the cell-specific total virus titers turned out to be more distinguishable under these infection conditions (MOI 10, 48 hpi) but not to be as similar as concluded from the previous screening experiments. The two clusters of clones were assigned low cell specific virus titers (small cell clones) and high cell specific virus titers (big cell clones) with a statistically significant two-fold difference of the respective average total virus titers among the cluster associates (Figure 5-14).

The single-cell approach employed by Heldt and Kupke et al. (2015) included the measurement of the cell size of IAV infected (non-clonal) MDCK cells and the amount of PFU produced by the cell, though no correlation was found between both parameters. But this not necessarily discounts the findings of the present thesis and vice versa. The cell size data which the previously described clusters of small cell clones and big cell clones are based on were population averages that thus represent an overall average cellular state. In contrast, the cell size determined in the course of the single-cell approach provides a snapshot of the individual cell, accounting not only for a specific clonal cell size but also for the cellular state, such as the current cell cycle stage (Boucrot and Kirchhausen, 2008; Heldt and Kupke et al., 2015). Furthermore, the cell-to-cell variability in virus yields shown by Heldt and Kupke et al. (2015)

was too high (spanning three orders of magnitude) as to allow the recognition of two-fold differences in virus yields (as indicated at the population level among small cells and big cells). Zhu et al. (2009) argue that “larger cells may provide more resources for biosynthesis than smaller cells” and that thus “the total yield of viral progeny from an infected cell may correlate with the size of the cell”. The group had performed single-cell analyses of vesicular stomatitis virus (VSV) infected baby hamster kidney (BHK) cells and indeed found a positive correlation between the cell size and the amount of PFU produced by the cell.

Potential of the clonal MDCK cell populations

The aim of the screening experiments was to reveal the variability in IAV yields among clonal MDCK cell populations. On the one hand, this served for assessing the potential of high yielding clones for improving the virus (and thus the vaccine) production process. Liu et al. (2010) claimed that the “biological cloning of MDCK cell lines is a useful approach to improve influenza vaccine productivity”. Indeed, the virus titer difference between the highest yielding clone and the parental MDCK cell population was low (less than two-fold) and thus not promising, likewise regarding the fluctuations of virus titers among replicated experiments. The prospect of slightly increased virus titers in the production process would not compensate the effort to be put in until the clonal population is ready for that (for instance, the adaption to serum-free medium), especially since the stability of the virus yield over several passages is not known.

Moving on to research applications, the clonal MDCK cell populations remain interesting. The screening of the virus titers among the clones helped to select candidates for the single-cell analysis, one individual representative of the small cell clones and the big cell clones, respectively. Moreover, the further characterization of the clonal MDCK cells, such as metabolic or genomic analyses, potentially contribute to the understanding of clonal heterogeneity.

6.2.2 Single-cell analysis

Two clonal MDCK cell populations, representing a small cell clone (clone 8) and a big cell clone (clone 26), were picked for single-cell analysis of IAV replication in comparison to the parental MDCK cell population. The cells were infected at MOI 10 and the number of PFU released per cell as well as the intracellular amount of vRNA segments were analyzed at 12 hpi.

Population-based experiment versus single-cell approach

Single-cell approaches separate single cells from a population and analyze specific parameters of the isolated cells. Similar conditions for single-cell analysis compared to population-based experiments should be ensured. Further, the behavior of the single cell should not be influenced by the experimental setup but resemble its behavior in the population context. Obviously, this is not completely realizable in single-cell approaches, but experiments comparing (means of) single-cell and population-derived measurements can confirm their feasibility.

The single-cell approach used in the present thesis was adapted from Heldt and Kupke et al. (2015) who confirmed “that the experimental procedure did not interfere with virus replication”. The authors showed that both, the virus yield and the intracellular vRNA levels were in the same order of magnitude when comparing the respective mean values. In the framework of the present thesis, there was a larger difference between the mean cell-specific virus yields obtained on population and single-cell level, but it still did not exceed one order of magnitude. A comparison of the intracellular vRNA level was not possible, as measurements were only performed at the single-cell level. Nevertheless, the single-cell experiments resulted in a similar ratio between the mean virus yields of the parental MDCK cell population and those of the clonal MDCK cell populations. Clone 8, which is characterized by small cells, produced an approximately 20 % (population) or 40 % (single cells) lower virus yield and clone 26, which is characterized by big cells, produced an approximately 20 % or 40 % higher virus yield than the parental cells. Not only in the present thesis but also in other comparative studies the cell-specific virus titer was determined higher at the population level than at the single-cell level (Heldt and Kupke et al., Akpinar et al., 2016; 2015; Schulte and Andino, 2014; Zhu et al., 2009). One possible reason for that may be the loss of virus titers due to unspecific adsorption of virus particles to the plastic surface. The surface area is disproportionately high in a small cavity containing a single cell in comparison to a dish containing one million of cells, for instance. In order to reduce this effect, Heldt and Kupke et al. (2015) used a non-binding 384-well plate for their single-cell approach. Another reason for the different cell-specific virus titers comparing population based and single-cell experiments may be the population context itself. Akpinar et al. (2016) measured the cell-specific yields of VSV produced by BHK cells at different cell densities. Basically, the lower the cell density was, the lower was the cell-specific virus titer. For instance, one single cell produced a 4-fold lower cell-specific virus yield compared to a population of about 10^4 cells. The authors suggest “that the presence of cell neighbors affects the physical state of an infected cell” and that, in contrast, “antiproliferative conditions associated with cell isolation [may be the reason for] the lower virus yields associated with isolated infected cells” (Akpinar et al., 2016).

Regarding the population context of a cell population in contrast to an isolated cell, the early studies of Rodriguez-Boulan and Sabatini (1978) and Rodriguez-Boulan et al. (1983) are also relevant. The group analyzed the polarized budding of virus particles from influenza virus infected MDCK cells attached to a surface in a population context or as an individual cell. In polarized monolayers of infected cells virus budding was found to take place at the apical surface (the medium facing site). After trypsinization, single cells in suspension lost their characteristic polarity (virus particles budded all over the cell surface). But the attachment to a surface triggered the reformation of the cellular polarity and virus particles were again found to bud from the apical surface (Rodriguez-Boulan et al., 1983; Rodriguez-Boulan and Sabatini, 1978). These findings indicate that the single-cell approach used in the present thesis allows a similar behavior of single cells and cells in a population context regarding the ability to release progeny viruses.

Cell size is associated with PFU but not with vRNA

Based on the growth characteristics of the clonal MDCK cells, two subpopulations were found, these clones with small cells growing to high cell densities and those clones with big cells growing to low cell densities. For single-cell analysis the most extreme representative of either group was selected, clone 8 (one of the clones with the smallest average cell diameter) and clone 26 (one of the clones with the biggest average cell diameter). At the population level, the screening of virus yields after IAV infection showed that the clones of small cells produced lower cell-specific virus titers and the clones of big cells produced higher cell-specific virus titers. The parental cells produced intermediate cell-specific virus titers. This tendency could be reproduced at the single-cell level and was confirmed statistically significant. Clone 8 yielded the lowest virus titer while clone 26 yielded the highest virus titer. The association of the cell-specific virus yield to the cell size was discussed before at the population level referring to Zhu et al. (2009). According to this, the resources for biosynthesis are limiting in the smaller cells.

At the single-cell level another aspect, the intracellular vRNA content, was considered. Both, clone 8 and clone 26 cells contained similar numbers of vRNA copies compared to the parental cells with no statistically significant difference. This was found for both vRNA segments that were analyzed, segment 5 (coding the NP protein) and segment 8 (coding the NS1 and NEP proteins). Thus, no association was found between the vRNA content and the virus yield. Schulte and Andino (2014), who analyzed the poliovirus replication in a HeLa cell line, also found that the infectious particle production is independent of the RNA production. Strikingly, in their studies the intracellular RNA content was different under different infection conditions but led to

a similar virus yield. The authors considered the differences in the nature of viral genome replication and virus particle production, arguing that the “replication is dependent on the polymerase , which [...] can be utilized repeatedly, while virion production is dependent on capsid proteins, which are continuously consumed during virion synthesis” (Schulte and Andino, 2014). Nevertheless, a similar conclusion can be drawn from the results of the present thesis, even if it may seem contradictory. It is assumed that the cellular resources are relatively rich in big cells and relatively sparse in small cells. Then, the vRNA replication may be seen as a process that is not restricted to cellular resources and thus can be carried out in small cells and in big cells in a similar manner. This may give an account for the similar distributions of intracellular vRNA copy numbers among single cells of all the populations analyzed. Further, the production of viral proteins may be seen as a process dependent on cellular resources, such as amino acids, and a much higher number of proteins than of vRNA is required for virus assembly. Assuming smaller cells to possess a lower quantity of cellular resources than bigger cells would limit them in the expression of viral proteins and thus lead to the release of fewer virus particles compared to bigger cells. This, in turn, may give an account for the shifted distributions of virus yields among the populations analyzed.

Apart from the limiting resources for protein production, there might be a second limiting factor that contributes to the lower virus yields of the small cells. For virus budding, parts of the host cell membrane are required since the virus envelop consists of the host cell membrane. As the surface of small cells is smaller than that of big cells, the budding surface may be limiting for the release of progeny viruses. Regarding the ratio of the cell size (diameter of suspended cells 12-16 μm) and the size of the virus particles (diameter approximately 100 nm), the availability of cell membrane for budding should not be the most limiting factor in virus replication. But nevertheless, the apical MDCK cell surface can be very crowded with budding influenza viruses as electron microscopy images, such as given by Rodriguez-Boulan and Sabatini (1978), indicate.

Cell-to-cell variability

Heldt and Kupke et al. (2015) have first revealed the large cell-to-cell variability among non-clonal MDCK cells regarding both, the virus yield and the intracellular vRNA content. The virus yield has been shown to range from 1 to 970 PFU per cell. Similarly, the intracellular vRNA levels have spanned three orders of magnitude (Heldt and Kupke et al., 2015). This extent of cell-to-cell variability also resulted from the single-cell experiments of the present thesis. The

virus yield as well as the intracellular vRNA levels spanned (at least) three orders of magnitudes (Figure 5-16 and Figure 5-18).

Large cell-to-cell variability is a common attribute of virus replication in cell lines and well illustrates that population averages incompletely represent the system. Several studies with different animal RNA viruses and hosts rely on single-cell analysis for virus infection studies and have demonstrated stochastic cell-to-cell variability in viral infections. For instance, the virus yield and the RNA content of 106 poliovirus infected cells of a HeLa cell line had spanned an up to 15-fold and 50-fold difference, respectively (Schulte and Andino, 2014). The virus yield of 192, 10 or less than 20 VSV infected BHK cells had spanned three orders of magnitude, an over 300-fold difference or one order of magnitude, respectively, in different studies (Akpınar et al., 2016; Timm and Yin, 2012; Zhu et al., 2009). Single Western equine encephalomyelitis virus infected chicken embryo cells had resulted in yields spanning two orders of magnitude (Dulbecco and Vogt, 1954). Different from the viruses mentioned before, the genome of the influenza virus is segmented which is thought to introduce an additional source of biological noise and thus an even larger heterogeneity during the virus replication (Heldt and Kupke et al., 2015).

The distributions of RNA and virus yields produced by single cells are commonly skewed to the left, meaning that the fraction of low-productive cells is high whereas the fraction of high-productive cells is low (Akpınar et al., 2016; Delbrück, 1945; Dulbecco and Vogt, 1954; Schulte and Andino, 2014; Timm and Yin, 2012; Zhu et al., 2009). In case of the intracellular vRNA levels in IAV infected single MDCK cells, a lognormal distribution has been described for most of the segments (Heldt and Kupke et al., 2015). However, the distributions of intracellular vRNA copy numbers among single cells obtained in the present thesis were mostly not distributed lognormally, although appearing to (investigating a bigger number of single cells might result in a better approximation of a lognormal distribution). Those skewed or lognormal distributions are generally widespread in nature and are directly linked to stochasticity (which is biological noise) in the underlying processes. The noise occurring in individual stages of a cascading process are multiplicatively effects is multiplicatively propagated (Koch, 1966; Limpert et al., 2001). For instance, all the stages of virus replication underlie random fluctuations and as a result the variability of possible outcomes is extremely high, which is reflected by the large cell-to-cell variability in intracellular vRNA copy numbers and virus yields.

Effect of clonal heterogeneity on cell-to-cell variability

The new information regarding cell-to-cell variability in IAV replication is that it is not only found in the heterogeneous parental MDCK cell population (as described by Heldt and Kupke et al. (2015)) but that also clonal MDCK cell populations are affected. In particular, the variances of the virus yield and the vRNA content were even confirmed not to be statistically significantly different comparing clonal and parental cells. As a result, the large cell-to-cell variability in IAV replication is not reduced when reducing the heterogeneity of the MDCK cell population by cloning. To put it in other words, the clonal heterogeneity does not contribute to the cell-to-cell variability in IAV replication.

Given the fact that a large cell-to-cell variability of IAV infection is present not only in the non-clonal MDCK cell population but also among clonal cells, this indicates the predominance of biological noise rather than the presence of different initial conditions. It has often been claimed that even among clonal populations, virtually composed of genetically identical cells, there is possibly variability in their behavior (Arriaga, 2009; Di Carlo et al., 2012; Pelkmans, 2012; Warrick and Timm et al., 2016).

Origin of cell-to-cell variability

In general, it is expected that cell-to-cell variability on the one hand has stochastic sources (which include intrinsic and extrinsic noise) and on the other hand may be deterministic and regulated (Pelkmans, 2012). In case of the IAV replication in single cells, several deterministic factors that may contribute to the large cell-to-cell variability have been taken into account by the study of Heldt and Kupke et al. (2015). The cell size (virtually associated with the cell cycle stage) as well as the diversity of the influenza A virus population and the presence of DIPs apparently did not affect the cell-to-cell variability. Additionally, the present thesis excluded the clonal heterogeneity of the host cell to be a major contributing factor. Finally, the question which else factors may play a role remains. Still, several more factors can potentially lead to cell-to-cell variability. For instance, such may be derived from the cellular component since heterogeneity can be present even in clonal cell populations (Arriaga, 2009; Di Carlo et al., 2012; Pelkmans, 2012; Warrick and Timm et al., 2016). This includes the regulatory and metabolic state of the cell, the cell cycle or apoptosis state, the expression level of involved structural and regulatory proteins and the availability of cellular resources for transcription and translation. Also, the antiviral state of the cell (innate immune response) and the present conditions for all individual stages of the replication cycle may play a role. In general, the interaction between the viral and cellular components (virus-host cell interaction) may influence the outcome of the infection.

Beyond that, the effective MOI underlying the Poisson distribution differs among the individual cells and thus may provide different conditions for the virus replication. Overall, the virus replication can be considered a multivalent system with multiple factors contributing to the outcome in a certain extent. Furthermore, the presence of stochasticity is likely to be an important factor. Heldt and Kupke et al. (2015) provide a detailed insight into the intrinsic and extrinsic noise present in IAV replication and its inferences for cell-to-cell variability.

7 Conclusions and outlook

From a parental MDCK cell population, 31 clonal populations were derived. These reflect the heterogeneity of the parental population. The morphological features did not allow a substantial classification of the clones. Instead, their growth characteristics when stationary growth phase was reached, enabled the identification of two subpopulations which were called small cells and big cells. A further characterization of the clones in terms of a comprehensive growth kinetic, the analysis of metabolites and a genomic analysis may help to understand the occurrence of both subpopulations. Possibly, also outstanding features could be inferred and benefits of specific clones in comparison to the parental population and the other clonal populations could be made use of.

One aim was to identify possible high or low yielding clones when screened for IAV replication at the population level. The achievable virus titers per mL apparently did not differ significantly among the clones employing two different infection protocols. Instead, the two subpopulations were distinguishable in terms of the cell-specific virus titer they produce. It is obviously associated to the cell size, small cells producing lower and big cells producing higher cell-specific virus titers. Nevertheless, this difference is too small as to be used for virus production processes aiming high virus yields. A further characterization of the IAV replication in the two subpopulations could potentially provide a better understanding for this, for instance regarding the localization of specific viral components in the cells. For this, a flow cytometry approach could be applied specifically staining distinct viral components. With those results, a strategy of manipulating cells could be derived, finally leading to an optimization of virus production.

The major aim was to reveal the contribution of the clonal heterogeneity to the cell-to-cell variability in IAV replication. At the single-cell level the virus yield and the intracellular vRNA content were compared using the parental cells and clonal cells, one representative out of both subpopulations. In accordance with the population based results, the clonal cells produced a lower or higher mean virus yield than the parental cells. In contrast, the mean vRNA contents of the cells of either population resembled each other. It can be assumed that the vRNA synthesis is not the limiting stage of IAV replication but that the availability of cellular resources for the virus particle production as well as the availability of host cell membrane for virus budding are limited by the cell size, but this hypothesis still has to be confirmed.

Regarding the distribution of the virus yields and the intracellular vRNA content among the single cells of either population, they were similar, spanning at least three orders of magnitude. By this, it was shown that the cell-to-cell variability remains the same, regardless of using

parental or clonal MDCK cells. It was inferred that the clonal heterogeneity of the MDCK cell population does not contribute to the large cell-to-cell variability in IAV replication. This was one more factor to exclude as the origin of cell-to-cell variability. The actual contributing factors still remain unknown, but the virus replication is considered a multivalent system with numerous variables that are not easy to account for. Additionally, biological noise it is likely to play an important role.

8 Bibliography

- Ackermann, W.W. and Maassab, H.F.** (1954). Growth characteristics of influenza virus. Biochemical differentiation of stages of development. *The Journal of Experimental Medicine*, **100**(4), 329-339.
- Akpinar, F., Timm, A. and Yin, J.** (2016). High-throughput single-cell kinetics of virus infections in the presence of defective interfering particles. *Journal of Virology*, **90**(3), 1599-1612.
- Arriaga, E.A.** (2009). Single cell heterogeneity Trans.). In: **Anselmetti, D.** (Ed.), *Single cell analysis. Technologies and applications.* (Ch. 11, pp. 223-234) Weinheim: Wiley-VCH.
- Arthur, J.M.** (2000). The mdck cell line is made up of populations of cells with diverse resistive and transport properties. *Tissue & Cell*, **32**(5), 446-450.
- American Type Culture Collection (ATCC)** (2016). Cells and microorganisms. Retrieved from https://www.lgcstandards-atcc.org/Products/Cells_and_Microorganisms, Accessed on November 24th, 2016.
- Audsley, J.M. and Tannock, G.A.** (2008). Cell-based influenza vaccines: Progress to date. *Drugs*, **68**(11), 1483-1491.
- Avital, G., Hashimshony, T. and Yanai, I.** (2014). Seeing is believing: New methods for *in situ* single-cell transcriptomics. *Genome Biology*, **15**(3), 110.
- Barker, G. and Simmons, N.L.** (1981). Identification of two strains of cultured canine renal epithelial cells (mdck cells) which display entirely different physiological properties. *Quarterly Journal of Experimental Physiology*, **66**(1), 61-72.
- Boehlke, C., Kotsis, F., Patel, V., Braeg, S., Voelker, H., Brecht, S., Beyer, T., Janusch, H., Hamann, C., Gödel, M., Müller, K., Herbst, M., Hornung, M., Doerken, M., Köttgen, M., Nitschke, R., Igarashi, P., Walz, G. and Kuehn, E.W.** (2010). Primary cilia regulate mtorc1 activity and cell size through lkb1. *Nature Cell Biology*, **12**(11), 1115-1122.
- Boucrot, E. and Kirchhausen, T.** (2008). Mammalian cells change volume during mitosis. *PLoS One*, **3**(1), e1477.
- Bouvier, N.M. and Palese, P.** (2008). The biology of influenza viruses. *Vaccine*, **26S**(4), D49-D53.
- Buckland, B.C.** (2015). The development and manufacture of influenza vaccines. *Human Vaccines & Immunotherapeutics*, **11**(6), 1357-1360.
- Burleson, F.G., Chambers, T.M. and Wiedbrauk, D.L.** (1992). *Virology. A laboratory manual* San Diego: Academic Press.
- Cao, X., Surma, M.A. and Simons, K.** (2012). Polarized sorting and trafficking in epithelial cells. *Cell Research*, **22**(5), 793-805.
- Cassio, D.** (2013). Long term culture of mdck strains alters chromosome content. *BMC Research Notes*, **6**, 162.

- Chen, X., Love, J.C., Navin, N.E., Pachter, L., Stubbington, M.J.T., Svensson, V., Sweedler, J.V. and Teichmann, S.A.** (2016). Single-cell analysis at the threshold. A discussion of some of the challenges and promise of single-cell technology. *Nature Biotechnology*, **34**(11), 1111-1118.
- Clarke, J., Porter, A. and Davis, J.M.** (2011). Cloning Trans.). In: **Davis, J.M.** (Ed.), *Animal cell culture. Essential methods.* (Ch. 8, pp. 231-254) Chichester: Wiley-Blackwell.
- Combe, M., Garijo, R., Geller, R., Cuevas, J.M. and Sanjuán, R.** (2015). Single-cell analysis of rna virus infection identifies multiple genetically diverse viral genomes within single infectious units. *Cell Host & Microbe*, **18**(4), 424-432.
- Cros, J.F. and Palese, P.** (2003). Trafficking of viral genomic rna into and out of the nucleus: Influenza, thogoto and borna disease viruses. *Virus Research*, **95**(1-2), 3-12.
- Delbrück, M.** (1945). The burst size distribution in the growth of bacterial viruses (bacteriophages). *Journal of Bacteriology*, **50**(2), 131-135.
- Delvigne, F. and Goffin, P.** (2014). Microbial heterogeneity affects bioprocess robustness: Dynamic single-cell analysis contributes to understanding of microbial populations. *Biotechnology Journal*, **9**(1), 61-72.
- Di Carlo, D., Tse, H.T.K. and Gossett, D.R.** (2012). Introduction: Why analyze single cells? Trans.). In: **Lindström, S. and Andersson-Svahn, H.** (Eds.), *Single-cell analysis. Methods and protocols.* (Methods in molecular biology Vol. 853, Ch. 1, pp. 1-10) New York: Humana Press.
- Dukes, J.D., Whitley, P. and Chalmers, A.D.** (2011). The mdck variety pack: Choosing the right strain. *BMC Cell Biology*, **12**, 43.
- Dulbecco, R. and Vogt, M.** (1954). One-step growth curve of western equine encephalomyelitis virus on chicken embryo cells grown in vitro and analysis of virus yields from single cells. *The Journal of Experimental Medicine*, **99**(2), 183-199.
- European Collection of Authenticated Cell Cultures (ECACC)** (2016). Culture collections. Cell lines and hybridomas. Retrieved from <http://www.phe-culturecollections.org.uk/products/celllines/index.aspx>, Accessed on November 24th, 2016.
- Eisfeld, A.J., Neumann, G. and Kawaoka, Y.** (2014). At the centre: Influenza a virus ribonucleoproteins. *Nature Reviews Microbiology*, **13**(1), 28-41.
- Elowitz, M.B., Levine, A.J., Siggia, E.D. and Swain, P.S.** (2002). Stochastic gene expression in a single cell. *Science*, **297**(5584), 1183-1186.
- Elton, D., Digard, P., Tiley, L. and Ortin, J.** (2006). Structure and function of the influenza virus rnp Trans.). In: **Kawaoka, Y.** (Ed.), *Influenza virology. Current topics.* (Ch. 1, pp. 1-36) Wymondham: Caister Academic Press.
- Erlinger, S. and Saier, M.H.** (1982). Decrease in protein content and cell volume of cultured dog kidney epithelial cells during growth. *In Vitro*, **18**(3), 196-202.
- Flint, J.S., Enquist, L.W., Racaniello, V.R. and Skalka, A.M.** (2009). Molecular biology (*Principles of virology.* Vol. I, 3 ed.) Washington: ASM Press.

- Fournier, E., Moules, V., Essere, B., Paillart, J.-C., Sirbat, J.-D., Isel, C., Cavalier, A., Rolland, J.-P., Thomas, D., Lina, B. and Marquet, R.** (2011). A supramolecular assembly formed by influenza a virus genomic rna segments. *Nucleic Acids Research*, **40**(5), 2197-2209.
- Freising, T., Kupke, S.Y., Bachmann, M., Fritzsche, S., Gallo-Ramírez, L.E. and Reichl, U.** (2016). Influenza virus intracellular replication dynamics, release kinetics, and particle morphology during propagation in mdck cells. *Applied Microbiology and Biotechnology*, **100**(16), 7181-7192.
- Fritzsche, F.S.O., Dusny, C., Frick, O. and Schmid, A.** (2012). Single-cell analysis in biotechnology, systems biology, and biocatalysis. *Annual Review of Chemical and Biomolecular Engineering*, **3**, 129-155.
- Galler, K., Bräutigam, K., Große, C., Popp, J. and Neugebauer, U.** (2014). Making a big thing of a small cell – recent advances in single cell analysis. *Analyst*, **139**(6), 1237-1273.
- Gaush, C.R., Hard, W.L. and Smith, T.F.** (1966). Characterization of an established line of canine kidney cells (mdck). *Proceedings of the Society for Experimental Biology and Medicine*, **122**(3), 931-935.
- Gekle, M., Wunsch, S., Oberleithner, H. and Silbernagel, S.** (1994). Characterization of two mdck-cell subtypes as a model system to study principal cell and intercalated cell properties. *Pflügers Archiv - European Journal of Physiology*, **428**(2), 157-162.
- Genzel, Y., Freising, T. and Reichl, U.** (2013). Zellkultur statt hühnerei. Herstellung moderner grippeimpfstoffe. *Chemie in unserer Zeit*, **47**(1), 12-22.
- Genzel, Y. and Reichl, U.** (2007). Vaccine production. State of the art and future needs in upstream processing Trans.). In: **Pörtner, R.** (Ed.), *Animal cell biotechnology. Methods and protocols. (Methods in biotechnology Vol. 24, 2 ed., Ch. 21, pp. 457-473)* Totowa: Humana Press.
- Genzel, Y. and Reichl, U.** (2009). Continuous cell lines as a production system for influenza vaccines. *Expert Review of Vaccines*, **8**(12), 1681-1692.
- Graf, T. and Stadtfeld, M.** (2008). Heterogeneity of embryonic and adult stem cells. *Cell Stem Cell*, **3**(5), 480-483.
- GraphPad Software** (2015). Extremely significant? . Retrieved from http://www.graphpad.com/guides/prism/6/statistics/index.htm?extremely_significant_results.htm, Accessed on December 29th, 2016.
- Gregersen, J.-P., Schmitt, H.-J., Trusheim, H. and Bröker, M.** (2011). Safety of mdck cell culture-based influenza vaccines. *Future Microbiology*, **6**(2), 143-152.
- Gross, A., Schoendube, J., Zimmermann, S., Steeb, M., Zengerle, R. and Koltay, P.** (2015). Technologies for single-cell isolation. *International Journal of Molecular Sciences*, **16**(8), 16897-16919.

- Hansson, G.C., Simons, K. and van Meer, G.** (1986). Two strains of the madin darby canine kidney (mdck) cell line have distinct glycosphingolipid compositions. *The EMBO Journal*, **5**(3), 483-489.
- Haselgrübler, T., Haider, M., Ji, B., Juhasz, K., Sonnleitner, A., Balogi, Z. and Hesse, J.** (2014). High-throughput, multiparameter analysis of single cells. *Analytical and Bioanalytical Chemistry*, **406**(14), 3279-3296.
- Hegde, N.R.** (2015). Cell culture-based influenza vaccines: A necessary and indispensable investment for the future. *Human Vaccines & Immunotherapeutics*, **11**(5), 1223-1234.
- Heldt, F.S., Frensing, T., Pflugmacher, A., Gröpler, R., Peschel, B. and Reichl, U.** (2013). Multiscale modeling of influenza a virus infection supports the development of direct-acting antivirals. *PLoS Computational Biology*, **9**(11), e1003372.
- Heldt, F.S., Frensing, T. and Reichl, U.** (2012). Modeling the intracellular dynamics of influenza virus replication to understand the control of viral rna synthesis. *Journal of Virology*, **86**(15), 7806-7817.
- Heldt, F.S., Kupke, S.Y., Dorl, S., Reichl, U. and Frensing, T.** (2015). Single-cell analysis and stochastic modelling unveil large cell-to-cell variability in influenza a virus infection. *Nature Communications*, **6**, 8938.
- Hensel, S.C., Rawlings, J.B. and Yin, J.** (2009). Stochastic kinetic modeling of vesicular stomatitis virus intracellular growth. *Bulletin of Mathematical Biology*, **71**(7), 1671-1692.
- Heppner, G.H. and Miller, B.E.** (1983). Tumor heterogeneity: Biological implications and therapeutic consequences. *Cancer Metastasis Reviews*, **2**(1), 5-23.
- Hierholzer, J.C. and Killington, R.A.** (1996). Virus isolation and quantitation Trans.). In: **Mahy, B.W.J. and Kangro, H.O.** (Eds.), *Virology methods manual*. (Ch. 2, pp. 25-46) London: Academic Press.
- Holland, J.J., Kennedy, S.I.T., Semler, B.L., Jones, C.L., Roux, L. and Grabau, E.A.** (1980). Defective interfering rna viruses and the host-cell response Trans.). In: **Fraenkel-Conrat, H. and Wagner, R.R.** (Eds.), *Virus-host interactions. Viral invasion, persistence, and disease*. (*Comprehensive virology* Vol. 16, Ch. 3, pp. 137-192) New York: Plenum Press.
- Huang, A.S. and Baltimore, D.** (1970). Defective viral particles and viral disease processes. *Nature*, **226**(5243), 325-327.
- Husted, R.F., Welsh, M.J. and Stokes, J.B.** (1986). Variability of functional characteristics of mdck cells. *The American Journal of Physiology - Cell Physiology*, **250**(2), C214-221.
- Japanese Collection of Research Bioresources (JCRB) Cell Bank** (2016). Jcrb cell bank. Retrieved from <http://cellbank.nibiohn.go.jp/english/>, Accessed on November 24th, 2016.
- Julkunen, I., Sareneva, T., Pirhonen, J., Ronni, T., Melén, K. and Matikainen, S.** (2001). Molecular pathogenesis of influenza a virus infection and virus-induced regulation of cytokine gene expression. *Cytokine & Growth Factor Reviews*, **12**(2-3), 171-180.

- Kalbfuss, B., Knöchlein, A., Kröber, T. and Reichl, U.** (2008). Monitoring influenza virus content in vaccine production: Precise assays for the quantification of hemagglutination and neuraminidase activity. *Biologicals*, **36**(3), 145-161.
- Kawakami, E., Watanabe, T., Fujii, K., Goto, H., Watanabe, S., Noda, T. and Kawaoka, Y.** (2011). Strand-specific real-time rt-pcr for distinguishing influenza vna, crna, and mrna. *Journal of Virological Methods*, **173**(1), 1-6.
- Kersting, U., Schwab, A., Treidtel, M., Pfaller, W., Gstraunthaler, G., Steigner, W. and Oberleithner, H.** (1993). Differentiation of madin-darby canine kidney cells depends on cell culture conditions. *Cellular Physiology and Biochemistry*, **3**(1), 42-55.
- Klenk, H.-D., Rott, R., Orlich, M. and Blödorn, J.** (1975). Activation of influenza a viruses by trypsin treatment. *Virology*, **68**(2), 426-439.
- Koch, A.L.** (1966). The logarithm in biology. 1. Mechanisms generating the log-normal distribution exactly. *Journal of Theoretical Biology*, **12**(2), 276-290.
- Laske, T., Heldt, F.S., Hoffmann, H., Frensing, T. and Reichl, U.** (2016). Modeling the intracellular replication of influenza a virus in the presence of defective interfering rnas. *Virus Research*, **213**, 90-99.
- Li, B. and You, L.** (2013). Predictive power of cell-to-cell variability. *Quantitative Biology*, **1**(2), 131-139.
- Limpert, E., Stahel, W.A. and Abbt, M.** (2001). Log-normal distributions across the sciences: Keys and clues. *BioScience*, **51**(5), 341-352.
- Liu, J., Mani, S., Schwartz, R., Richman, L. and Tabor, D.E.** (2010). Cloning and assessment of tumorigenicity and oncogenicity of a madin-darby canine kidney (mdck) cell line for influenza vaccine production. *Vaccine*, **28**(5), 1285-1293.
- Liu, J., Shi, X., Schwartz, R. and Kemble, G.** (2009). Use of mdck cells for production of live attenuated influenza vaccine. *Vaccine*, **27**(46), 6460-6463.
- Lloyd, A.C.** (2013). The regulation of cell size. *Cell*, **154**(6), 1194-1205.
- Lugovtsev, V.Y., Melnyk, D. and Weir, J.P.** (2013). Heterogeneity of the mdck cell line and its applicability for influenza virus research. *PLoS One*, **8**(9), e75014.
- Macaulay, I.C. and Voet, T.** (2014). Single cell genomics: Advances and future perspectives. *PLoS Genetics*, **10**(1), e1004126.
- Madin, S.H. and Darby, N.B.** (1958). Established kidney cell lines of normal adult bovine and ovine origin. *Proceedings of the Society for Experimental Biology and Medicine*, **98**(3), 574-576.
- Maldonado, V. and Meléndez-Zajgla, J.** (2007). A modified method for cloning adherent mammalian cells. *Bioquímica*, **32**(2), 70-72.

- McCauley, J.W., Hongo, S., Kaverin, N.V., Kochs, G., Lamb, R.A., Matrosovich, M.N., Perez, D.R., Palese, P., Presti, R.M., Rimstad, E. and Smith, G.J.D.** (2012). *Orthomyxoviridae* Trans.). In: **King, A.M.Q., Adams, M.J., Carstens, E.B. and Lefkowitz, E.J.** (Eds.), *Virus taxonomy. Classification and nomenclature of viruses*. (9 ed., pp. 749-761) London: Elsevier Academic Press.
- Meier, K.E., Snavely, M.D., Brown, S.L., Brown, J.H. and Insel, P.A.** (1983). A₁- and β₂-adrenergic receptor expression in the madin-darby canine kidney epithelial cell line. *The Journal of Cell Biology*, **97**(2), 405-415.
- Merten, O.-W., Hannoun, C., Manuguerra, J.-C., Ventre, F. and Petres, S.** (1996). Production of influenza virus in cell cultures for vaccine preparation Trans.). In: **Cohen, S. and Shafferman, A.** (Eds.), *Novel strategies in the design and production of vaccines. (Advances in experimental medicine and biology Vol. 397, Ch. 19, pp. 141-151)* New York: Springer Science+Business Media.
- Milián, E. and Kamen, A.A.** (2015). Current and emerging cell culture manufacturing technologies for influenza vaccines. *BioMed Research International*, **2015**, 504831.
- Modrow, S., Falke, D., Truyen, U. and Schätzl, H.** (2013). *Molecular virology* Heidelberg: Springer.
- Muzzey, D. and van Oudenaarden, A.** (2009). Quantitative time-lapse fluorescence microscopy in single cells. *Annual Review of Cell and Developmental Biology*, **25**, 301-327.
- Nakazato, Y., Suzuki, H. and Saruta, T.** (1989). Characterization of subclones of madin-darby canine kidney renal epithelial cell line. *Biochimica et Biophysica Acta*, **1014**(1), 57-65.
- Nayak, D.P., Balogun, R.A., Yamada, H., Zhou, Z.H. and Barman, S.** (2009). Influenza virus morphogenesis and budding. *Virus Research*, **143**(2), 147-161.
- Nayak, D.P., Chambers, T.M. and Akkina, R.K.** (1985). Defective-interfering (di) rnas of influenza viruses: Origin, structure, expression and interference Trans.). In: **Cooper, M., Eisen, H., Goebel, W., Hofschneider, P.H., Koprowski, H., Melchers, F., Oldstone, M., Rott, R., Schweiger, H.G., Vogt, P.K. and Wilson, I.** (Eds.), *Current topics in microbiology and immunology. (Current topics in microbiology and immunology Vol. 114, pp. 103-151)* Berlin: Springer-Verlag.
- Nichols, G.E., Lovejoy, J.C., Borgman, C.A., Sanders, J.M. and Young, W.W., Jr.** (1986). Isolation and characterization of two types of mdck epithelial cell clones based on glycosphingolipid pattern. *Biochimica et Biophysica Acta*, **887**(1), 1-12.
- Oh, D.Y., Barr, I.G., Mosse, J.A. and Laurie, K.L.** (2008). Mdck-siat1 cells show improved isolation rates for recent human influenza viruses compared to conventional mdck cells. *Journal of Clinical Microbiology*, **46**(7), 2189-2194.
- Pelkmans, L.** (2012). Using cell-to-cell variability - a new era in molecular biology. *Science*, **336**(6080), 425-426.
- Pietuch, A. and Janshoff, A.** (2013). Mechanics of spreading cells probed by atomic force microscopy. *Open Biology*, **3**(7), 130084.

- Portela, A. and Digard, P.** (2002). The influenza virus nucleoprotein: A multifunctional rna-binding protein pivotal to virus replication. *Journal of General Virology*, **83**(4), 723-734.
- Rehberg, M., Ritter, J.B., Genzel, Y., Flockerzi, D. and Reichl, U.** (2013). The relation between growth phases, cell volume changes and metabolism of adherent cells during cultivation. *Journal of Biotechnology*, **164**(4), 489-499.
- Resa-Infante, P., Jorba, N., Coloma, R. and Ortín, J.** (2011). The influenza rna synthesis machine. Advances in its structure and function. *RNA Biology*, **8**(2), 207-215.
- Richardson, J.C.W., Scalera, V. and Simmons, N.L.** (1981). Identification of two strains of mdck cells which resemble separate nephron tubule segments. *Biochimica et Biophysica Acta*, **673**(1), 26-36.
- Rodriguez-Boulan, E., Paskiet, K.T. and Sabatini, D.D.** (1983). Assembly of enveloped viruses in madin-darby canine kidney cells: Polarized budding from single attached cells and from clusters of cells in suspension. *The Journal of Cell Biology*, **96**(3), 866-874.
- Rodriguez-Boulan, E. and Sabatini, D.D.** (1978). Asymmetric budding of viruses in epithelial monolayers: A model system for study of epithelial polarity. *PNAS*, **75**(10), 5071-5075.
- Schulte, M.B. and Andino, R.** (2014). Single-cell analysis uncovers extensive biological noise in poliovirus replication. *Journal of Virology*, **88**(11), 6205-6212.
- Shaw, M.L. and Palese, P.** (2013). *Orthomyxoviridae* Trans.). In: **Knipe, D.M. and Howley, P.M.** (Eds.), *Fields virology*. (6 ed., Ch. 40, pp. 1151-1185) Philadelphia: Lippincott Williams & Wilkins.
- Sheskin, D.J.** (2000). Handbook of parametric and nonparametric statistical procedures (2 ed.) Boca Raton: Chapman & Hall/CRC.
- Sidorenko, Y. and Reichl, U.** (2004). Structured model of influenza virus replication in mdck cells. *Biotechnology and Bioengineering*, **88**(1), 1-14.
- Siegel, S. and Tukey, J.W.** (1960). A nonparametric sum of ranks procedure for relative spread in unpaired samples. *Journal of the American Statistical Association*, **55**(291), 429-445.
- Simmons, N.L.** (1981). Cultured monolayers of mdck cells: A novel model system for the study of epithelial development and function. *General Pharmacology*, **13**(4), 287-291.
- Snijder, B., Sacher, R., Rämö, P., Damm, E.-M., Liberali, P. and Pelkmans, L.** (2009). Population context determines cell-to-cell variability in endocytosis and virus infection. *Nature*, **461**(7263), 520-523.
- Spiller, D.G., Wood, C.D., Rand, D.A. and White, M.R.H.** (2010). Measurement of single-cell dynamics. *Nature*, **465**(7299), 736-745.
- Steinhauer, D.A.** (1999). Role of hemagglutinin cleavage for the pathogenicity of influenza virus. *Virology*, **258**(1), 1-20.
- Steinhauer, D.A. and Skehel, J.J.** (2002). Genetics of influenza viruses. *Annual Review of Genetics*, **36**, 305-332.

- Svec, D., Andersson, D., Pekny, M., Sjöback, R., Kubista, M. and Ståhlberg, A.** (2013). Direct cell lysis for single-cell gene expression profiling. *Frontiers in Oncology*, **3**, 274.
- Timm, A. and Yin, J.** (2012). Kinetics of virus production from single cells. *Virology*, **424**(1), 11-17.
- Toriello, N.M., Douglas, E.S., Thaitrong, N., Hsiao, S.C., Francis, M.B., Bertozzi, C.R. and Mathies, R.A.** (2008). Integrated microfluidic bioprocessor for single-cell gene expression analysis. *PNAS*, **105**(51), 20173-20178.
- Tsioris, K., Torres, A.J., Douce, T.B. and Love, J.C.** (2014). A new toolbox for assessing single cells. *Annual Review of Chemical and Biomolecular Engineering*, **5**, 455-477.
- Tzur, A., Kafri, R., LeBleu, V.S., Lahav, G. and Kirschner, M.W.** (2009). Cell growth and size homeostasis in proliferating animal cells. *Science*, **325**(5937), 167-171.
- Ulmer, J.B., Valley, U. and Rappuoli, R.** (2006). Vaccine manufacturing: Challenges and solutions. *Nature Biotechnology*, **24**(11), 1377-1383.
- Valentich, J.D.** (1981). Morphological similarities between the dog kidney cell line mdck and the mammalian cortical collecting tubule. *Annals of the New York Academy of Sciences*, **372**, 384-405.
- Vinegoni, C., Dubach, J.M., Thurber, G.M., Miller, M.A., Mazitschek, R. and Weissleder, R.** (2015). Advances in measuring single-cell pharmacokinetics and pharmacology *in vivo*. *Drug discovery today*, **20**(9), 1087-1092.
- Wang, D. and Bodovitz, S.** (2010). Single cell analysis: The new frontier in 'omics'. *Trends in Biotechnology*, **28**(6), 281-290.
- Warrick, J.W., Timm, A., Swick, A. and Yin, J.** (2016). Tools for single-cell kinetic analysis of virus-host interactions. *PLoS One*, **11**(1), e0145081.
- Weaver, W.M., Tseng, P., Kunze, A., Masaeli, M., Chung, A.J., Dudani, J.S., Kittur, H., Kulkarni, R.P. and Di Carlo, D.** (2014). Advances in high-throughput single-cell microtechnologies. *Current Opinion in Biotechnology*, **25**, 114-123.
- Webb, C.P., Kane, L., Dawson, A.P., Vande Woude, G.F. and Warn, R.M.** (1996). C-met signalling in an hgf/sf-insensitive variant mdck cell line with constitutive motile/invasive behaviour. *Journal of Cell Science*, **109**(9), 2371-2381.
- Webster, R.G., Bean, W.J., Gorman, O.T., Chambers, T.M. and Kawaoka, Y.** (1992). Evolution and ecology of influenza a viruses. *Microbiological Reviews*, **56**(1), 152-179.
- Whittaker, G.R. and Digard, P.** (2006). Entry and intracellular transport of influenza virus Trans.). In: **Kawaoka, Y.** (Ed.), *Influenza virology. Current topics.* (Ch. 2, pp. 37-64) Wymondham: Caister Academic Press.
- World Health Organization (WHO)** (2014). Influenza virus infections in humans. Retrieved from www.who.int/influenza/human_animal_interface/virology_laboratories_and_vaccines/influenza_virus_infections_humans_feb14.pdf, Accessed on December 05th, 2016.

- World Health Organization (WHO)** (2016a). Influenza (seasonal). Retrieved from <http://www.who.int/mediacentre/factsheets/fs211/>, Accessed on January 13th, 2017.
- World Health Organization (WHO)** (2016b). Virology of human influenza. Retrieved from <http://www.euro.who.int/en/health-topics/communicable-diseases/influenza/data-and-statistics/virology-of-human-influenza>, Accessed on December 02nd, 2016.
- World Health Organization (WHO)** (2017). Influenza vaccine viruses and reagents. Retrieved from <http://www.who.int/influenza/vaccines/virus/>, Accessed on January 13th, 2017.
- Wills, Q.F. and Mead, A.J.** (2015). Application of single-cell genomics in cancer: Promise and challenges. *Human Molecular Genetics*, **24**(R1), R74-R84.
- Wright, P.F., Neumann, G. and Kawaoka, Y.** (2013). Orthomyxoviruses Trans.). In: **Knipe, D.M. and Howley, P.M.** (Eds.), *Fields virology*. (6 ed., Ch. 41, pp. 1186-1243) Philadelphia: Lippincott Williams & Wilkins.
- Wu, M. and Singh, A.K.** (2011). Single-cell protein analysis. *Current Opinion in Biotechnology*, **23**(1), 83-88.
- Zhu, L., Gao, D., Yang, J. and Li, M.** (2012). Characterization of the phenotype of high collagen-producing fibroblast clones in systemic sclerosis, using a new modified limiting-dilution method. *Clinical and Experimental Dermatology*, **37**(4), 395-403.
- Zhu, Y., Yongky, A. and Yin, J.** (2009). Growth of an rna virus in single cells reveals a broad fitness distribution. *Virology*, **385**(1), 39-46.
- Zinserling, V.A. and Dedov, V.A.** (2016). Influenza virus Trans.). In: **Hofman, P.** (Ed.), *Infectious disease and parasites. (Encyclopedia of pathology* pp. 179-182) Springer International Publishing.

List of abbreviations

AM	arithmetic mean
ATCC	American Type Culture Collection
avg	average
BAEE U/mL	trypsin activity according to N _α -Benzoyl-L-arginine ethyl ester enzymatic assay
BEVS	baculovirus expression vector system
BHK cells	baby hamster kidney cells
BSA	Bovine serum albumin
cDNA	complementary desoxyribonucleic acid
cRNA	complementary ribonucleic acid
cRNP	complementary ribonucleoprotein
c _T	cycle threshold
CV	coefficient of variation
DIP	defective interfering particle
DI RNA	defective interfering ribonucleic acid
DMSO	dimethyl sulfoxide
DNA	desoxyribonucleic acid
dNTP	desoxynucleoside triphosphate
ECACC	European Collection of Authenticated Cell Cultures
FACS	fluorescence activated cell sorting
FBS	fetal bovine serum
GMEM	Glasgow's minimum essential medium
HA	hemagglutinin, hemagglutination
HA assay	hemagglutination assay
hpi	hours post infection
IAV	influenza A virus
JCRB	Japanese Collection of Research Bioresources
LAIV	live attenuated influenza vaccine
M1	matrix protein 1
M2	matrix protein 2
MDCK cells	Madin-Darby canine kidney cells
MOI	multiplicity of infection

mRNA	messenger ribonucleic acid
n	number of independent experiments
n _s	number of analyzed single cells
NA	neuraminidase
NEP	nuclear export protein
NES	nuclear export signal
NIBSC	National Institute for Biological Standards and Control
NLS	nuclear localization signal, nuclear import signal
NP	nucleoprotein
P _{cloning}	passage number used for seeding
P _{expansion}	number of passages during expansion
P _{total}	total passage number of cryopreserved cells
PA	polymerase acidic
PB1	polymerase basic 1
PB2	polymerase basic 2
PBS	phosphate buffered saline
PCR	polymerase chain reaction
PFU	plaque-forming unit
qPCR	quantitative PCR, realtime PCR
RBC	red blood cells
RdRp	RNA-dependent RNA polymerase
RKI	Robert Koch Institute
RNA	ribonucleic acid
RT	reverse transcriptase
RT PCR	reverse transcriptase PCR, reverse transcription
RT-qPCR	real-time reverse transcription quantitative PCR
SCA	single-cell analysis
SD	standard deviation
SOP	standard operating procedure
TCID ₅₀	50% tissue culture infective dose
vRNA	viral ribonucleic acid
vRNP	viral ribonucleoprotein
VSV	vesicular stomatitis virus
WHO	World Health Organization

List of symbols

α	significance level of statistical tests	[-]
a	slope of the linear regression	[-]
b	intercept of the linear regression	[-]
c_i	cell count in the i^{th} bin	[-]
c_{standard}	concentration of standard dilution applied for RT	[ng/ μ L]
c_T	threshold cycle	[-]
c_{total}	total cell count	[-]
c_{well}	cell number per well	[cells/well]
D	dilution factor	[-]
d_i	cell diameter in the i^{th} bin	[μ m]
F_{qPCR}	coefficient for dilution of RT reaction in qPCR reaction	[-]
i	bin index	[-]
k	average mass of one nucleotide	[g/mol]
$\log_{10} \text{HAU}/100 \mu\text{L}$	logarithmic HA titer per 100 μ L	[-]
MOI	multiplicity of infection	[virus particles/cell]
m_{qPCR}	mass of cDNA in qPCR reaction	[ng]
m_{RT}	mass of vRNA in RT reaction	[ng]
n	number of plaques	[plaques]
N_A	Avogadro constant	[molecules/mol]
N_{bases}	number of nucleotides (fragment length) of qPCR product	[-]
$N_{\text{molecules cell}}$	number of vRNA molecules per cell	[-]
$N_{\text{molecules qPCR}}$	number of standard cDNA molecules in qPCR reaction	[molecules]
$N_{\text{molecules RT}}$	number of vRNA molecules in RT reaction	[-]
$n_{\text{RBC, well}}$	number of RBC per well	[RBC/well]
p	p-value, probability of type I error in hypothesis tests	
PFU_{cell}	number of PFU per single cell	[PFU/cell]
t_{HA}	virus titer based on HA assay	[virus particles/mL]

t_{PFU}	virus titer based on plaque assay	[PFU/mL]
$t_{\text{TCID}_{50}, \text{ virus stock}}$	virus titer of the virus stock based on TCID ₅₀ assay	[virus particles/mL]
V_i	cell volume in the i^{th} bin	[μL]
$V_{\text{infection medium}}$	volume of infection medium per well	[$\mu\text{L}/\text{well}$]
$V_{\text{infection mixture}}$	volume of infection mixture per well	[$\mu\text{L}/\text{well}$]
$V_{\text{lysate qPCR}}$	volume of sample single-cell lysate applied for RT	[μL]
$V_{\text{lysate total}}$	total volume of sample single-cell lysate	[μL]
$V_{\text{RBC, well}}$	volume of RBC suspension per well	[mL/well]
V_{RT}'	volume of RT reaction after dilution	[μL]
$V_{\text{RT/qPCR}}$	volume of diluted RT reaction aliquot in qPCR reaction	[μL]
V_s	average cell-specific cell volume	[$\mu\text{L}/\text{cell}$]
V_{sample}	volume of sample	[mL]
V_{standard}	volume of standard dilution in RT reaction	[μL]
V_{total}	total cell volume	[μL]
$V_{\text{virus stock}}$	volume of virus stock per well	[$\mu\text{L}/\text{well}$]
V_{well}	cell volume per well	[$\mu\text{L}/\text{well}$]

List of figures

Figure 2-1: Milestones of the present thesis and questions to be addressed.	2
Figure 3-1: Schematic depiction of the influenza A virus particle structure; the complex of RNA polymerases, NP and a viral RNA segment is called viral ribonucleoprotein complex (vRNP); NEP: nuclear export protein; PB1 and PB2: polymerase basic 1 and 2; PA: polymerase acidic; adapted from Flint et al. (2009).....	4
Figure 3-2: Intracellular replication cycle of influenza A virus; only one out of eight vRNP segments is depicted for simplicity; enzymes and structure proteins: RdRp RNA-dependent RNA polymerase, NP nucleoprotein, HA hemagglutinin, NA neuraminidase, M1 matrix protein 1, M2 matrix protein 2 NEP nuclear export protein; ribonucleic acid (RNA) types: vRNA viral RNA, vRNP viral ribonucleoprotein, mRNA messenger RNA, cRNA complementary RNA, cRNP complementary ribonucleoprotein; adapted from Heldt et al. (2013).....	7
Figure 3-3: Examples for heterogeneity of cellular characteristics masked by population average; single-cell analysis is capable to reveal the extent of cell-to-cell variability (distributional dispersion)(A) and the occurrence of subpopulations (multimodal distributions)(B,C); population average can be misleading (B) or discriminate rare subpopulations (C); partly adapted from Di Carlo et al. (2012).....	13
Figure 4-1: Linear correlation between the decadic logarithm of the number of standard cDNA molecules present a qPCR reaction cavity (\log_{10} molecules qPCR) and the threshold cycle (cT) value; the according linear equation is given in Equation 12.	39
Figure 5-1: Examples for adverse particles (A,B) and single cells (C,D) on a 384-well plate; single cells were either adherent (C) or round shaped (D); phase contrast microscopic images taken with 40-fold magnification; scale bars equal 20 μ m.	42
Figure 5-2: Propagation of a clonal MDCK cell population (clone 31) from one single cell on a 384-well plate; phase contrast microscopical images taken at 0 (A), 1 (B), 2 (C), 3 (D), 5 (E), 6 (F), 9 (G) and 13 (H) days post seeding on a 384-well plate with 20-fold (A-E), 10-fold (F) and 5-fold (G-H) magnification; scale bars equal 100 μ m.	43
Figure 5-3: Timeline of the expansion of 31 clonal MDCK cell populations in culture vessels with increasing growth area; different colors indicate different culture vessels; solid lines between different or identical culture vessels indicate trypsinization and (re)seeding; except for clone 1, the 24-well plate was skipped.....	45
Figure 5-4: Morphological characteristics during the spread of a clonal MDCK cell population; black arrows: elongated cells, grey arrows: flattened cells, white arrows: detaching round cells; phase contrast microscopical images taken at 5 (A) and 20 (B) days post seeding on a 384-well plate with 20-fold magnification; scale bars equal 100 μ m.	46
Figure 5-5: Morphological characteristics of subconfluent clonal MDCK cell populations; A-D depict types A-D which are described in Table 5-1; phase contrast microscopical images taken on 75 cm ² flasks with 2.5-fold magnification; scale bars equal 100 μ m.	47
Figure 5-6: Morphological characteristics of a confluent clonal MDCK cell population (clone 20); phase contrast microscopical image taken on 6-well plate with 10-fold magnification; scale bar equals 100 μ m.	48

Figure 5-7: Correlation between average cell number and diameter of cells grown to confluency from clonal and non-clonal MDCK cell populations; colors and shapes of the dots indicate the distinct clusters containing populations with similar growth characteristics (respective clones listed above); $0.5 \cdot 10^6$ cells were seeded in 6-well plates 7 d prior to measurement; $n=2-3$ (independent experiments). 49

Figure 5-8: Distribution of the average cell diameter (A), cell number (B) and cell volume (C) per well at confluency among the clonal and non-clonal MDCK cell populations; $0.5 \cdot 10^6$ cells were seeded in 6-well plates 7 d prior to measurement; average means are used for binning; $n=2-3$ (independent experiments)..... 50

Figure 5-9: Virus titers per mL produced by IAV-infected clonal (1-31) and parental (a-c) MDCK cell populations (MOI 10, 12 hpi) measured by HA assay (A), TCID₅₀ assay (B) and plaque assay (C); $n=2-3$ (independent experiments); avg: average; error bars indicate SD. 52

Figure 5-10: Cell-specific virus titers produced by IAV-infected clonal (1-31) and parental (a-c) MDCK cell populations (MOI 10, 12 hpi) measured by HA assay (A), TCID₅₀ assay (B) and plaque assay (C); avg: average; cell counts at 12 hpi were used for calculation of cell-specific titers; $n=2-3$ (independent experiments); avg: average; error bars indicate SD..... 54

Figure 5-11: Cell-specific virus titers produced by IAV-infected clonal (1-31) and parental (a-c) MDCK cell populations plotted on a log₁₀ scale (MOI 10, 12 hpi) measured by HA assay (A), TCID₅₀ assay (B) and plaque assay (C); avg: average; logarithmic scale; cell counts at 12 hpi were used for calculation of cell-specific titers; $n=2-3$ (independent experiments); avg: average; error bars indicate SD..... 55

Figure 5-12: Virus titers produced by IAV-infected clonal (1-31) and parental (a-c) MDCK cell populations (MOI 10, 48 hpi) measured by HA assay; virus titers are shown per mL on a linear scale (A) and per cell (cell-specific virus titers) on a linear scale (B) as well as on a logarithmic scale (C); $n=1$; avg: average..... 56

Figure 5-13: Relation between cell number and virus titer per mL produced by IAV-infected clonal and parental MDCK cell populations (MOI 10, 48 hpi) measured by HA assay; colors and shapes of the dots indicate the distinct clusters containing populations with similar growth characteristics (see paragraph 5.1.3); $n=1$ 57

Figure 5-14: Cell-specific virus titers produced by IAV-infected clonal and parental MDCK cell populations (MOI 10, 48 hpi) measured by HA assay; A Correlation between average cell diameter and cell-specific virus titer; colors and shapes of the dots indicate the distinct clusters containing populations with similar growth characteristics (see paragraph 5.1.3); $n=1$; B arithmetic mean of the cell-specific virus titers of either cluster: populations of small cells ($n = 14$) and populations of big cells ($n = 16$); error bars indicate SD; arithmetic means of the cell-specific virus titers of the two clusters is extremely significantly different according to *t*-test (**** $p \leq 0.0001$). 58

Figure 5-15: Relation between total cell volume and virus titer per mL produced by IAV-infected clonal and parental MDCK cell populations (MOI 10, 48 hpi) measured by HA assay; colors and shapes of the dots indicate the distinct clusters containing populations with similar growth characteristics (see paragraph 5.1.3); $n=1$ 59

Figure 5-16: Distribution of the virus yield expressed as plaque-forming units (PFU) per cell on a linear (A-C) and logarithmic (D-F) scale produced by IAV-infected (MOI 10, 12 hpi) single cells of different MDCK cell populations: clone 8 (A,D), parental (B,E) and clone 26 (C,F); the first bar on the left indicates the number of non-productive cells (0 PFU); data were pooled from independent experiments (n=3); the number of analyzed cells is indicated as n_s; the vertical line indicates the arithmetic mean (AM); the coefficient of variation is indicated as CV; lognormal distributions are fitted to the data (solid lines in D,E,F); *p*-value indicates the result of Shapiro-Wilk normality test on logarithmized data. 62

Figure 5-17: Boxplot of virus yield expressed as plaque-forming units (PFU) per cell produced by IAV-infected (MOI 10, 12 hpi) single cells of different MDCK cell populations; logarithmic scale; non-productive cells included; hinges cover 25 to 75 %, whiskers mark min-max range; lines within boxes show median (solid) and arithmetic mean (dashed); data were pooled from independent experiments (n=3); the median of clone 8 or clone 26 is significantly lower (** *p* ≤ 0.01) or higher (***) *p* ≤ 0.001) than the median of non-clonal cells according to Mann-Whitney *U* test. 63

Figure 5-18: Distribution of the number of segment 5 (A,B,C) and segment 8 (D,E,F) vRNA copies per cell on a logarithmic scale produced by IAV-infected (MOI 10, 12 hpi) single cells of different MDCK cell populations: clone 8 (A,D), parental (B,E) and clone 26 (C,F); the vertical line indicates the arithmetic mean (AM); data were pooled from independent experiments (n=3); lognormal distributions are fitted to the data (solid lines); *p*-value indicates the result of Shapiro-Wilk normality test on logarithmized data. 66

Figure 5-19: Boxplot of the number of segment 5 (A) and segment 8 (B) vRNA copies per cell produced by IAV-infected (MOI 10, 12 hpi) single cells of different MDCK cell populations; logarithmic scale; hinges cover 25 to 75 %, whiskers mark min-max range; lines within boxes show median (solid) and arithmetic mean (dashed); data were pooled from independent experiments (n=3); for both, segment 5 and segment 8 vRNA levels, the median of clone 8 and clone 26 is not significantly (ns) lower or higher than median of non-clonal cells according to Mann-Whitney *U* test (*p* > 0.05). 67

Figure A-1: Exemplary cell size distributions of three different MDCK cell populations directly obtained from Vi-Cell XR cell viability analyzer after trypsinization of cells grown to confluency; 0.5·10⁶ cells were seeded in 6-well plates 7 d prior to measurement; vertical lines and numbers indicate the average cell diameter (arithmetic mean); A clone 8, B parental, C clone 26. XXII

List of tables

Table 3-1: Length of the eight vRNA segments of IAV and proteins encoded by them; adapted from Bouvier and Palese (2008).....	5
Table 4-1: List of technical equipment used for the present thesis; specific software is provided.	18
Table 4-2: List of plastic ware used for the present thesis.	18
Table 4-3: List of commercial chemicals and reagents used for the present thesis.	19
Table 4-4: List of primers used for reverse transcription (RT); underlined letters indicate tag sequence; 100 μ M stock solutions were prepared in RNase-free water.	22
Table 4-5: List of primers used for realtime PCR (qPCR); underlined letters indicate tag sequence; 100 μ M stock solutions were prepared in RNase-free water.	22
Table 4-6: Volumes of buffers and media for passaging of MDCK cells for maintenance or expansion in different cell culture vessels.....	23
Table 4-7: Volumes for passaging of clonal MDCK cells for expansion in different cell culture vessels; arrows indicate the transfer of the cells to the next cell culture vessel; 24-well plate optionally skipped.	26
Table 4-8: Composition of the RT mastermix; one of the primers given in Table 4-4 was used; the mastermix was prepared in an excess of 10 %.....	35
Table 4-9: Composition of the RT hot start mastermix; Maxima H Minus Reverse Transcriptase (40 U/ μ L) was used as the enzyme with the respective buffer; the mastermix was prepared in an excess of 25 %.....	35
Table 4-10: RT temperature program; a hot start was realized; the lid temperature was 99 °C...36	
Table 4-11: Composition of the qPCR mastermix; the commercial Quanti Tect SYBR Green PCR master mix (2x) contains polymerase, dNTP mix, fluorescent dye and buffer; one of the primer pairs given in Table 4-5 was used; the mastermix was prepared in an excess of 25 %...37	
Table 4-12: qPCR temperature and signal recording program; # indicates recording of signal intensity.	37
Table 4-13: Summary of possible outcomes of hypothesis tests; symbols (asterisks) and the respective p-values and meanings are given; α significance level; p probability of type I error; adapted from GraphPad Software (2015).....	40
Table 5-1: Morphological characteristics of subconfluent clonal MDCK cell populations; Types A-D were distinguished according to cell shape, colony formation, motility and propagation; generic images are provided in Figure 5-5)	47

Table 5-2: Features of clone 8, clone 26 and the parental MDCK cell population. All features obtained on 6-well plates; photos for morphology taken after 2 d of growth (40x magnification); cell diameter and density measured after 7 d of growth; n=3 (independent experiments); cell-specific virus titers produced by IAV-infected cell populations (MOI 10, 12 hpi, $1 \cdot 10^6$ cells were seeded in 6-well plates 24 h prior to infection; cell counts at 12 hpi were used for calculation of cell-specific titers) (paragraph 5.2.1.1); PFU: plaque-forming units.61

Table A-1: Passage numbers of the clonal MDCK cell populations; P_{cloning} : passage number used for seeding; $P_{\text{expansion}}$: number of passages during expansion; P_{total} : total passage number of cryopreserved cells; for population based screening experiments the cells were used one to two passages post thawing; for single-cell experiments the clonal cells were used three to seven passages post thawing and the non-clonal cells were used at passages 6, 11 and 14.XXI

A Appendix

A 1 Standard operating procedures (SOPs)

A 1.1 SOP V/05, version 2.2 (20.01.2011): Hemagglutination assay (HA assay)

SOP V/05 HA-Assay

Version: 2.2 (20.01.2011) Author: Verena Lohr Approved:

Hemagglutination assay (HA assay)

This SOP is based on the SOP written by Bernd Kalbfuß, Version 2.1 (04.12.2006)

1. Introduction

The HA assay is used to detect influenza virus particles (infectious and non-infectious). Influenza viruses carry the protein hemagglutinin (HA) on their surface which binds to specific glycosylation patterns on proteins which are located on the outer membrane of a cell. Thus, virus particles bind to cells and by using erythrocytes as cell system, influenza virus particles can cross-link erythrocytes with each other. This agglutination of erythrocytes can be observed in wells of a round bottom well plate as agglutinated erythrocytes sediment like a carpet at the bottom of the well instead of a point-like sedimentation.

By titrating the virus containing sample, one can determine a critical concentration of the sample at which this switch in sedimentation behaviour occurs. The negative logarithm of this dilution has been defined as the logarithmic HA titer (or simply log-titer) and is a measure for the concentration of influenza virus particles in the sample. The inverse of the dilution has been termed HA activity with units HAU/100 µL and is also supposed to be proportional to the number of virions in the sample.

There are two ways in which one can analyze the HA assay (procedure of pipetting is the same for both methods):

- i) a classical analysis in which the experimenter visually evaluates the HA titer
- ii) a photometric analysis which uses an automated procedure in order to minimize subjectivity and which includes an additional dilution step that increases sensitivity and reduces the error of the method

2. Materials

- Protective clothing: lab coat, protective gloves (Nitrile)
- Centrifuge (e.g. Primo R, Hera, N1.06)
- Sterile cryotubes
- Influenza virus samples (active or chemically inactivated)
- Internal HA standard (= control which is an chemically inactivated influenza virus sample with defined HA titer, stored at -80°C in N1.11, produced as described in SOP HA assay from Bernd Kalbfuß, Version 2.1 (04.12.2006))
- Erythrocyte suspension (conc. approximately 2.0×10^7 erythrocytes/mL, stored at 4 °C in N1.06, produced as described in SOP V/07 from Claudia Best (07.06.2007))
- Unsterile phosphate buffered saline, PBS (stored in N1.06, produced as described in SOP M/01 from Claudia Best (26.09.2007))
- Unsterile transparent 96well round bottom microtiter plates (stored in N1.06, e.g. Greiner Bio-One, Cat.No. 650101) + transparent disposable lids (stored in N1.06, e.g. Greiner Bio-One, Cat.No. 656101)
- 100 µL micropipette + disposable tips
- 8x100 µL or 8x300 µL multichannel micropipette + disposable tips
- Electronic 8x1200 µL multichannel pipette + 1250 µL disposable tips
- 2 reservoirs for multichannel micropipette (PBS, erythrocyte suspension)
- Plate photometer (e.g. Tecan spectra, Tecan Instruments, N1.07)

3. Sample preparation

Infected cell culture with cells and without microcarrier should be filled directly into sterile kryotubes or other sterile tubes and centrifuged at 300xg for 5 min at 4 °C. If cells can not be settled at this g force, choose an appropriate centrifugation setting. After the centrifugation step transfer the supernatant into a new sterile kryotube and freeze at -80 °C.

4. Assay procedure

It is absolutely necessary to pipet exactly in this assay!!

Active samples have to be handled under S2 work bench! For handling outside the safety hood (e.g. when scanning the microtiter plate with the spectrometer), keep disinfectant or citric acid ready in case of accidental spillage!

4.1 Classical method

The titration of influenza virus by the classical method is based on the method described by Mahy and Kangro [1].

1. Pre-dilute samples which are known to be highly concentrated in PBS (all samples which have a HA activity above 3.0 log HA units/100 µL should be diluted). Typically, a 1:10 pre-dilution is sufficient. Samples from cell culture normally do not require this pre-dilution. However, this has to be decided from the assay performer.
2. Fill the wells of column 2-12 with 100 µL PBS each. Wells B, D, F and H of column 1 and 2 are filled with 29.3 µL PBS.
3. Perform the following steps with a 100 µL pipette under S2 work bench! Don't spray disinfectant onto reservoirs and microtiter plates.
The wells 1 and 2 of row A are filled with 100 µL of internal HA standard. Beneath these, a pre-dilution of internal HA standard is prepared by adding 70.7 µL of HA standard to wells 1 and 2 of row B. These 4 wells are prepared accordingly for the samples in rows 3 to 8. This means that on each plate 3 samples can be prepared. If there are more samples, an additional plate is necessary. Standard is necessary on every second plate.

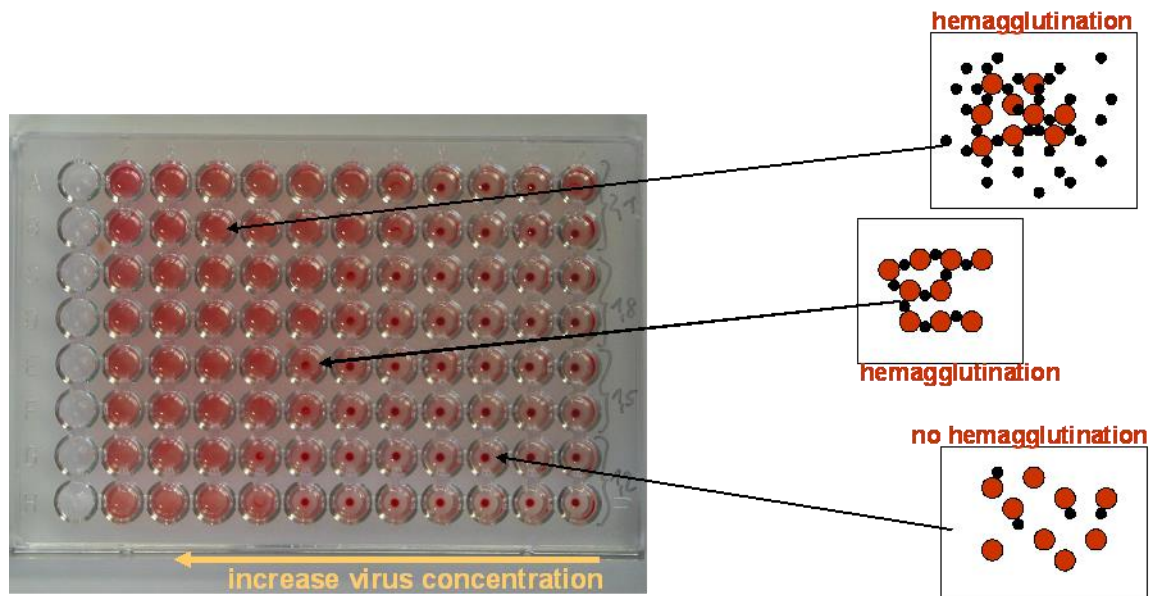
Pipetting scheme for pipetting internal HA standard and samples onto microtiter plate

	1	2	3
A	100 µL HA standard	100 µL HA standard	...
B	70.7 µL HA standard 29.3 µL PBS	70.7 µL HA standard 29.3 µL PBS	...
C	100 µL sample 1	100 µL sample 1	...
D	70.7 µL sample 1 29.3 µL PBS	70.7 µL sample 1 29.3 µL PBS	...
E

4. Mix column 2 three times with a multichannel pipette and transfer 100 µL of column 2 to column 3. Empty the pipette tips completely once before the transfer. Mix again three times and continue the serial dilution until the end of the plate (column 12). The remaining 100 µL should be disposed. Each well has to be filled with 100 µL after finishing these steps. Add 100 µL of erythrocyte suspension into each well by using an electronic multichannel pipette. Mix the suspension well before you start! Start pipetting at the column with the highest dilution (column 12. *For each plate new tips have to be used!*)
5. Each well which has been pipetted faulty should be marked as the values from these wells need to be eliminated during assay evaluation!
6. Incubate the plates for at least 3 hours under the work bench. If the assay is not analyzable, incubation must be prolonged (over night if necessary).
7. Evaluate the results visually. Therefore, mark every well which shows a perfect erythrocyte dot with a (●) and each imperfect dot with a (○). Record your findings by taking the

document "AB-HA_Testauswertung_3.pdf". The last dilution with an imperfect dot is the end point of the titration and is expressed as log HA units per test volume (100 μ L). The inverse of this dilution gives the HA activity [HAU/100 μ L].

8. Compare the measured titer of the internal standard with its nominal titer. The difference (*nominal-measured*) has to be added to the titer of each sample. If two or more standards were analyzed (e.g. because 3 plates were assayed) use the mean difference. If the measured titer of internal standard is more than 0.3 log HAU/100 μ L different from its nominal titer, re-do the whole assay!
9. After evaluation of the titer microtiter plates scan them (see section 4.1) or dispose them into S2 waste!!



Scheme for determination of HA titers in micro titer plate (example shows HA titers from 1.2-2.1 log HA units/100 μ L in double determination)

Overview on dilutions and resulting HA titers (log HA units/100 μ L)

	1	2	3	4	5	6	7	8	9	10	11	12
Dilution	1:1	1:2	1:4	1:8	1:16	1:32	1:64	1:128	1:256	1:512	1:1024	1:2048
HA titer (100 μ L sample)	0	0.3	0.6	0.9	1.2	1.5	1.8	2.1	2.4	2.7	3.0	3.3
HA titer (70.7 μ L sample)	0.15	0.45	0.75	1.05	1.35	1.65	1.95	2.25	2.55	2.85	3.15	3.45

4.1.1 Points to consider

- The detection limit of this assay is 0.15 log HAU/100 μ L. This corresponds to approximately 2.0×10^7 virions/mL; assuming that the number of erythrocytes is proportional to the number of virus particles (each virus particle binds to one erythrocyte).
- The assay has been validated with a standard deviation of ± 0.03 log HAU/100 μ L which is the dilution error.
- The confidence interval for HA activity was determined to be $\pm 15\%$ - 13% (with a confidence level of 95 %).
- The validation has been made for the assay procedure which is described here. If you change singular steps in your procedure, be aware that validation is not valid then.
- Before you start with serious analyses, train yourself in pipetting accurately and precisely, e.g. by measuring standard samples several times.
- HA activity may suffer depending on sample treatment and storage conditions. Thus, do not freeze a measured sample and re-thaw it. Probably, HA titer has then been changed.

4.2 Photometric analysis

In order to minimize subjectivity (dependence on the experimenter), the titration result is evaluated photometrically using an automated procedure. However, this evaluation is restricted to samples with titer >1.0 log HAU/100 μ L. Otherwise, sample titers have to be evaluated with the classical method.

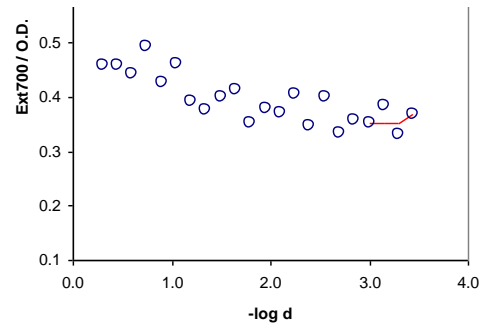
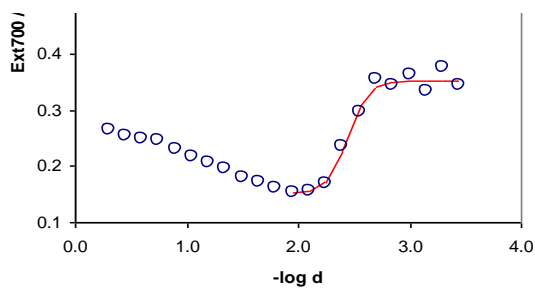
4.2.1 Measurement of extinction

1. Perform all steps which are described for the classical method.
2. Cover microtiter plates containing active virus samples with an appropriate lid.
3. Make sure that Tecan photometer is switched on. Open the software "iControl" and choose "HA protocol" from the list of used protocols. The settings should be defined as follows: Messfilter 700 nm, Referenzfilter none, 10 Blitze, Temperatur 0.0 °C, Schüttelmodus none. (Changes can be made by clicking on button "Messparameter definieren", but should not be done for standard HA protocol.)
4. After having inserted the plate into the reader, click the button "Messung starten". You will be asked for a file name first and to put your plate onto the tray afterwards. The measurement will be carried out immediately afterwards.
It is of utmost importance to remove either the lid before scanning and to remove any condensed water from the bottom of a microtiter plate before scanning!!
5. Save extinction data as Excel-file in the folder "/bpt/data/Tecan/HA_assay/2010/..." using the file name pattern "<Number>-<Date>_<Experimenter>.xls (e.g. 145_10-03-31_CB). If more than one plate will be measured, let the excel file from the first plate open. Then, the results from the following plate will be saved as a new sheet in this file. You have to rename the sheets after your measurement in order to document which sheet belongs to which plate.
6. Repeat step 4 and 5 for each plate of the assay run.

4.2.2 Evaluation of HA titers

A data evaluation template (Excel-file) has been prepared. The evaluation procedure is described in the following. You have to enable macros for the sheet to work properly!

7. Open the data evaluation template ("/bpt/Labor/HA_neu/Data_Evaluation_Template.xls") and save a **copy** in the appropriate folder (/bpt/usp/Labor/HA_neu/data/2010/...).
8. Import your extinction data. Therefore, copy all values and paste them into data-sheet. Delete extinction values of all wells that suffered from erroneous pipetting! As long as affected wells are not within the zone of transition, the assay result may be unaffected.
9. Adjust the sample names and dilutions in the "Report" sheet. Fill all empty header fields and transfer the remarks from the run protocol. Specify the internal standard used and the position of the internal standard (normally, position 1 and 9). If only one standard was measured, specify the same position twice.
10. Click "Evaluate" to start HA titer evaluation.
11. Check difference between nominal titer of the standard and the evaluated titer. Re-do the assay if both values differ more than 0.3 log HAU/100 μ L.
12. Check all fitted curves in the "Evaluation" sheet. If fitting of extinction values has not been made by a sigmoidal curve, then re-analyze the sample. Be careful, if this maybe is due to a low titer of the sample. Then take titers evaluated by the classical method.



Evaluation of the transition point by a Boltzmann function. Left: correct fitting, right: erroneous fitting which would lead to high titer evaluation if curve is not checked and rejected

13. Compare the evaluated titers with the results obtained by the classical method. The discrepancy should be less than 0.3 log HAU/100 μ L.
14. Save the document and make at least one hardcopy of the "Report" and "Evaluation" sheets. Documents are collected in a folder located in N1.07 and N0.13.

5. Sample storage

If samples are kept at below -70 °C, they can be stored up to five years without loss of HA activity. Anyway, this holds true for samples which have been prepared as described in this document (see sample preparation). After this period, it cannot be guaranteed that measured HA activities resemble the original values.

- [1] Mahy B.W.J., Kangro H.O. "Virology Methods Manual": Academic Press Limited, 1996.

Instructions V/08 Version2.1 english

Datum: 2.06.08

Autor: Iona Behrendt

geprüft:

geändert: 09.01.2013

Autor: Verena Lohr

geprüft:

TCID₅₀ Assay

1.0 Objective

Determine the virus sample dilution that infects 50 % of adherent MDCK cells.

2.0 Material

2.1. Cell cultivation and infection with virus

- 6-8 day old MDCK cells from cell culture flasks (T75, T175 or roller bottle)
- Sterile PBS (see instruction M/01)
- Trypsin 10000 BAEE / mL in Milli-Q water, sterile filtered (Trypsin, Sigma, No. T-7409), stored at -80 °C for infection with virus
- Cell culture medium (= Z medium; GMEM + 1% Lab-M-Pepton + 10% FCS, see instruction M/04)
- Virus medium (=V medium; GMEM + 1% Lab-M-Pepton, see instruction M/04)
- Gentamicin 10 mg/mL (Invitrogen, No. 11130-036), stored at room temperature
- 96well plates 400 µL for cell culture, sterile with flat bottom and lid (Cellstar, Greiner bio-one, No. 655180), for each sample one plate is needed!
- Sterile reaction tubes 1.5 mL, for dilution series
- Sterile pipettes, pipettor
- 100 µL pipette
- Electronic single-channel pipette 1 mL (Eppendorf)
- Electronic 8-channel pipette 1250 µL (Eppendorf)
- Pipette tips 100 µL (Plastibrand, sterile)
- Pipette tips 1250µL (Eppendorf, sterile)
- Multipipette with Combitips 10 mL (Eppendorf, Combitips plus biopure)
- 1 sterile Schott bottle (250 or 500 mL)
- 4 sterile reservoirs
- 2 small sterile basins
- Biohazard warning sticker

2.2. Fixation and staining

- 96well plates with confluent MDCK cells
- Sterile and non-sterile PBS (instruction M/01)
- 80% acetone solution in water, icecold (Acetone, p.A.)
- Primary antibody (normally from NIBSC) depending on the virus strain that will be analyzed; e.g.
 - o Influenza Anti A/Wisconsin/67/2005 H3N2 (HA serum sheep) in a 1:200 dilution in PBS
 - o Influenza Anti B/Malaysia/2506/2004 (HA serum sheep), 1:200 dilution
 - o Influenza Anti A/PR/8/34 H1N1 (HA serum sheep), 1:200 dilution
 - o Equine Influenza A (goat serum, final bleed, goat 613 from 02.08.2001, nano tools) , 1:100 dilution

- Secondary antibody (Invitrogen, No.: A-11015)
- 100 μ L 8-channel pipette with sterile tips
- Basin
- 3 reservoirs
- Waste bottle for acetone

3.0 Method

Note for the preparation of virus samples: Generally, the infection supernatant is not centrifuged before storing it at -80 °C. However, in some cases (e.g. with MDCK.SUS2 cells), samples can be centrifuged with a speed <5000 x g. This does not influence the TCID₅₀ value.

3.1 Cell cultivation and infection with virus

A) Cell seeding

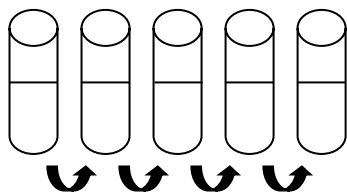
- Wash confluent MDCK cells in cell culture flasks 3x with PBS and trypsinize with the mandatory amount of trypsin for 20 min at 37 °C, then stop the reaction with Z medium (see also instruction Z/04) and count the cell solution in the ViCell XR
- Add 1 % gentamicin to the medium (1 mL gentamicin for 100 mL medium)
- Dilute the trypsinized cells with Z medium (containing gentamicin) to a cell concentration of 4-5x10⁵ cells/mL (see also instruction “Zellzahlbestimmung”), you will need 10 mL of cell suspension for one 96well plate
- Pipet 100 μ L of the cell suspension to each well of the 96well plate, use the electronic 8-channel pipette for this
- Incubate the cells for 1-2 days at 37 °C and 5 % CO₂ (afterwards check for confluence of the cells under the microscope; **if they are not confluent, stop the assay at this point**)

B) Virus sample dilutions

- Add 1 % gentamicin and 0.02 % trypsin to V medium (for 100 mL medium you need to add 20 μ L trypsin and 1.0 mL gentamicin (100 mL V medium are enough for 10 dilution series
- Prepare 8-10 tubes with 900 μ L of V medium each (the number of tubes can vary with the needed number of dilutions; the dilutions are done as follows: give 100 μ L of sample or standard into the first tube (use an Eppendorf pipette), mix 5 times by pipetting up and down, discard the tip, take a new one and transfer 100 μ L from this tube into the next tube, go on like this to the last tube

Sample V medium

Standard



100 μ L 100 μ L 100 μ L 100 μ L

10⁰	10¹	10²	10³	10⁴	10⁵	10⁶	10⁷	10⁸
-----------------------	-----------------------	-----------------------	-----------------------	-----------------------	-----------------------	-----------------------	-----------------------	-----------------------

C) Infection with virus dilutions

- Wash the cell culture plates 2 times with 100 μ L PBS for each well with an electronic 8-channel pipette (dump the PBS in the basin to remove it)
- Add 100 μ L of each dilution in the 8 wells of one column of the cell culture plate belonging to this dilution (start with the highest dilution, then you don't have to change the tip)
- Only V medium is added in columns 1, 2, 11 and 12 (also 100 μ L per well), these wells/columns are used as negative controls, edge effects can be neglected
- Dilutions to do:
 With a HA value of the sample > 2.7 : $10^3 - 10^{10}$
 With a HA between 2.1 and 2.7 (Standard, Seed virus for fermentations): $10^1 - 10^8$
 With a HA < 2.1 : $10^0 - 10^7$

	1	2	3	4	5	6	7	8	9	10	11	12
A	Virus Medium	Virus Medium	10^1	10^2	10^3	10^4	10^5	10^6	10^7	10^8	Virus Medium	Virus Medium
B	Virus Medium	Virus Medium	10^1	10^2	10^3	10^4	10^5	10^6	10^7	10^8	Virus Medium	Virus Medium
C	Virus Medium	Virus Medium	10^1	10^2	10^3	10^4	10^5	10^6	10^7	10^8	Virus Medium	Virus Medium
D	Virus Medium	Virus Medium	10^1	10^2	10^3	10^4	10^5	10^6	10^7	10^8	Virus Medium	Virus Medium
E	Virus Medium	Virus Medium	10^1	10^2	10^3	10^4	10^5	10^6	10^7	10^8	Virus Medium	Virus Medium
F	Virus Medium	Virus Medium	10^1	10^2	10^3	10^4	10^5	10^6	10^7	10^8	Virus Medium	Virus Medium
G	Virus Medium	Virus Medium	10^1	10^2	10^3	10^4	10^5	10^6	10^7	10^8	Virus Medium	Virus Medium
H	Virus Medium	Virus Medium	10^1	10^2	10^3	10^4	10^5	10^6	10^7	10^8	Virus Medium	Virus Medium

- Put a biohazard sticker onto the plates and incubate them for 1 day at 37 °C and 5 % CO₂

D) Trypsin addition

- Add 1 % gentamicin and 0.04 % trypsin to V medium (for 100 mL medium add 40 μ L trypsin and 1 mL gentamicin)
- Add 100 μ L of this medium to each well (use an electronic 8-channel pipet); take care that no virus is carried along other columns, therefore start pipetting at the highest dilution and end at the lowest dilution), remember to change the tips after each plate
- Place the plates in the incubator (37 °C, 5 % CO₂) for one more day

3.2 Fixation and staining

A) Prepare the primary antibody (**only necessary for the Equine Influenza A goat serum if no purified antibody is available!**):

- The Equine Influenza A primary antibody is a polyclonal antibody against equine influenza, but also against cell compounds; therefore, antibodies against cells have to be absorbed; otherwise, they will outperform the fluorescent signal from virus infected cells
- Wash 1-2 day old confluent cell culture flasks 3 times with PBS

- Add 1 mL (for T75) or 3 mL (for T175) of diluted primary antibody against equine influenza and incubate for 30 min at 37 °C, 1 mL 1:100 diluted antibody is enough for one cell culture plate, prepare and incubate an appropriate amount
- The purified primary antibody can be frozen and stored at -20 °C

B) Fixation

- Discard the medium from plates into a basin that already contains 2% acidic acid, pour this into a waste bottle for acetone waste and dispose it appropriately
- add 100 µL icecold 80 % acetone solution to each well
- place the plates for 30 min in the cooling room for fixation, the virus is inactivated after this step so that the following steps can be done outside of the clean bench
- wash the plates twice with PBS (collect the acetone/PBS mix in the same waste as acetone before, call Jan Schäfer to dispose it)

C) Staining

- dilute the purified primary antibody against equine influenza A 1 : 100 in PBS; for other antibodies a 1:200 dilution is sufficient
- add 50 µL of primary antibody solution to each well (electronic 8-channel pipette) and incubate the plates for 60 min at 37 °C
- wash the plates twice with PBS
- in the meantime prepare a 1:500 dilution of secondary antibody in PBS
- add 50 µL of second antibody solution to each well (electronic 8-channel pipette) and again incubate for 60 min at 37 °C
- wash twice with PBS, add 100 µL PBS to each well at the end

The following table summarizes the available antibodies and for which strain they are used.

The following table summarizes the available antibodies and for which strain they are used.

Virus strain	1st antibody	2nd antibody
Human Influenza Virus A/PR/8/34 (H1N1)	anti-influenza A/PR/8/34 H1N1 HA Serum (NIBSC 03/242)	Alexa Fluor 488 donkey anti- sheep IgG (Invitrogen A 11015)
Human Influenza Virus B/Florida/4/2006	anti-B/Florida HA Serum (NIBSC 07/356)	
Human Influenza Virus B/Brisbane/60/2008	anti-B/Brisbane/60/2008 (NIBSC 08/354)	
Human Influenza Virus A/Uruguay/10/2007	anti-A/Brisbane/10/2007 (NIBSC 08/136)	
Human Influenza Virus A/Hongkong/10/2007 (cold-adapted strain)	anti-A/Brisbane/59/2007 (NIBSC 08/112)	
Human Influenza Virus A/Victoria/210/09	anti-A/Perth/16/2009 (NIBSC 10/182)	
Human Influenza Virus B/Vienna/1/1999/37 (cold-adapted strain)	anti-B/Yamagata /16/88 (NIBSC 07/356)	
Human Influenza Virus A/California/7/2009	anti-A/California/7/2009 (NIBSC 10/118)	

4.0 Analysis and calculation of TCID₅₀ titer

- The analysis of plates is done at a fluorescence microscope
- Each well where a fluorescent well (which means a virus is present) will be evaluated as positive (1), each well without any fluorescent cell as negative (0); record the results in a TCID₅₀ worksheet
- The calculation will be done according to the equation of Spearman and Kärber:

$$(\log \text{ virus } 100\%) + (0.5) - \frac{\text{cumulative } 100 \%}{\text{number of tests (per dilution)}} = \log \text{ virus}/100 \mu\text{L}$$

Example analysis:

	1	2	3	4	5	6	7	8	9	10	11	12
A	0	0	1	1	1	1	1	1	1	0	0	0
B	0	0	1	1	1	1	1	1	1	0	0	0
C	0	0	1	1	1	1	1	1	0	0	0	0
D	0	0	1	1	1	1	1	1	0	0	0	0
E	0	0	1	1	1	1	1	1	0	0	0	0
F	0	0	1	1	1	1	1	1	1	0	0	0
G	0	0	1	1	1	1	1	0	0	0	0	0
H	0	0	1	1	1	1	1	1	1	0	0	0

0	0	10 ⁻¹	10 ⁻²	10 ⁻³	10 ⁻⁴	10 ⁻⁵	10 ⁻⁶	10 ⁻⁷	10 ⁻⁸	0	0
---	---	------------------	------------------	------------------	------------------	------------------	------------------	------------------	------------------	---	---

0: no fluorescent cell (= no virus, negative well)

1: fluorescent cell (= virus, positive well)

dilution	Number positive wells/ total number of wells	Cumulative number of positive wells
10 ⁻⁵	8 / 8	19
10 ⁻⁶	7 / 8	11
10 ⁻⁷	4 / 8	4
10 ⁻⁸	0 / 8	0

Example calculation:

$$(-5) + 0.5 - 19/8 = - 6.875 = y ; 10^{6.875} \text{ virions}/100\mu\text{L} = 10^{7.875} \text{ v/mL} = 7.50 \times 10^7 \text{ virions/mL}$$

5.0 Determination of a standard or seed virus reference titer

For each standard or seed virus, samples shall be analyzed at least twice in a 6-fold replication and from 2 people. From all values obtained in these analyses, a reference titer will be calculated.

A 2 Supplemental material

Table A-1: Passage numbers of the clonal MDCK cell populations; P_{cloning} : passage number used for seeding; $P_{\text{expansion}}$: number of passages during expansion; P_{total} : total passage number of cryopreserved cells; for population based screening experiments the cells were used one to two passages post thawing; for single-cell experiments the clonal cells were used three to seven passages post thawing and the non-clonal cells were used at passages 6, 11 and 14.

Clone	P_{cloning}	$P_{\text{expansion}}$	P_{total}	Clone	P_{seeding}	P_{cloning}	P_{total}
1	19	6	25	17	6	5	11
2	6	5	11	18	6	5	11
3	6	5	11	19	6	5	11
4	6	5	11	20	6	6	12
5	6	5	11	21	6	5	11
6	6	6	12	22	6	5	11
7	6	5	11	23	6	6	12
8	6	5	11	24	6	6	12
9	6	5	11	25	6	6	12
10	6	6	12	26	6	7	13
11	6	5	11	27	6	8	14
12	6	5	11	28	6	6	12
13	6	5	11	29	6	5	11
14	6	5	11	30	6	5	11
15	19	6	25	31	6	5	11
16	19	6	25	non-clonal population			11

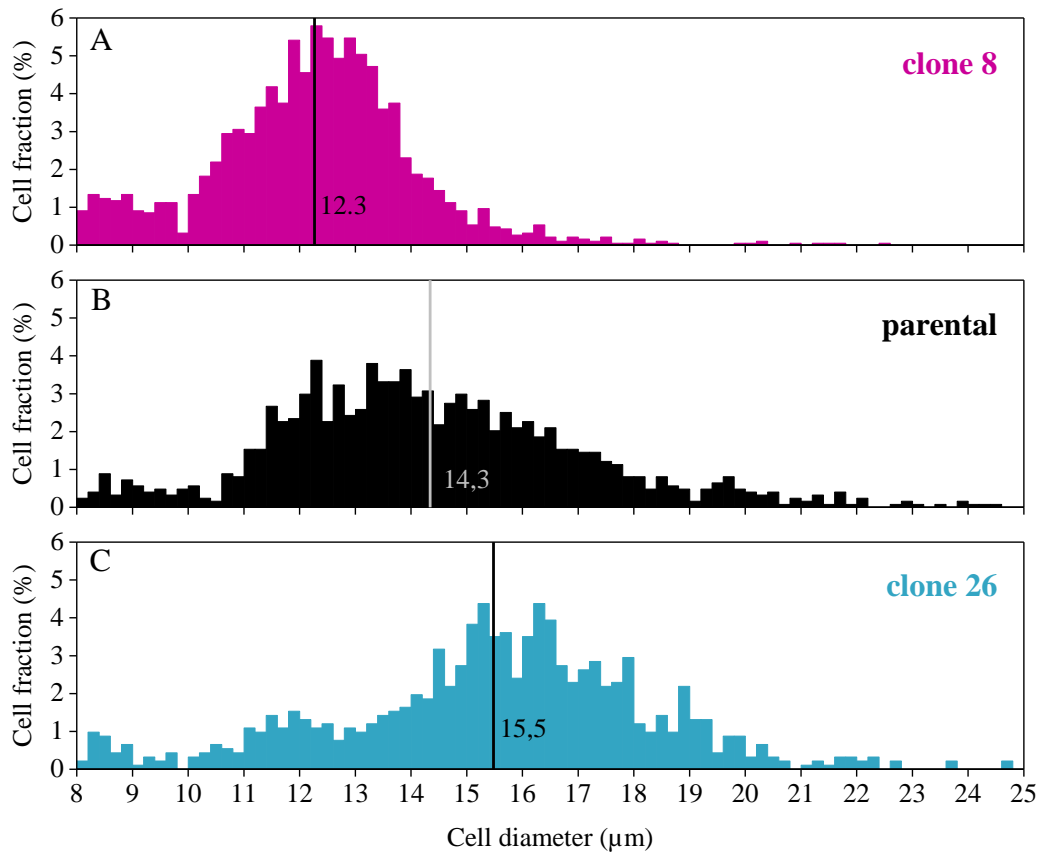


Figure A-1: Exemplary cell size distributions of three different MDCK cell populations directly obtained from Vi-Cell XR cell viability analyzer after trypsinization of cells grown to confluency; $0.5 \cdot 10^6$ cells were seeded in 6-well plates 7 d prior to measurement; vertical lines and numbers indicate the average cell diameter (arithmetic mean); A clone 8, B parental, C clone 26.